UNIVERSIDAD DE ANTIOQUIA

EFFECT OF HYDROCARBONS ON THE AMMONIA SELECTIVE CATALYTIC REDUCTION OF NITROGEN OXIDES UNDER TYPICAL DIESEL ENGINE EXHAUSTS CONDITIONS OVER COPPER-BASED ZEOLITES

Andrés Camilo Álvarez Montoya

Universidad de Antioquia
Facultad de Ingeniería
Departamento de Ingeniería Química

Medellín, Colombia
2020

Efecto de hidrocarburos en la reducción catalítica selectiva de óxidos de nitrógeno bajo condiciones típicas de motores diésel en zeolitas basadas en cobre

Andrés Camilo Álvarez Montoya

Tesis presentada como requisito parcial para obtar al título de:
Doctor en Ingeniería Química

Asesora:
Lina María González Rodríguez
Ph.D. en Ciencias Químicas

Línea de Investigación:
Fijación de gases de efecto invernadero y control de la contaminación del aire
Grupo de Investigación:
Catálisis Ambiental

Universidad de Antioquia
Falcultad de Ingeniería, Departamento de Ingeniería Química
Medellín, Colombia
2020.

UNIVERSIDAD DE ANTIOQUIA

TESIS DOCTORAL

Effect of hydrocarbons on the ammonia selective catalytic reduction of nitrogen oxides under typical diesel engine exhausts conditions over copper-based zeolites

---

Autor:
Andrés Camilo ÁLVAREZ MONTOYA

Asesora:
Dr. Lina María GONZÁLEZ RODRÍGUEZ

Tesis como requisito parcial para optar al título de Doctor en Ingeniería Química

Departamento de Ingeniería Química
Universidad de Antioquia

2020

UNIVERSITY OF ANTIOQUIA

DOCTORAL THESIS

Effect of hydrocarbons on the ammonia selective catalytic reduction of nitrogen oxides under typical diesel engine exhausts conditions over copper-based zeolites

Author:
Andrés Camilo ÁLVAREZ MONTOYA

Advisor:
Dr. Lina María GONZÁLEZ RODRÍGUEZ

A thesis submitted in partial fulfillment of the requirements for the degree of PhD in Chemical Engineering

in the

Department of Chemical Engineering
University of Antioquia

2020

Declaration of Authorship

I, Andrés Camilo ÁLVAREZ MONTOYA, declare that this thesis titled, "Effect of hydrocarbons on the ammonia selective catalytic reduction of nitrogen oxides under typical diesel engine exhausts conditions over copper-based zeolites" and the work presented in it are my own. I confirm that:

- This work was done wholly or mainly while in candidature for a research degree at this University.
- Where any part of this thesis has previously been submitted for a degree or any other qualification at this University or any other institution, this has been clearly stated.
- Where I have consulted the published work of others, this is always clearly attributed.
- Where I have quoted from the work of others, the source is always given. With the exception of such quotations, this thesis is entirely my own work.
- I have acknowledged all main sources of help.
- Where the thesis is based on work done by myself jointly with others, I have made clear exactly what was done by others and what I have contributed myself.

Signed:

Date:

"That which does not kill us makes us stronger."

Friedrich Nietzsche

UNIVERSIDAD DE ANTIOQUIA

Abstract

Faculty of Engineering
Department of Chemical Engineering

PhD in Chemical Engineering

Effect of hydrocarbons on the ammonia selective catalytic reduction of nitrogen oxides under typical diesel engine exhausts conditions over copper-based zeolites

by Andrés Camilo ÁLVAREZ MONTOYA

The use of diesel engines is growing due to their advantages over the gasoline engines, but they increase nitrogen oxides (NO_X) emissions. The ammonia selective catalytic reduction (NH_3-SCR) with Cu-based zeolites is the most promising and studied technique for the abatement of NO_X. However, research under more realistic conditions, such as including hydrocarbons on the simulated gas, needs to be studied deeply. We selected Cu-ZSM-5, Cu-SSZ-13, and Cu-SAPO-34 (three of the most successful and investigated catalysts in the NH_3-SCR of NO_X) to perform a series of experiments regarding the effect of propylene and dodecane (two hydrocarbons that can be present in diesel exhausts) on the NH_3-SCR of NO and adsorption of NH_3. We synthesized the catalysts by ion exchange and confirmed their structure by X-ray diffraction. We found that both propylene and dodecane reduced the amount NH_3 adsorbed on the catalysts. Also, we determined that experiments of temperature-programmed desorption of NH_3 of Cu-ZSM-5 and Cu-SAPO-34 saturated with propylene changed the parameters of the desorption kinetic of the catalysts, and mainly affected the acid sites that not concern copper. We confirmed that dodecane (a long-chain hydrocarbon) affected the performance of Cu-SSZ-13 (a small-pore zeolite) on the NH_3-SCR and NH_3 oxidation. Finally, we found that the hydrocarbons decreased the activation energy and changed the parameters of a power-law kinetic of Cu-ZSM-5 and Cu-SSZ-13 in the NH_3-SCR of NO.

UNIVERSIDAD DE ANTIOQUIA

Resumen

Facultad de Ingeniería
Departamento de Ingeniería Química

Doctor en Ingeniería Química

Efecto de hidrocarburos sobre la reducción catalítica de óxidos de nitrógeno bajo condiciones típicas de exostos de motores diésel sobre catalizadores zeolíticos basados en cobre

por Andrés Camilo ÁLVAREZ MONTOYA

El uso de motores diésel está creciendo debido a sus ventajas sobre los motores a gasolina, pero aumentan las emisiones de óxidos de nitrógeno (NO_X). La reducción catalítica selectiva con amoniaco (NH_3-RCS) utilizando zeolitas basadas en cobre es la técnica más prometedora y estudiada para la reducción de NO_X. Sin embargo, su investigación bajo condiciones más reales, como la inclusión de hidrocarburos en el gas simulado, necesitan ser estudiadas profundamente. Se seleccionaron Cu-ZSM-5, Cu-SSZ-13 y Cu-SAPO-34 (tres de los catalizadores más exitosos e investigados en la NH_3-RCS de NO_X) para desarrollar una serie de experimentos concernientes al efecto del propileno y el dodecano (dos hidrocarburos que pueden estar presentes en exhostos de motores diésel) en procesos relacionados con la NH_3-RCS de NO_X. Los catalizadores se sintetizaron por intercambio iónico y su estructura fue corroborada por difracción de rayos X. Se encontró que tanto el propileno como el dodecano redujeron la cantidad de amoniaco desorbida en los catalizadores, la cual es una etapa muy importante para que la reacción de NH_3-RCS ocurra. Además, se determinó que experimentos de desorción a temperatura programada de amoniaco de Cu-ZSM-5 y Cu-SAPO-34 saturados con propileno cambia los parámetros de la cinética de desorción de ambos catalizadores y principalmente afecta los sitios ácidos no relacionados con cobre. Se encontró que el dodecano (un hidrocarburo de cadena larga) afecta el desempeño la Cu-SSZ-13 (una zeolita de poro pequeño) en la NH_3-RCS de NO y en la oxidación de NH_3. Finalmente, se encontró que los hidrocarburos disminuyeron la energía de activación y cambiaron los parámetros de una cinética de ley de potencias de la Cu-ZSM-5 y la Cu-SSZ-13 en la reacción de NH_3-RCS de NO.

Acknowledgements

A lot of people make it possible for me to finish this thesis, but unfortunately, I do not have enough space for writing all their names. Here I am naming the more significant to my work and life:

- My advisor Professor Lina González for her help in the experimental section, support in everything I asked, comments, and suggestion throughout the doctoral;
- Professor Aída Luz Villa for allowing me to work in Environmental Catalysis Research Group and including me in the project "NH_3-SCR over Cu-SSZ-13 in the presence of hydrocarbons", which was part of Chapter 3 of the thesis;
- Professor Sven Kureti for the opportunity and kindly reception at the "Institut für Energieverfahrenstechnik und Chemieingnenireurwesen" in Freiberg, Germany;
- MSc. Christoph Hahn, first for his help by email asking my question and then for training me in all the experimental part at IEC in Freiberg that was part of Chapter 2;
- Dipl.-Eng Chelo for her extraordinary support in Spanish at the laboratory and daily issues during my stay in Germany, also for her availability to help in everything I asked;
- Juan Miguel González, who synthesized the H-SSZ-13 at Purdue University and gave us the catalysts for performing such as amazing experiments;
- my colleagues at the Catálisis Ambiental group and IEC institute for their friendship at both laboratories;
- technicians and scientific staff who make some of the catalysts characterizations and some of them help me in Germany with the facilities;
- Colciencias for the loan-scholarship through the call 647 and DAAD for its scholarship to my stay in Germany;
- my girlfriend for her support and love who came at the right time and makes my doctoral studies more enjoyable and with the better companion;
- my parents, Nancy and Albeiro, and my aunt Stella who kindly offer me to live with her all this time;
- the rest of the people, especially my personal friends, who directly or indirectly help me to perform my doctoral studies.

Contents

List of Figures

List of Tables

List of Abbreviations

BET	**B**runauer-**E**mmett-**T**eller
DEF	**D**iesel **E**xhaust **F**luid
DOC	**D**iesel **O**xidation **C**atalyst
DPF	**D**iesel **P**articulate **F**ilter
DRIFTS	**D**iffuse-**R**eflenctance **I**nfrared **F**ourier **T**ransformm **S**pectroscopy
EDS	**E**nergy **D**ispersive **Spectroscopy**
EGR	**E**xhaust **G**as **R**ecirculation
FTIR	**F**ourier **T**ansform **I**nfra**R**ed
GHSV	**G**as **H**ourly **S**pace **V**elocity
HC	**H**ydro**C**arbon
MFC	**M**ass **F**low **C**ontroller
MOR	**MOR**pholine
NO_X	**N**itrogen **O**xides
NSR	**N**O_X **S**torage **R**eduction
PAH	**P**oly **A**romatic **Hydrocarbon**
PLS	**P**artial **L**east **S**quares
SCR	**S**elective **C**atalytic **R**eduction
SEM	**S**canning **E**lectron **M**icroscope
SNCR	**S**elective **N**on-**C**atalytic **R**eduction
TEOS	**TE**tra**e**thyl **O**rtho**S**ilicate
TPD	**T**emperature **P**rogrammed **D**esorption
TPR	**T**emperature **P**rogrammed **R**eduction
TWC	**T**hree-**W**ay **C**atalysts
TOR	**T**urn**O**ver **R**ate
w/	**w**ith
w/o	**w**ith**o**ut
WHO	**W**orld **H**ealth **O**rganization
XRD	**X**-**R**ay **D**iffraction

Physical Constants

Boltzmann constant	$k_B = 1.38 \times 10^{-23} \mathrm{J\,K^{-1}}$
Gas constant	$R = 8.314 \mathrm{J\,mol^{-1}\,K^{-1}}$
Avogadro number	$\mathrm{N_A} = 6.022 \times 10^{23}$

List of Symbols

A	pre-exponential factor	$\mathrm{m\,s^{-1}}$, $\mathrm{mol\,m^{-2}\,s^{-1}}$
A_{ads}	pre-exponential factor of the adsorption	$\mathrm{m\,s^{-1}}$
A_{des}	pre-exponential factor of the desorption	$\mathrm{mol\,m^{-2}\,s^{-1}}$
B	width at half maximum of the X-ray diffraction peak	radian
c	concentration	ppm
c_i^{exit}	NH_3 content in the gas	ppm
C_i	initial mass of coating	g
C_f	final mass of coating	g
CML	coating mass loss	%
C_s	gas concentration	$\mathrm{mol\,m^{-3}}$
D	dispersion	dimensionless
D_{eff}	effective diffusivity	$\mathrm{m^2\,s^{-1}}$
D_{hkl}	crystallite size in the direction perpendicular to the lattice plane	m
d_p	crystallite grain size	m
E	activation energy	$\mathrm{kJ\,mol^{-1}}$
$E(0)$	activation energy at zero coverage	$\mathrm{kJ\,mol^{-1}}$
E_a	apparent activation energy	$\mathrm{kJ\,mol^{-1}}$
E_{ads}	activation energy of the adsorption	$\mathrm{kJ\,mol^{-1}}$
E_{des}	activation energy of the desorption	$\mathrm{kJ\,mol^{-1}}$
F	total flow	$\mathrm{mL\,min^{-1}}$
$F_{N_{2,\ in}}$	nitrogen flow in	$\mathrm{mL\,min^{-1}}$
K	crystallite-shape factor	dimensionless
m	catalyst mass	g, mg
M_i	initial mass of monolith	g
M_f	final mass of monolith	g
ML	metal loading	mg
MML	monolith mass loss	%
MW_{Cu}	molecular weight of Cu	$\mathrm{g\,mol^{-1}}$
n_{Des}	mol desorbed from a TPD	mol
$N_{2,\ NH_3}$	N_2 from NH_3	ppm
$N_{2,NO}$	N_2 from NO_X	ppm
$NH_{3,\ C}$	NH_3 converted	ppm
NO_C	NO converted	ppm
$NO_{2,\ C}$	NO_2 converted	ppm
$\mathrm{N}w-p$	Weisz-Prater number	dimensionless
r_{ads}	rate of adsorption	$\mathrm{m\,s^{-1}}$
r_{des}	rate of desorption	$\mathrm{mol\,m^{-2}\,s^{-1}}$

r_{cal}	calculated reaction rate	$\mathrm{mol\,kg^{-1}\,s^{-1}}$
r_M	rate measured	$\mathrm{mol\,s^{-1}}$
R_p	radius of a particle	m
t	time	s
T	temperature	K, °C
$\mathrm{T_{ads}}$	temperature of adsorption	°C
T_0	initial temperature	K, °C
T_{end}	final temperature	K, °C
TMS	total metal surface	$\mathrm{mol_{Cu}\,g_{cat}^{-1}}$
TOR	turnover rate	$\mathrm{mol_{NO}\,mol_{Cu}^{-1}\,s^{-1}}$
V	volume	mL
$\dot{V}_{Ar}$	flow of Ar	$\mathrm{cm^3\,min^{-1}}$
V_m	molar volume	$\mathrm{m^3\,mol^{-1}}$, $\mathrm{cm^3\,mol^{-1}}$
$\dot{V}_{N_2}$	flow of nitrogen	$\mathrm{cm^3\,min^{-1}}$
w_i	width of the peak i	
	at half of the height	dimensionless
X_{NH_3}	NH_3 conversion	%
X_{NO}	NO conversion	%

Greek letters

α	coverage dependence of the E	$\mathrm{kJ\,mol^{-1}}$
β	heating rate	$\mathrm{°C\,min^{-1}}$
λ	wavelength	m, nm
ν	average velocity	$\mathrm{m\,s^{-1}}$
ρ	apparent density	$\mathrm{kg\,m^{-3}}$
ρ_2	apparent density	$\mathrm{kg\,m^{-3}}$
θ	coverage	dimensionless
θ	Bragg angle	radian

Dedicated to my parents, Nancy and Albeiro; and my aunt Stella, who contributed in my entire life to my success.

Chapter 1

Background

This chapter aims to give the basic concepts and definitions for the understanding of the main topics of this thesis. It begins defining diesel engines, diesel fuel, and emissions, emphasizing on nitrogen oxides. It lists the main categories for NO_X abatement and explains the NH_3-SCR of NO_X, which was the technique for reducing NO_X studied in this work. It gives a general review of the catalysts used in this process and emphasizes zeolites. It explains the principles of adsorption in materials like zeolites and depicts the equations needed for simulating the kinetics of the adsorption/desorption process. It gives a thorough state of the art in the effect of hydrocarbons on catalysts based on zeolites used in the NH_3-SCR of NO_X that let us propose some of the objectives dealt in this thesis. It finally gives an overview and explains some of the decisions made for the topics of each chapter.

1.1 General concepts

1.1.1 Diesel engine

A diesel engine is an internal combustion engine, in which compressed air ignites the diesel fuel to convert its chemical energy into mechanical force [1]. It has a higher compression ratio, hence more efficient than a gasoline engine. However, it is more expensive due to the materials that need to resist the high pressures and temperatures inside the engine [2].

1.1.2 Diesel fuel

A report from the United Nations Environment Programme, the International Labour Organisation, and the World Health Organization (WHO) defines the diesel fuel as a mixture of normal, branched, and cyclic alkanes (60 to 90% v/v), with hydrocarbon chains length between C_9 and C_{30}; aromatic compounds, especially alkylbenzenes (5 to 40% v/v); and small amounts of alkanes (0 to 10% v/v) obtained from the middle-distillate, gas-oil fraction during petroleum separation [3]. Benzene, toluene, ethylbenzene, xylenes, and polycyclic aromatic hydrocarbons (PAHs), may be present at levels of parts per million [3].

Diesel fuel can also derive from animals or plants—biodiesel. It is obtained subjecting the animal fat or vegetable oil to a chemical reaction called transesterification [4].

1.1.3 Emissions

The major combustion products in a diesel engine exhaust are nitrogen (∼67%), carbon dioxide (∼12%), water vapor (∼11%), oxygen (∼9%), nitrogen oxides (∼0.5%), and ∼0.5% composed of pollutants such as particulate matter, carbon monoxide, hydrocarbons, and some sulfur dioxide depending on the fuel source [5]. Among all the pollutants emitted, NO_X has the highest proportion of diesel pollutant emissions with a rate of more than 50%. Diesel engines are responsible for about 85% of all the NO_X emissions from mobile sources, primarily in the form of NO [5]. Benzene and toluene are present in the lower weight percent range in the gaseous part of the hydrocarbon fraction. Other components are low-relative-molecular-mass polycyclic aromatic hydrocarbons (PAHs) [3]. According to Liang et al. [6], the composition of gases from a diesel engine exhaust suggests that they may originate from unburned diesel fuel, engine oil evaporation or combustion generated products. Compared with diesel fuel, the exhaust contains fewer fractions of alkanes and more PAH compounds. Liang et al. [6] reported that the gases of a diesel engine exhaust might contain 8339 μg/g n-alkanes, 7592 μg/g of branched alkanes, 242 μg/g saturated cycloalkanes, 246 μg/g of polycyclic aromatic

hydrocarbons (PAHs), 10997 μg/g of alkylated PAHs, 71.1 μg/g of alkylbenzenes, and 7012 μg/g of alkanoic acids.

1.1.4 Nitrogen oxides

Nitrogen oxides (NO_X) are a gaseous mixture of nitric oxide (NO) and nitrogen dioxide (NO_2). Naturally, they are present in the atmosphere due to bacterial decomposition, forest fires, volcanic activity, trees, and yeast. Anthropogenically, they are produced from fossil fuel combustion such as coal, petroleum, and natural gas in solid waste incinerators, refineries, glass and cement industries, and power plants. According to the type of NO_X formation, they are classified as:

- prompt NO_X, formed in the reaction of hydrocarbon fragments with atmospheric nitrogen to produce HCN or H_2CN that can oxidize to NO and NO_2 or N_2O;
- fuel NO_X, produced from the combustion of nitrogen present in fuels like coal and heavy oils; and
- thermal NO_X, formed from the reaction of nitrogen from the air with oxygen at high temperature (~1000 °C) according to the Zeldovich mechanism (Reactions 1.1–1.3)

$$N_2 + O_2 \longleftrightarrow 2\,NO \tag{1.1}$$

$$N_2 + O\cdot \longleftrightarrow NO + N\cdot \tag{1.2}$$

$$N\cdot + O_2 \longleftrightarrow NO + O\cdot \tag{1.3}$$

1.1.5 Nitrogen oxides abatement

The Three main categories to reduce NO_X [7] are:

a) treating the fuel, which consists of reducing any nitrogen bounded to the fuel;

b) minimizing the formation of NO_X at the source, which consists of modifying combustion parameters to reduce the amount of oxygen [8], eg., staged air addition, steam and water injection, reburning, exhaust gas recirculation (EGR), and design modifications in the burner, furnace or boiler [7]; and

c) removing NO_X before expelling them into the atmosphere, which consists of reducing the NO_X by a technique such as selective catalytic reduction (SCR), selective non-catalytic reduction (SNCR), NO_X storage reduction (NSR), and scrubbing methods.

From techniques described previously, SCR with NH_3 is the most promising for the reduction of NO_X.

1.1.6 NH_3-SCR of NO from diesel engines

NH_3-SCR of NO_X consists of injecting NH_3, which reacts with NO_X, into the gaseous stream to produce molecular nitrogen and water (Reaction 1.4). Commercial SCR systems reduce NO_X between 70 and 95% at the temperature range 250–400 °C. The working temperatures depend on the catalyst used; for titanium and vanadium oxide catalysts is about 340–400 °C; for zeolite catalyst, it is about 200–300 °C.

NO_X in diesel exhaust is usually composed of 90% NO. Therefore, the main reaction of SCR is Reaction 1.4, which is called standard SCR. With equimolar amounts of NO and NO_2 (Reaction 1.5), it is called fast SCR; and with only NO_2 (Reaction 1.6), it is called slow SCR.

$$4\,NH_3 + 4\,NO + O_2 \longrightarrow 4\,N_2 + 6\,H_2O \tag{1.4}$$

$$4\,NH_3 + 2\,NO + 2\,NO_2 \longrightarrow 4\,N_2 + 6\,H_2O \tag{1.5}$$

$$8\,NH_3 + 6\,NO_2 \longrightarrow 7\,N_2 + 12\,H_2O \tag{1.6}$$

Another important reaction is the oxidation of NO (Reaction 1.7)

$$2\,NO + O_2 \longrightarrow 2\,NO_2 \tag{1.7}$$

Others reaction that can occur in the process are the following:

$$4\,NH_3 + 5\,O_2 \longrightarrow 4\,NO + 6\,H_2O \tag{1.8}$$

$$4\,NH_3 + 3\,O_2 \longrightarrow 2\,N_2 + 6\,H_2O \tag{1.9}$$

$$2\,NH_3 + 2\,O_2 \longrightarrow N_2O + 3\,H_2O \tag{1.10}$$

Reaction 1.8, Reaction 1.9, and Reaction 1.10 represent the oxidation of NH_3 to NO, N_2 and N_2O, respectively.

The Gibbs free energy for Reaction 1.4 ($\Delta G^0_{298} = -1651\text{kJ mol}^{-1}$) is lower with respect to the one of Reaction 1.7 ($\Delta G^0_{298} = -70\text{kJ mol}^{-1}$) [9]. Since Reaction 1.5 is limited by Reaction 1.7, it is concluded that Reaction 1.4 dominates the reduction of NO as Zhang et al. [9] point out.

Figure 1.1 shows a typical diesel after-treatment system, which consists of a diesel oxidation catalyst (DOC), a diesel particulate filter (DPF), and the selective catalytic reduction (SCR) system itself. The DOC oxidizes hydrocarbons and CO to CO_2, and NO to NO_2; the DPF traps the particulate matter from the exhaust gas; then a diesel exhaust fluid (DEF, generally a urea solution) is added in the SCR unit to reduce the nitrogen oxides to N_2 and H_2O. Because of the complex composition of the exhaust gases and diesel engine operational conditions, the diesel after-treatment system could have some problems. For example, DOC might oxidize neither HC nor the CO, if it is saturated after a long-time use or in the long idling or cold start of the engine, in which the DOC does not reach its operating temperature.

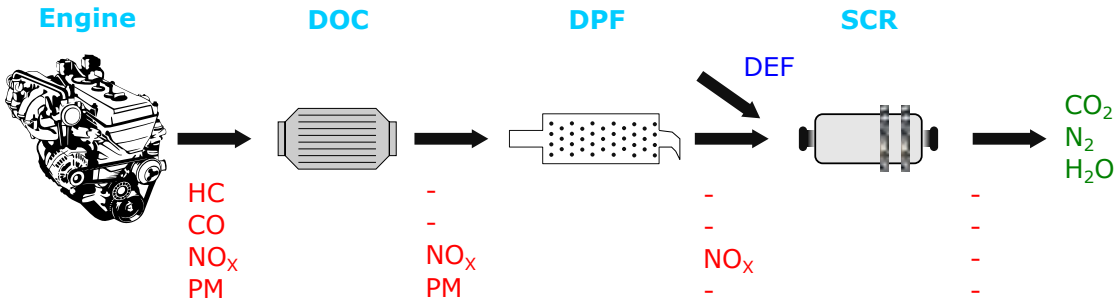

Figure 1.1: Schematic of a diesel after-treatment system. *The figure of the diesel engine was taken from* [10].

1.1.7 Catalysts for NH_3-SCR of NO_X

Generally, SCR of NO_X emitted from stationary sources uses catalysts consisting of vanadium pentoxide (V_2O_5) and tungsten trioxide (WO_3) supported by high-surface-area anatase-form titania (TiO_2) [11]. Those catalysts have high activity for NO_X reduction at the medium temperature range 350–450 °C and resistance to sulfur poisoning [12]. However, they lack thermal stability under harsh environments due to the phase change of TiO_2 from anatase to rutile above 550 °C [13]. Also, vanadium, which is toxic, could evaporate from the surface at 550 °C [13]. On the other hand, the automobile industry, which uses gasoline as a fuel, uses the TWC (Three-Way Catalysts), which can deal with hydrocarbons, CO, and NO_X at the same time.

However, in diesel engines, using the TWC and the $V_2O_5/WO_3/TiO_2$ is not possible because they operate at lean conditions (i.e., excess of air). They have a narrow working temperature window, are unstable, and deactivates easily caused by the anatase-rutile transition in V_2O_5-WO_3/TiO_2 catalysts [14]. For that reason, the automobile industry that works with diesel engines prefers the metal-exchange zeolite-based catalysts because they operate on a broader temperature window (200–450 °C), increase stability, and reduced deactivation problems [14]. ZSM-5 and beta zeolite frameworks with medium and large pores, promoted by transition metals like Cu and Fe, have high NO_X

reduction over a wide range of conditions [15–19], but the presence of water can cause dealumination of these catalysts at high temperatures [20]. Zeolites having the CHA framework, which possesses small pores, are an alternative due to their high thermal stability [21–24].

1.1.8 Zeolites

According to Collela [25], "a zeolite is a crystalline substance with a structure characterized by a framework of linked tetrahedra, each consisting of four O atoms surrounding a cation. This framework contains open cavities in the form of channels and cages. These are usually occupied by H_2O molecules and extra-framework cations that are commonly exchangeable. The channels are large enough to allow the passage of guest species. In the hydrated phases, dehydration occurs at temperatures mostly below about 400 °C and is largely reversible. The framework may be interrupted by (OH, F) groups; these occupy a tetrahedron apex that is not shared with adjacent tetrahedra".

The Structure Commission of the International Zeolite Association (IZA-SC) is the organization that promotes and encourages the development of all aspects of zeolite science and technology [26]. Until 2016, it has registered 232 frameworks of zeolites, including the MFI (Figure 1.2a) and CHA (Figure 1.2b) frameworks that were subject of study in this thesis. ZSM-5 corresponds to the framework type MFI, while SAPO-34 (a silicoaluminophosphate) and SSZ-13 (an aluminosilicate) correspond to the framework type CHA.

MFI framework is composed of several pentasil units linked together by oxygen bridges to form pentasil chains, and mirror images that form corrugated sheets with 10-ring holes [27]. Each sheet is linked by oxygen bridges to the next to form the 3-dimensional structure. Adjacent sheets are related to one another by an inversion center producing straight 10-ring channels perpendicular to the sheets (along x). The following channels link the straight channels to one another to form a 3-dimensional 10-ring channel system [27].

CHA framework has an ABC stacking of double 6-rings arrays (or and AAB-BCC stacking of single 6-ring arrays. This stacking produces an elongated cavity with six 8-ring pores and a 3-dimensional channel system [27]. The pore size of the CHA and MFI framework are 3.8 and 5.4–5.6 Å[28].

1.1.9 Adsorption in zeolites

Adsorption is the enrichment of a solid surface by an interface of a fluid [29]. The fluid available for adsorption, which can be either a gas or liquid, is the adsorbate; the solid, on which the adsorption takes place, is called the adsorbent [29]. Zeolites can adsorb molecules, without changing their structure, due to their high specific surface area

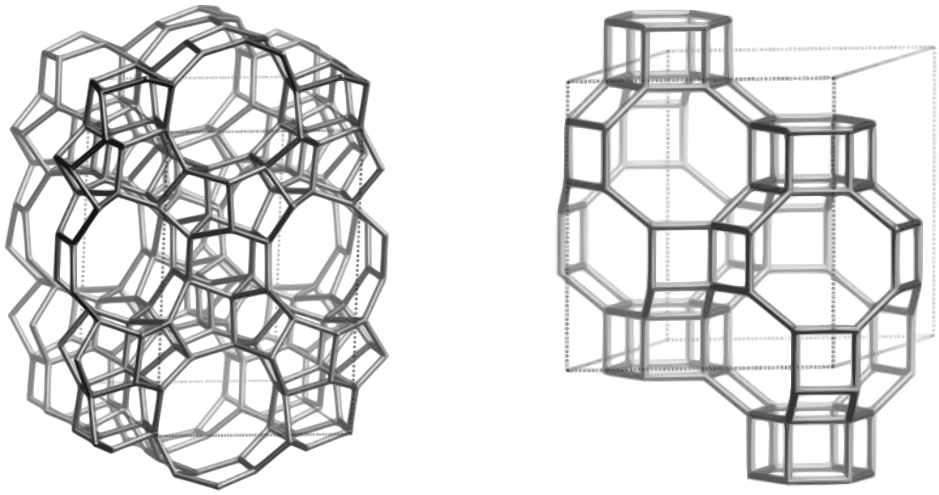

(a) MFI framework viewed along [010]

(b) MFI framework viewed to normal [001]

Figure 1.2: Frameworks of the catalyst worked in this thesis.
Frameworks of the catalyst worked in this thesis. *Adapted from* [28].

(40–800 m^2/g), some hydrophobic-hydrophilic surface effects and their structure itself [30].

One of the main steps in the NH_3-SCR of NO_X is the adsorption of ammonia on the catalyst surface. Since several gaseous compounds are present in the diesel engines exhausts, they could avoid the successful adsorption of ammonia due to adsorption competition or blockage of the active sites.

1.1.9.1 Kinetic modeling of adsorption/desorption of NH_3

Arrhenius expressions (Equations 1.11 and 1.12) [31] describe the kinetic of the adsorption/desorption process, where r_{ads} and r_{des} are the rate of adsorption and desorption, respectively; A_{ads} and A_{des} are the pre-exponential factor of the adsorption and desorption, respectively; E_{ads} and E_{des} are the activation energy of adsorption and desorption, respectively; c_{NH_3} is the concentration of NH_3 in the gas phase; R is the universal gas constant; and T is the temperature. For the complete model, it is assumed that the adsorbate does not adsorb onto the walls of the reactor and that not re-adsorb (nonactivated adsorption, i.e., $Eads = 0$) onto the sample. The activation energy of the desorption depends on the coverage—Temkin type desorption—according to Equation 1.13, in which α is the coverage dependence of the activation energy, θ_{NH_3} is the surface coverage of NH_3, and E_0 is the activation energy at zero coverage.

$$r_{\text{ads}} = A_{\text{ads}} \exp\left[\frac{-E_{\text{ads}}}{RT}\right] c_{NH_3} \left(1 - \theta_{NH_3}\right) \tag{1.11}$$

$$r_{des} = A_{des} \exp\left[\frac{-E_{des}}{RT}\right] \theta_{NH_3} \tag{1.12}$$

$$E_{des} = E(0)\,(1 - \alpha \cdot \theta_{NH_3}) \tag{1.13}$$

1.1.10 Kinetic diameter

The kinetic diameter gives an idea of the molecule as a target. It is applied to atoms and molecules to measure the probability that a gas molecule will collide with another molecule [32]. Table 1.1 shows the kinetic diameters found in the literature of NH_3 C_3H_6, and n-$C_{12}H_{26}$, the more critical compounds in this thesis. Those values can be compared with the pore size of the zeolites to indicate how likely the molecule could enter the pores of the zeolites.

Table 1.1: Kinetic diameter taken from [33–35] of the more representative compounds in this thesis.

Molecule	Kinetic diameter / Å
NH_3	2.6
C_3H_6	4.5
n-$C_{12}H_{26}$	4.9
CO	3.8
CO_2	3.3

1.2 State of the art in the effect of HCs on the NH_3-SCR of NO_X

Since the first report about the abatement of NO_X using zeolite materials [19], several studies have been reported changing the type of catalyst [36–38], the reaction conditions [39], and pollutants such as SO_2 [40–42]. In addition to SO_2, the effect of hydrocarbons is one of the topics studied. This section lists the main works related to the study of the effect of hydrocarbons on the NH_3-SCR of NO_X and describes their main findings.

Montreuil et al. [43] investigated at the Ford Company, the effect of hydrocarbons (1100 ppm ethylene, 700 ppm propylene, 130 ppm benzene, and 110 ppm decane) on two different catalyst formulations (first and second generation catalysts). They used a base gas concentration of 15% oxygen, 350 ppm NO, 350 ppm NH_3, 5% CO_2, and 4.6% water. They found that hydrocarbons affected the NO_X conversion in the first generation catalyst but little or nothing in the second generation catalyst at 200 °C. It was the first report about the effect of hydrocarbons in the NH_3-SCR of NO_X. However, the authors do not reveal information on the catalysts.

In another work, Sultana et al. [44] added decane to a simulated gas from a diesel engine to study its effect on the NH_3-SCR of NO_X with Cu/HZSM-5 and Cu/NaZSM-5 catalysts. They study the NH_3-SCR of NO with 200 ppm NO, 200 ppm NH_3, 10% O_2, 6% H_2O, 1 ppm SO_2, and 10 ppm $C_{10}H_{22}$ at a temperature range 160–400 °C. They reported that Cu/NaZSM-5 behaved better than Cu/HZSM-5 with and without $C_{10}H_{22}$ due to a promoting effect of the Na^+ cations in the formation of Cu^+, nitrite, and nitrate intermediates species and retardation of coke formation. They confirmed their results by FT-IR of adsorbed NO but did not study the adsorption of NH_3.

Later, He et al. [45] reported that propylene deactivates Fe/Beta and Fe/ZSM-5 catalysts (synthesized by incipient wetness impregnation), however cutting off the propylene restores the conversion. They used a reactant composition of 1000 ppm NH_3, 1000 ppm NO, 2% O_2, and He for balance and with 1000 ppm C_3H_6 when used. They found by FT-IR analysis that deposits of carbon species on Fe/Beta formed N_2O, and by XPS that C_3H_6 partially reduced Fe^+, confirming that both could reduce NO conversion. These results were significant at that time, but synthesizing the catalysts by incipient wetness impregnation lacks good dispersion of the active sites in the catalysts.

Li et al. [13] reported that in the NH_3-SCR of NO_X (1000 ppm NO or NO_2, 1000 ppm NH_3, 1000 ppm C_3H_6 when used, 5% O_2, and He as balance in the temperature range 150–550 °C) with Fe-ZSM-5 (prepared by ion exchange), the NO conversion decreased in the presence of propylene by 24, 55, 51, and 25% at 200, 300, 400, and 500 °C, respectively; however, the effect was insignificant when they replaced NO by NO_2 in the feed. They proposed that propylene residues may deactivate the catalyst by blocking the Fe^{3+} active site, on which NO oxidized to NO_2. The zeolite crystal structure did not change either before nor after propylene poisoning, and no graphitic phase formed over propylene-poisoned catalyst. The surface area and pore volume of the catalysts decreased due to carbonaceous deposition. The activity for NO oxidation to NO_2 was significantly inhibited in a propylene poisoned catalyst below 400 °C. The adsorption of NH_3 on the Brønsted acid sites to form NH_4^+ was not hindered even on the propylene poisoned catalyst, and the amount of absorbed NH_3 was still abundant and enough to react with NO_2 to generate N_2. They also reported hydrocarbon oxygenates such as formate, acetate, and containing nitrogenated organic compounds on the catalyst's surface. This work was significant because they proposed a mechanism for the activation in Fe-ZSM-5; however, they did not deal with Cu-based zeolites, which are more active at low temperatures.

Heo et al. [46] studied the effect of hydrocarbon slip on NO removal activity of CuZSM5, FeZSM5, and V_2O_5/TiO_2 catalyst by NH_3 at the conditions of 500 ppm NO, 500 ppm NH_3, 5% O_2, 10% H_2O, N_2 balance, and 500 or 2000 ppm of C_3H_6 when used in the temperature range 150–550 °C. Their results show that propylene decreased the

activity in the NH_3-SCR of NO of CuZSM5 and FeZSM5 due to the competitive adsorption of NH_3 and C_3H_6 and due to the consumption of NH_3 by side reactions as NH_3 oxidation and ammoxidation. In the high-temperature region, the HC-SCR reaction by C_3H_6contributes to restoring the CuZSM5 activity, while the recovery was not possible in FeZSM5.

Malpartida et al. [47] used a gas composition of 14% O_2, 4% CO_2, 1% H_2O, 300 ppm CO, 150 ppm NO, 150 ppm NH_3, and 85 ppm of HC's (43 ppm $C_{10}H_{22}$, 25 ppm toluene, and 17 ppm C_3H_6) diluted in Ar to study the unburnt HC effect on the activity of commercial automotive catalyst for the NH_3-SCR. They studied the reaction in the temperature range 438–673 k and found that propylene, decane, and toluene blocks the pores of a commercial zeolite by forming carbonaceous material on the surface of the catalyst. That reduces its activity in the NH_3-SCR of NO_X and oxidation properties but depends on the kind of hydrocarbon. This report proved that HCs could adsorb on the catalyst but not reveal the kind of catalyst they tested.

Luo et al. [48] studied the effect of C_3H_6 and $C_{12}H_{26}$ on the NH_3-SCR performance of Cu/Beta and Cu/SPZ catalysts. The feed gas composition was 600 ppm NH_3, 600 ppm NO_X, 8% O_2, 5% H_2O in the temperature range 150–500 °C. Cu/SPZ had less hydrocarbon inhibition and less N_2O formation than Cu/Beta. $C_{12}H_{26}$ did not affect the Cu/SPZ at temperatures lower than 300 °C and had little effect at 400 °C; propylene slightly inhibited the activity (less than 5% conversion reduction). They did not detect coke formation in the Cu/SPZ catalyst, C_3H_6 affected Cu/beta due to the partial oxidation intermediates on the catalyst surface, and dodecane inhibited the NO conversion over the whole temperature range. At 150 °C, NO_X conversion decreased due to the strong adsorption of $C_{12}H_{26}$ blocking sites either directly or indirectly by blocking pores. At 300 °C, due to both partial oxidation intermediates and strong hydrocarbon adsorption. The authors highlight that the differences of resistance to hydrocarbon poisonings, such as hydrocarbon adsorption and coke formation, are related to the pore structure of the zeolite. They concluded that the small pores in the Cu/SPZ catalyst do not allow the diffusion of large hydrocarbon molecules into the pores, hindering adsorption onto active sites, as well as the formation of coke-related molecules in the pores, and thus the active sites are preserved. This work was significant because it gave insights about the possible mechanism of HC poisoning on Cu based zeolite.

In related work, Luo et al. [49] studied the hydrocarbon poisoning of Cu-Zeolite SCR catalysts. They used a gas feed composition of 600 ppm NH_3, 600 ppm NO_X, 200 ppm C_3H_6, 8% O_2, 5% CO_2, and 2.5% H_2O from 150–500 °C. They concluded that C_3H_6 affects the Cu/Beta performance in the standard and fast SCR reactions by formation of intermediate surface species—acrolein-like and coke species—formed during C_3H_6 oxidation, and by reduction of NO_2 to NO, respectively. However, it had a positive effect on the slow SCR reaction. This work focused more on the mechanism, but Cu/Beta

zeolite is not the most suitable catalyst for the SCR reaction.

Ma et al. [50] tested a series of Fe-zeolite catalysts (Fe-MOR, Fe-ZSM-5, and Fe-BEA) prepared by ion exchange. They studied the reactions at the conditions of 500 ppm C_3H_6 (when used), 500 ppm NO, 500 ppm NH_3, and 5% O_2in the temperature range 150–500 °C. Fe-zeolites were active without propylene from 150—300 °C; however, C_3H_6 suppressed the catalytic activity. Fe-MOR was the most resistant because it has a one-dimensional structure that facilitates diffusion, lower acidity, and is not susceptible to deactivation compared to Fe-ZSM-5 and Fe-BEA. They observed nitrogenated-organic compounds (e.g., isocyanate) on the Fe-zeolite catalyst surface. The site blockage was mainly on Fe^{3+} sites, on which NO was activated and oxidized. In a Fe-BEA monolith catalyst coating modified with MOR, the deactivation due to propylene poisoning was less, and the NO_X conversion was higher than the catalyst in powder form.

Ye et al. [20] studied the effect of propylene on copper, iron, and mixed copper/iron exchanged zeolites containing ZSM-5 and chabazite-like zeolites (SSZ-13, SAPO-18, and SAPO-34) for the NH_3-SCR of NO. They used the standard reactant composition as follows: 400 ppm NO, 400 ppm NH_3, 700 ppm C_3H_6 (when used), 14% O_2, 2% H_2O, and a balance of He. The temperature studied was in the range of 150–550 °C. All the catalysts exhibited high NO conversions without propylene. Cu/SSZ-13, Cu/SAPO-18, and Cu-SAPO-34 were the most stable in the presence of propylene; coke formed on Cu/ZSM-5. C_3H_6 reduced the surface area, the Cu^+/Cu^{2+} ratio, and the copper contained in Cu/ZSM-5, but they slightly change in SSZ-13, SAPO-18, and SAPO-34. Cu/ZSM-5 showed a more significant decline in NO conversion with time and higher propylene adsorption than Cu/SSZ-13, Cu/SAPO-18, and Cu/SAPO-34. They concluded that the resistance to hydrocarbon poisoning depended on the pore geometry of the zeolites. For example, for medium-pore size zeolites like Cu/ZSM-5, hydrocarbon blocked the active sites and decreased the active intermediates needed for NO conversion. On the other hand, small-pore zeolites like Cu/SSZ-13, Cu/SAPO-18, and Cu/SAPO-34 showed a more considerable hydrocarbon poison resistance since they have small cage diameter and do not possess one-dimensional channel structures. This work was meaningful because it regarded the pore size of the catalyst, but the analysis was vague, and more characterization was needed.

Kumar et al. [51] investigated the hydrocarbon storage on small-pore Cu-zeolite SCR catalysts supported in a 300 cpsi cordierite substrate. They used a base feed of 10% O_2, 8% H_2O in N_2 with a HC storage concenctraion ofn-$C_{12}H_{26}$(∼1000 ppm C_1) or C_3H_6 (∼1000–5000 ppm C_1) at temperatures from 100–450 °C.They found that even small-pore zeolite catalysts can store substantial quantities of n-dodecane on the external surface, although the reactive transformation drives this process instead of adsorption.

Ma et al. [52] used, at steady state, a gas N_2 mixture containing 350 ppm NO, 350 ppm NH_3, 14% O_2, 500 ppm C_3H_6 (when used), and 2% H_2O in the temperature

range 150–550 °C to propose a mechanism of propene poisoning on Cu-SSZ-13 catalysts for SCR of NO_X by NH_3. The found that C_3H_6 inhibits the NO_X adsorption and activation on the catalyst surface of commercial Cu-SSZ-13, especially at temperatures around 350 °C. Below 250 °C, NO_X and C_3H_6 competes for adsorption; around 350 °C, coke depositions deactivates the Cu-SSZ-13. They report that submitting the poisoned catalysts to oxygen at temperatures above 450 °C could remove the coke and regenerate the catalysts.

Zheng et al. [53] investigate the effect of C_3H_6 on NH_3-SCR, NH_3 adsorption and oxidation, and N_2O production on a commercial Cu-SSZ-13 monolithic catalyst. The gas composition for the baseline NH_3-SCR reactions comprised 500 ppm NH_3 and 500 ppm NO for standard SCR (NO/NO_X = 1), 250 ppm NO and NO_2 for fast SCR (NO/NO_X = 0.5), and 500 ppm NO_2 for slow SCR (NO/NO_X = 0), in 0% and 5% O_2in a carrier gs of 2.5% H_2O, 2% CO_2 and balance Ar. When C_3H_6 was used, the concentration was 500 ppm. They found that C_3H_6 promotes NO_2 reduction to NO by the formation of organic intermediates and that it competes with NH_3 for adsorbed NO_2, which generates NO and thus increases the NO/NO_X ratio. They showed that organic intermediates play an essential role in blocking active sites as they confirmed by in situ DRIFTS (diffuse reflectance infrared Fourier transform spectroscopy).

Selleri et al [54] modeled the inhibition effects of short-chain hydrocarbons (C_2H_2, C_3H_6, and C_3H_8) on a small-pore Cu-zeolite NH_3-SCR catalyst. They carried out the steady-state experiments in the temperature range 150–550 °C with molar feed fractions of 180 ppm NO_X, 234 ppm NH_3, 0 or 180 ppm HC, 10% H_2O, and 10% O_2. They stated that they can rule out that the negative effect of HCs on DeNOx performance is due to HC competing with NH_3 for adsorption on the same catalyst site. They pointed out that is likely instead that HCs are partially oxidizez by O_2 (and NO_{arg}), leading to intermediate adspecies which block the active sites.

In another report, Selleri et al. [55] studied the impact of light and heavy hydrocarbons on the NH_3-SCR activity of commercial Cu- and Fe-zeolite catalysts. The steady-state NO_X conversion experiments were carried out in the temperature range 150–550 °C; molar feeds were: NO_X = 500 ppm, NH_3 = 550 ppm, HCs = 1500 ppm (on C_1 basis), H_2O = 10%, O_2 = 10%, and balance N_2. They found that both C_3H_6 and $C_{10}H_{22}$ affected a commercial Fe-zeolite, but not a commercial Cu-zeolite in the SCR reaction.

All the previous works focused on the effect of HCs on the catalytic activity of the catalysts tested. However, some of them lack thoroughly, and the conditions such as GHSV need to be studied. Parallel reactions, such as NO and NH_3 oxidation in the presence of HC, have not been studied intensely. Those works did not study the effect hydrocarbons on the kinetics of the adsorption or the SCR reaction.

1.2.1 Justification for materials and conditions

Considering the literature review about in the effect of HCs on the NH_3-SCR of NO_X, we selected the following materials for this work:

Cu-ZSM-5 because is the most studied catalyst in the NH_3-SCR of NO_X and we want to have a reference for compare our results; Cu-SSZ-13, because is the most promising catalysts for the NH_3-SCR of NO_X, and we want to evaluate more deeply its behavior under conditions with HCs; and Cu-SAPO-34 because is a catalyst with the same structure of the Cu-SSZ-13 with similar properties but still needs to be studied for how it behaves under several conditions. For the case of the HCs we chose propylene because it is the most used surrogate for diesel in the studies related to the effect of HC on the NH_3-SCR of NO_X; and n-dodecane because we wanted to use a more suitable surrogate for diesel and because it little reported in the literature. The conditions were chosen according to the standard concentrations used to study the effect of NH_3-SCR of NO_X over Cu-zeolite catalysts, that mean: 400 ppm NO, 500 ppm NH_3, 8% O_2, and 5% H_2O. In the temperature range 150–550 °C, which is usually used to determine the catalytic activity of Cu-zeolite catalysts.

1.2.2 Significance of the research

According to the literature, diesel vehicles are going to increase their worldwide use, because they are more thermodynamically efficient than spark-ignition engines, have better fuel economy and greater power density compared to conventional gasoline engines [56]. However, they produce higher NO_X and particulate matter emissions in comparison with spark-ignition engines. NO_X can cause a lot of environmental issues like acid rain, tropospheric ozone, and photochemical smog; in addition, they cause problems in people in breathing and visibility [57].

This research aimed to study the effect of hydrocarbons on the activity of Cu-based zeolite catalysts. The results of this project would help to understand how hydrocarbons affect the catalyst used for the NH_3-SCR at diesel engine conditions. In this project, we found by FTIR characterization how hydrocarbons can affect the acid sites in the studied catalysts. We used a kinetic model and fitted NH_3-TPD data using MATLAB® to understand a little how hydrocarbons can affect the kinetic of the adsorption/desorption of NH_3 in Cu-ZSM-5 related catalysts and Cu-SAPO-34. Another significant result was the study of the effect of HCs on the kinetics of Cu-ZSM-5 and Cu-SSZ-13—the most used catalysts in the NH_3-SCR. The results from this project would also help to analyze better the design of complete after-treatment gas system in diesel engines because we demonstrated that hydrocarbons can change the kinetics of the NH_3-SCR of NO reaction.

1.3 Objectives

Taking into account state of the art in the effect of HCs in the SCR and the need to understand the effect of hydrocarbons more deeply, we propose to give more depth to these studies. We proposed the following objectives:

1.3.1 General objective

To study the effect of propylene, dodecane on the ammonia selective catalytic reduction of nitrogen oxides (NH_3-SCR of NO).

1.3.2 Specific objectives

- To synthesize and characterize Cu-ZSM-5, Cu-SSZ-13, and Cu-SAPO-34.
- To evaluate the effect of hydrocarbons on the catalytic activity and stability of a selected catalyst under typical diesel engine exhaust conditions (400 ppm NO, 8% O_2, 5% H_2O).
- To study the effect of a hydrocarbon on the kinetics of the adsorption/desorption of NH_3 over Cu-based catalysts.
- To determine the effect of hydrocarbons on the kinetic of the NH_3-SCR of NO over Cu-based catalysts.

1.4 Thesis overview

Studying the effect of hydrocarbons on the catalytic activity and kinetic of Cu-based zeolites in the NH_3-SCR of NO is the main objective of this work. We chose propylene and n-dodecane as an unsaturated and long-chain hydrocarbons surrogates for diesel fuel. We chose the most reported and promising catalysts for the NH_3-SCR of NO_X such as Cu-ZSM-5, Cu-SSZ-13, and Cu-SAPO-34. Our purpose was to see an effect on the pore size of the catalysts.

Chapter 1 is a background that describes the basic concepts regarding the topics of this thesis. It gives state of the art in the effect hydrocarbons in the NH_3-SCR of NO. We wrote the primary studies of this thesis as three independents articles with their introduction, experimental section, the results, and discussion and conclusion.

In Chapter 2, we used C_3H_6 and Cu-based ZSM-5 catalysts to study the effect of pre-adsorbing C_3H_6 on the catalysts and compare to Cu-SAPO-34, which has smaller pore size to study the differences in the adsorption of C_3H_6. Adsorbing first the C_3H_6 is the worst scenario for studying how C_3H_6 affects the adsorption of NH_3, but it is the beginning to perform more realistic experiments adsorbing C_3H_6 and NH_3 at the same

time and study how they compete for the adsorption. We synthesized the Cu-based ZSM-5 catalysts by ion exchange and impregnation to study if the method of synthesis influences the adsorption. We used Matlab to obtain the parameters for the simulation of the kinetics of the adsorption/desorption and found that pre-adsorbing propylene on the catalysts, reduces the amount of ammonia adsorbed on the surface and changes the parameters in all the catalysts.

Chapter 3 compares the $C_{12}H_{26}$ resistance of Cu-ZSM-5 and Cu-SSZ-13. We found that $C_{12}H_{26}$ affected more Cu-ZSM-5 than Cu-SSZ-13. We chose Cu-SSZ-13 because it was the most resistant to HC for making a deeper study on several reactions such as NO oxidation and NH_3 oxidation. We impregnated a monolith with Cu-ZSM-5 catalyst and studied the NH_3-SCR of NO, the result was unexpected, and we did not perform more reactions. We found that $C_{12}H_{26}$ affects in several ways the activity of the Cu-SSZ-13 in the NH_3-SCR of NO, NH_3 oxidation, and NO oxidation.

We followed the studies with C_3H_6 in Chapter 4. In this case, we investigated the effect of propylene and $C_{12}H_{26}$ on the kinetics of the NH_3-SCR reaction with Cu-ZSM-5 and Cu-SSZ-13 to see any correlation between the hydrocarbon length and type of zeolite framework. We found that both propylene and dodecane affects in different extents the orders of the reaction and the apparent activation energies for both Cu-ZSM-5 and Cu-SSZ-13.

Chapter 5 concludes the whole thesis, describes all the limitations for the work done and states the recommendations for future work.

1.5 Scientific contributions

One of the main activities was the adequacy of the facilities for the determination of the catalytic activity of the materials. It consisted of designing the tubing system, choosing the feed gas system, and calibration of mass flow controllers (Appendix A.1) and FT-IR (Appendix A.2). In that sense, during this project we also collaborated with researchers from the Universidad Nacional for the evaluation of the catalytic activity of a natural zeolite and published the article "Activity of an iron Colombian natural zeolite as a potential geo-catalyst for NH_3-SCR of NO_X". Despite it was related with the reduction of NO_X, it was not related with the effect of hydrocarbons, and for that reason, its results were not included in this thesis.

Regarding the effect of hydrocarbons on the Cu-based zeolite catalysts, we publish or presented in the following works:

1.5.1 Journal articles

- John-Freddy Gelves, Ludovic Dorkis, Marco-A. Márquez, Andrés-Camilo Álvarez, Lina-María González, Aída-Luz Villa. Catalysis Today 320 (2019) 112-122.

doi = 10.1016/j.cattod.2018.01.025

1.5.2 National conference

- Andrés Álvarez, Juan González, Lina González y Aída Villa. Efecto del dodecano sobre la reducción catalítica selectiva de NO_X con amoniaco con el catalizador Cu-SSZ-13. XI Simposio Colombiano de Catálisis. Popayán. 23/09/2019.

1.5.3 International conference

- Andrés Camilo Álvarez Montoya. Efecto del dodecano sobre la oxidación de NO y NH_3 en Cu-SSZ-13. II Simposio Internacional de Catálisis Ambiental y Energías Renovables. Medellín. 28/10/2019.

1.5.4 Manuscripts to submit

- Effect of propylene on the NH_3-TPD over Cu-based ZSM-5 catalysts to be submitted to *Catalysis Letters* journal.
- Effect of hydrocarbons on the kinetic of NH_3-SCR over Cu-based zeolites to be submitted to *Applied Catalysis B: Environmental* journal.

Chapter 2

Effect of C_3H_6 on the adsorption/desorption of NH_3

NH_3-SCR—the leading technique for abating NO_X from diesel engines—still presents problems such us catalytic poisoning due to the presence of hydrocarbons in the gas exhaust. To understand how hydrocarbons poison SCR catalysts, this study aimed to evaluate Cu-containing catalysts (Cu-ZSM-5 and Cu-SAPO-34) in the NH_3-SCR, and the kinetics of the adsorption/desorption of NH_3 in the presence of C_3H_6 (a surrogate hydrocarbon that might be present in diesel exhausts). Cu-based ZSM-5 catalysts, synthesized by ion exchange and incipient wetness impregnation and characterized by XRD, UV-Vis, OH-DRIFTS, NH_3-TPD, and NH_3-DRIFTS were tested for the effect of C_3H_6 in the NH_3-SCR of NO, in the NH_3-TPD, and in the adsorption/desorption kinetics of NH_3 in an elementary mean field model considering two sites (Z–OH and S). Adsorbing C_3H_6 on the catalysts decreased the amount of NH_3 desorbed from all the studied catalysts in the NH_3-TPD. NH_3-DRIFTS showed that C_3H_6 affected to a significant extent the acid sites not related to copper (i.e., Brønsted acid sites). Concerning the kinetic modeling of the adsorption/desorption of NH_3, C_3H_6 changed the coverage dependence of the activation energy of the H-ZSM-5 in both acid sites maintaining the remaining constant. Still, it affected all the parameters in the Cu-containing samples suggesting that C_3H_6 modify the adsorption/desorption kinetics of NH_3 in the studied catalysts.

2.1 Introduction

Pursuing fewer pollutant emissions into the environment and improving costs in transportation have promoted alternatives in the vehicle market. Using diesel engines is increasing worldwide [5, 58] as they have have better thermodynamic efficiency, higher fuel economy, greater power density, and less of the greenhouse gas CO_2 emissions compared to the gasoline ones [59]. However, they release more nitrogen oxides (NO_X) into the atmosphere. NO_X contribute to global warming, acid rain, photochemical smog, tropospheric ozone, and breath and heart diseases in people. Techniques such as NO_X storage and reduction (NSR), selective NO_X recirculation (SNR), Selective non-catalytic reduction of NO_X (SNCR) are used to reduce NO_X [60]; though, selective catalytic reduction (SCR) of NO_X by ammonia (NH_3) is the most promising to abate NO_X from diesel engines. In the NH_3-SCR of NO, the gases from a diesel engine exhaust react with NH_3 in a catalyts to produce nitrogen and water according to Reaction 1.4.
A complete after treatment gas process in a vehicle, in addition to the NH_3-SCR system, can have two additional units: a diesel oxidation catalyst (DOC) unit to oxidize CO, NO, and hydrocarbons; and a diesel particulate filter (DPF) unit to retain particulate matter [46].

Vanadia/tungsten/titania ($V_2O_5/WO_3/TiO_2$) SCR catalysts have been the most used materials in stationary sources. However, they can have problems with the stability and toxicity of the vanadium, limiting their use in diesel vehicles. Recently, copper and iron-containing zeolites for the application in the vehicle industry are the focus of research groups [37, 61–67]; copper catalysts has better activity at lower temperature and less sensitive to NO/NO_2 changes than iron catalysts [21, 36, 61, 62, 68, 69]. Cu-zeolite catalysts can reduce NO_X emissions up to 1000% in the temperature range of 200–400 °C, but they can lack stability or can be poisoned by compounds in diesel exhaust such as unburned hydrocarbons CO, and SO_2. Hydrocarbons can poison the catalyst in the cold start period of a diesel engine, at which the catalyst has not reached its operating temperature [48], or when the diesel oxidation catalyst is aged, at which it is not able to oxidize hydrocarbons before entering the SCR unit [48].

Studies about the effect of hydrocarbons on Cu-based catalysts in the NH_3-SCR of NO focus on the catalytic activity[20, 46–48, 53], mechanism [52, 53], and adsorption [51, 70]. Heo et al. point out that C_3H_6 decreases the catalytic activity of Cu-ZSM5, and Fe-ZSM-5 [46]; Malpartida et al. conclude that the presence of HCs drops the conversion of a commercial catalyst for the NH_3-SCR [47], Luo et al. report that C_3H_6 negatively affect both Cu/beta and state of the art Cu-zeolite [48]; Ye et al. describe that propene degraded Cu/ZSM-5 catalytic activity, however, Cu/SSZ-13, Cu-SAPO-18, and Cu-SAPO-34 had better hydrocarbon coking resistance [20]; Zheng et al. state that C_3H_6

affects to some extent the NH_3-SCR activity of a commercial monolith made of Cu-SSZ-13 [53]; Ma et al. conclude that C_3H_6 could deactivate Cu-SSZ-13 in the NH_3-SCR of NO_X [52]. Regarding the adsorption of NH_3, Kim et al. report a strong temperature dependence of C_3H_6 on Cu-SSZ-13 [70], and Kumar et al. report that a state of the art small-pore Cu-zeolite can store C_3H_6 [51]. Regarding coke deposition, Ye et al. report that Cu/SSZ-13, Cu-SAPO-18, and Cu-SAPO-34 had better hydrocarbon coking resistance than Cu/ZSM-5 [20]. Although those studies have dealt with the effect of C_3H_6 on the mechanism, catalytic activity, and coke deposition on Cu-based catalysts, studies related to the kinetics of the adsorption/desorption of NH_3 over NH_3-SCR catalysts are still missing. The adsorption of NH_3 is a crucial step in the mechanism of the NH_3-SCR, is essential for simulating transient experiments and for describing detailed kinetic models [71].

This chapter aimed to study the effect of propylene-saturated ZSM-5-related and Cu-SAPO-34 catalysts on both the NH_3-TPD profile and NH_3 adsorption/desorption kinetics described by an elementary mean-field model.

2.2 Experimental

2.2.1 Catalyst synthesis

2.2.1.1 Cu-based ZSM-5

Cu-ZSM-5 (synthesized by ion exchange [38, 72]) and Cu/ZSM-5 (synthesized by incipient wetness impregnation) were prepared starting from a commercial NH_4-ZSM-5 purchased from Zeolyst International. It was calcined at 560 °C for 5 h, at a heating rate of 5 °C/min, to obtain the H-ZSM-5 form, which was either ion-exchanged or impregnated.

For ion exchange, the method according to [38, 72] was applied. For this, the sample was refluxed with a 160 ppm of $Cu(CH_3COO)_2$ in a ratio of 125 mL of solution per gram of catalyst at 65 °C for 24 h, filtered with distilled water, dried at 100 °C for 24 h, and calcined in 500 mL/min of synthetic air at 560 °C for 5 h at a heating rate of 5 K min^{-1}. From now, the ion-exchange ZSM-5 is name as 1.2Cu-ZSM-5.

For incipient wetness impregnation, H-ZSM-5 was impregnated with an aqueous $Cu(NO_3)_23{\cdot}H_2O$ solution with a nominal loading of 1.2% and 2% of copper. It was dried at 100 °C for 12 h and calcined in synthetic air at 560 °C, heating rate 5 K min^{-1}, for 5 h. From now, the impregnated samples are named as 1.2Cu/ZSM-5, and 2.0Cu/ZSM-5, respectively.

2.2.1.2 Cu-SAPO-34

H-SAPO-34 was synthesized according to the hydrothermal method, followed by Najafi et al. [73]. The sources of aluminum, phosphorous, and silicon were aluminum isopropoxide, orthophosphoric acid (H_3PO_4), and tetraethyl orthosilicate (TEOS), respectively. Morpholine was the structure-directing agent and water the solvent. The molar ratio of Al_2O_3:P_2O_5:SiO_2:SDA:H_2O was 1:1:0.6:4:70. Aluminum isopropoxide and morpholine were added to the water and stirred for 15 min. The TEOS was added to the solution under stirring for another 15 min. Finally, the H_3PO_4 was added dropwise and stirred for 1 h. The solution was transferred to TEFLON liners in stainless steel autoclaves for crystallization at 200 °C for 14 h. The final gel was centrifuged, dried at 120 °C overnight, and calcined at 560 °C for 12 h. Copper incorporation was made by the ion exchange method, according to the procedure by Leistner et al. [74]. SAPO-34 was submitted to ion exchange with a solution of NH_4NO_3 5.4 M in a ratio of 7 mL of solution per gram of catalyst at 80 °C for 1 h while maintaining the pH between 3.0–3.5. The solid was dried at 100 °C overnight, and the process was repeated once. Finally, the solid was calcined at 560 °C for 12 h, and the H-SAPO-34 form was obtained. H-SAPO-34 was ion-exchanged with $CuNO_3 \cdot 2.5H_2O$ 0.4 M in a ratio of 4 mL of solution per g of catalyst at 70 °C for 1 h. The final solution was centrifuged and washed several times with deionized water until the filtrate reached the pH of the water. The solid was dried at 100 °C overnight and calcined at 560 °C, heating rate of 5 K min^{-1}, for 12 h.

We named the bare SAPO-34 samples as H-SAPO-34 and the Cu-based SAPO-34 samples as 2.6Cu-SAPO-34.

2.2.2 Catalysts characterization

XRD patterns were measured on a Bruker AXS D8-ADVANCE diffractometer with a Co Kα ($\lambda = 1.788$ nm) radiation. The measuring range was 1–60° with a step of 0.01° at 0.6°/min. Copper content was obtained by XRF spectroscopy. BET surface area was determined in a Micromeritics ASAP 2020. The sample was pretreated at 350 °C for 2 h, and the isotherm was recorded at −196 °C. Diffuse reflectance UV-Vis spectra were obtained in a Lamba 850 Perkin Elmer spectrometer equipped with a Praying Mantis reflectance optics (Harrick Scientific). Measurements were performed under ambient conditions between 200–800 nm with a resolution of 0.9 nm. SEM-EDS were performed in a FEI Quanta FEG 250 scanning electron microscope. In situ FTIR experiments were performed in a Tensor 27 FTIR spectrometer (Bruker®) equipped with a liquid-nitrogen-cooled MCT detector and a Praying Mantis reflectance optics (Harrick Scientific) heatable stainless steel infrared cell with ZnSe windows connected to a gas-handling system. The sample was loaded into the cup of the cell and pretreated at 450 °C in 500 mL/min N_2 for 30 min. For OH-DRIFTS, spectra of a diluted sample in KBr in a mass ratio of 1:2

were taken at 50 °C, and the spectra of pure KBr were used as background. The spectra were normalized to the maximum intensity of the lattice vibration characteristic of the bare catalysts: for H-SZM-5 in the range 1200–400 cm^{-1} [75], and for SAPO-34 in the range 2000–650 cm^{-1} [76].

2.2.3 NH_3 adsorption/desorption experiments

2.2.3.1 Description of the bench for NH_3-TPD

Figure 2.1 shows the facilities for the study of the NH_3-TPD of the catalysts. The laboratory building supplied the N_2 and O_2 gases, while NH_3 and C_3H_6 were storage in gas bottles of 1000 ppm and 5% in N_2, respectively. The gases flowed by stainless steel tubes and were controlled by Bronkhorst mass flow controllers (MFC). All the MFCs were calibrated considering the heat capacity of the gas supplied. The reactor was a quartz tube i.d.: 9 mm, length: 0.8 m, and o.d.: 10 mm placed in a horizontal electric furnace, in which OMEGA temperature controllers controlled the temperatures and heating rates. Temperatures were measured in front of and behind the bed by NiCrNi thermocouple at about 1 cm from the bed. NH_3 content was measured via non-dispersive infrared (NDIR) spectrometer X-STREAM Rosemount Analytical and C_3H_6 via Fourier Transformed Infrared (FTIR) spectrometer Multigas Analyzer 2000 from MKS Instruments. The temperatures, flows, and concentrations were visualized and recorded on a computer by a LabVIEW® software.

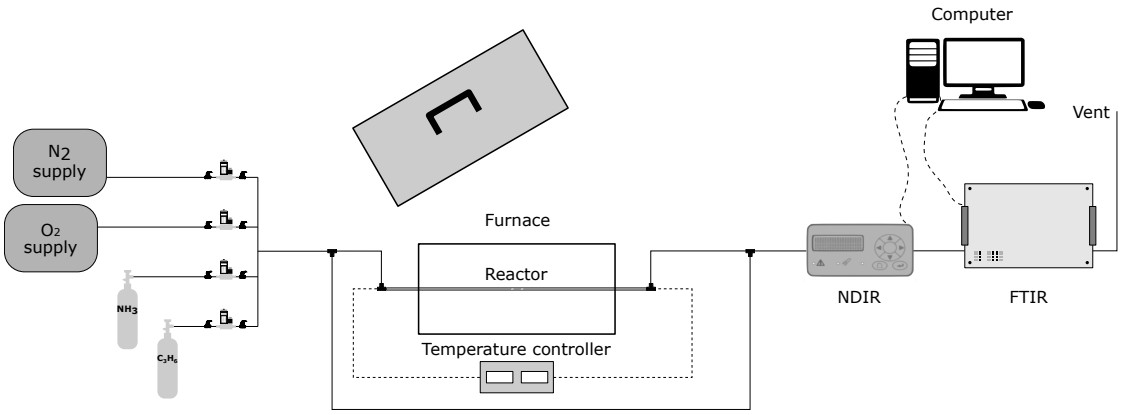

Figure 2.1: Diagram of the NH_3-TPD bench reactor used for the NH_3 adsorption/desorption experiments in this chapter.

2.2.3.2 NH_3-TPD experiments

The catalysts were first granulated by pressing the powder to about 10 kN for 5 min, then crushed and sieved to a particle size of 125–250 μm to avoid discharges; granulating the sample to bigger sizes does not change the BET surface area [77, 78]. For the NH_3-TPD experiments, we packed 200 mg of catalyst between two pieces of quartz wool

to fix it into a quartz reactor (i.d. 8 mm). Bronkhorst mass flow controllers were used to control the flows. The sample was pretreated in 500 mL/min (STP) of synthetic air (20% O_2, 80% N_2) at 450 °C for 30 min. It was cooled down to the adsorption temperature (50, 100, 150, or 200 °C) in 500 mL/min (STP) of N_2.

When propylene was used, the sample was pre-saturated with 5000 ppm C_3H_6/N_2 in a flow of 500 mL/min (STP) until complete saturation and then flushed in 500 mL/min (STP) of N_2 flow. NH_3 adsorption phase was performed with 1000 ppm NH_3/N_2 until complete saturation at a flow of 500 mL/min (STP) and flushed with 500 mL/min N_2 to remove physisorbed NH_3 and weakly adsorbed NH_3. The desorption was carried out at a heating rate of 10 K min^{-1} from adsorption temperature to 700 °C. NH_3 content was measured via non-dispersive infrared (NDIR) spectrometer X-STREAM Rosemount Analytical and C_3H_6 via Fourier Transform Infrared (FTIR) spectrometer MKS 2000.

The amount of NH_3 desorbed from the catalyst was calculated with Equation 2.1, in which n_{Des} is the mol of NH_3 desorbed from the surface, $\dot{V}_{N_2}$ is the flow of nitrogen, V_m is the molar volume at standard conditions, β is the heating rate, T_0 is the temperature of adsorption, T_{End} is the final temperature, c_i^{exit} is the NH_3 content in the gas, T is the temperature.

$$n_{\mathrm{Des}} = \frac{\dot{V}_{N_2}}{V_m} \cdot 10^{-6} \cdot \frac{1}{\beta} \cdot \int_{T_0}^{T_{\mathrm{end}}} c_i^{\mathrm{exit}} \cdot dT \tag{2.1}$$

2.2.3.3 NH_3-FTIR experiments

For NH_3-FTIR experiments we used the same FTIR equipment described in the catalyst characterization for the OH-DRIFTS. The sample was pre-treated with 500 mL/min (STP) of N_2 at 450 °C for 30 min and cooled down to 200, 150, 100, and 50 °C for taking background spectra. When C_3H_6 was used, it was saturated with 5000 ppm C_3H_6/N_2 at 50 °C for 30 min and flushed with N_2 for 40 min. The sample was saturated with 200 mL/min (STO) of 1000 ppm NH_3/N_2 for 30 min and flushed with N_2 for 40 min. DRIFTS Spectra were taken from 50 °C to 200 °C, collected in the range of 4000–650 cm^{-1} by accumulating 600 scans at 4 cm^{-1} resolution and subtracting the background spectra taken in the previous step.

2.2.3.4 Py-DRIFTS

Approximately 80 mg of sample were calcined at 550 °C for 5 h at a heating rate of 5 K min^{-1}. The sample was divided into two parts: one directly for Py-DRIFTS and the other one for C_3H_6 saturation in 100 mL/min (STP) of 1% C_3H_6 in helium at 30 °C for 30 min and flushed with 100 mL/min (STP) of Ar for 1 h. The Py-DRIFTS was performed in a Perkin Elmer FTIR equipped with an MCT detector and a DIFFUSIR$_{\mathrm{TM}}$

in-situ DRIFT cell from PIKI Technologies. The sample was heated up to 400 °C at a heating rate of 10 K min^{-1} in helium and let it to cool to 30 °C to take blank spectra. The pyridine was adsorbed at 30 °C for 30 min and flush with helium for 30 min. The desorption was carried out up to 400 °C at a heating rate of 10 K min^{-1}, taking spectra each 50 °C, which was subtracted to the blank spectra. For the C_3H_6-saturated sample, the blank spectra from the fresh catalyst were used, and the adsorption and desorption phases were the same as for the fresh sample. The software Spectrum 10 STD® transformed the spectra with the Kubelka-Munk function.

2.2.4 SCR experiments

SCR experiments were performed with a total flow of 1 L/min (STP) with 500 ppm NO_X, 500 ppm NH_3, 5% O2, 10% H_2O with 200 and 500 ppm C_3H_6 when used and balance nitrogen. A sample of 200 mg of granulated (125–250 μm) catalyst was heated at 500 °C, and then the temperature was decreased to 150 °C in steps of 50 K. The traces of the components were measured by an MKS 2000 FTIR spectrometer. Conversions of NO and NH_3 were calculated by Equation 2.2, where X_i is the conversion of component i, y_{initial} is the gas phase trace y_T is the gas phase trace at the measured temperature.

$$X_i = \frac{y_{\text{initial}} - y_T}{y_{\text{initial}}} \cdot 100\% \tag{2.2}$$

2.2.5 Modeling and simulation

We used an elementary mean-field approach, which considers all respective sites equivalent, to model the NH_3 adsorption/desorption kinetics [78]. It assumes that NH_3 adsorbs onto two sites—(Brønsted (Z−OH) and Lewis (S) acid sites) according to Reactions 2.3 and 2.4. Arrhenius type expressions can describe the reaction rates of the adsorption/desorption steps (Equations 2.5–2.8), where A_i is the pre-exponential factor, E_i is the activation energy, α_i is the coverage dependence of the activation energy, which considers that the activation energy changes depending on the amount of NH_3 on the surface due to repulsive interactions of the adsorbates [78–80], θ_i is the surface coverage of site i, R is the universal gas constant, T is the temperature, and c_{NH_3} is the concentration of NH_3.

$$NH_3(g) + Z{-}OH \underset{r_2}{\overset{r_1}{\rightleftharpoons}} NH_4{}^+ + Z{-}O^- \tag{2.3}$$

$$NH_3(g) + S \underset{r_4}{\overset{r_3}{\rightleftharpoons}} H_3N{-}S \tag{2.4}$$

$$r_1 = A_1 \exp\left(-\frac{E_1}{RT}\right) c_{NH_3}(1 - \theta_{Z-OH}) \tag{2.5}$$

$$r_2 = A_2 \exp\left(-\frac{E_2(0) - \alpha_{NH_4^+} \cdot \theta_{NH_4^+}}{RT}\right) \theta_{NH_4^+} \tag{2.6}$$

$$r_3 = A_3 \exp\left(-\frac{E_3}{RT}\right) c_{NH_3}(1 - \theta_S) \tag{2.7}$$

$$r_4 = A_4 \exp\left(-\frac{E_4(0) - \alpha_{NH_3} \cdot \theta_{NH_4^+}}{RT}\right) \theta_{NH_3} \tag{2.8}$$

The mass balance of a continuous stirred tank reactor (Equation 2.9) is useful to obtain the concentration of NH_3 in the gas phase [78, 79, 81, 82], in which F_{N_2} is the nitrogen flow, S_{act} is the active surface area. Equation 2.10 and Equation 2.11 represent the coverage ($\theta_{NH_4^+}$ and θ_{NH_3}) change with respect to temperature, in which Γ_{Z-OH} and Γ_S are the adsorption capacities of the Brønsted and Lewis acid sites, respectively, and β is the heating rate. Summarizing, the adsorption/desorption kinetic model involves ten parameters: A_1, A_2, E_1 E_2, $\alpha_{NH_4^+}$, A_3, A_4, E_3, E_4, α_{NH_3}. However, to reduce the number of parameters, pre-exponential factors of the desorption A_1 and A_3 were taken from the literature as 0.87 m/s [78] and the chemisorption of NH_3 was considered nonactivated (i.e. $E_1 = E_3 = 0$) [31, 79, 82–88]. It simplified the model to six parameters. MATLAB® functions lsqcurvefit and ode15s were used to adjust the parameters that fit the experimental data and to solve the differential and algebraic equations system, respectively.

$$0 = F_{N_2}\left(c_{NH_3,\,in} - c_{NH_3,\,out}\right) - S_{act}\left(r_1 - r_2 + r_3 - r_4\right) \tag{2.9}$$

$$\Gamma_{Z-OH} \cdot \beta \cdot \frac{d\theta_{NH_4^+}}{dT} = r_1 - r_2 \tag{2.10}$$

$$\Gamma_S \cdot \beta \cdot \frac{d\theta_{NH_3}}{dT} = r_3 - r_4 \tag{2.11}$$

2.2.5.1 Procedure for determining the parameters of the kinetic modeling

The raw data obtained from the experiments at a temperature of adsorption of 50 °C explained in Subsection 2.2.3, were organized to calculate the heating rate with the slope of a line from the data of T vs. time. We calculated the amount of NH_3 desorbed from the TPD profile considering the peaks obtained by deconvolution with a Gaussian function (Equation 2.12), where y is the function to model (NH_3 content with respect to temperature), y_0 is the baseline, A_i is the area of the peak i of the experimental data, w_i represents the standard deviation of the peak i (geometrically is the width at half of the height of the peak), $T_{c,i}$ is the temperature in the peak at which $dy/dT = 0$ (statistically is the expected value), and T is the temperature values to be fitted in the curve. The ratio

of areas under the curve and the BET surface area were used to calculate the adsorption capacity of each peak. Then the initial coverages were assumed: for the peaks at low temperature, it was assumed near to 1.0, for the other peaks less than the previous one. For the fitting, the data of the temperature needed to be in ascending order for solving the differential equation required for the numerical method. We used the function interp1d [89] from scipy.interpolate in Python to interpolate the data to have the temperatures always increasing and evenly spaced. The fitting program, written in MATLAB®, was provided by Christoph Hahn, who obtained it from previous studies on his group and modified it for better organization of the script. The initial values were based on the literature to start the fitting [78]. The solver runs with a second-generation core i5 on Windows 10 for about 6 to 12 h. Then, the initial coverages were calculated with the adsorption part using the parameters obtained in the fitting of the TPD experiment and run again until obtaining similar values. Finally, with the parameters obtained, we simulated the TPD profiles at temperatures of adsorption of 100, 150, and 200 °C. We usually repeated between three to five times the iteration until having the less χ^2 and R^2 near to 1.0. For validating, we simulated the remaining NH_3-TPD profiles with the parameters obtained in the fitting.

$$y = y_0 + \sum_{0}^{i} \frac{A_i}{w_i \sqrt{\frac{\pi}{2}}} \exp\left[\frac{-2\left(T - T_{c,i}\right)^2}{w_i}\right] \tag{2.12}$$

2.3 Results and discussion

2.3.1 Catalyst characterization

2.3.1.1 XRD

XRD patterns Figure 2.2 revealed that the catalysts retained their structures after either ion exchange or impregnation with copper. Figure 2.2a and Figure 2.2b do not show any peaks related to CuO, which generally appears at diffraction angles around 35.5° and 38.7° [72, 90]. The absence of CuO is also related to a low concentration of copper solution in the synthesis and to a low copper loading in the catalyst [22, 91]. Nanba et al. [91] synthesized a series of Cu-ZSM-5 catalysts and just detect CuO in the XRD in catalysts with copper loading greater than 3.3%. Nakhostin et al. suggest that the no detection of copper species in the XRD (Cu, Cu_2O, and CuO) implies that copper exists either as isolated ions at the exchange sites or due to high dispersion of the copper oxides it could be below the detection limit [92]. However, despite the XRD did not show peaks of CuO, it might be present in the impregnated samples at high copper loading [38].

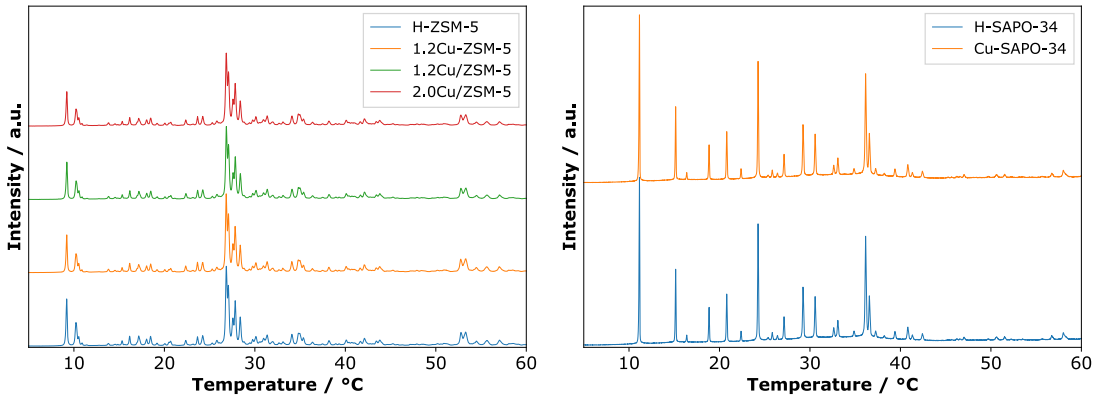

(a) ZSM-5 based catalysts. **(b)** SAPO-34 based catalysts.

Figure 2.2: XRD patterns of the catalysts.

2.3.1.2 UV-Vis

UV-VIS spectra (Figure 2.3) shows characteristic bands of zeolites with copper; the band around 200 nm referred to a charge transfer from lattice oxygen (O) to Cu^{+}/Cu^{2+} and the band around 750 nm to d-d transitions of isolated Cu^{2+} [93]. Both bands were present in the samples synthesized by ion exchange [90] and incipient wetness impregnation [94]. The relative intensity refers to the Cu species content in the sample, for the band around 750 nm, the ion exchange sample introduced more isolated Cu^{2+} species than the impregnated ones. Those results might suggest that the Cu incorporated into the ion exchange samples manly as Cu^{2+}.

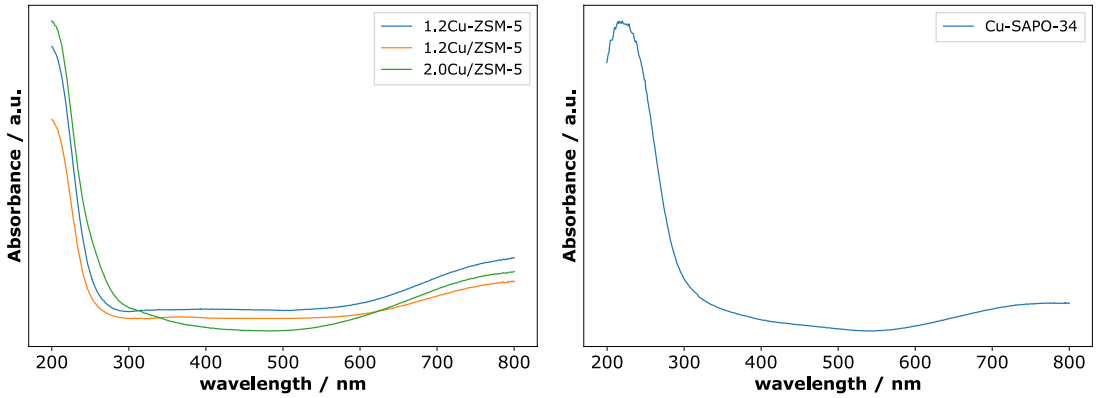

(a) ZSM-5 based. **(b)** Cu-SAPO-34.

Figure 2.3: UV-Vis spectra of the catalysts. The spectra were taken with their corresponding bare zeolite as the blank.

2.3.1.3 BET surface area

Table 2.1 shows that incorporating copper by either ion exchange or by incipient wetness impregnation slightly reduced the surface area, being the reduction more notorious in the impregnated samples with 2% copper (6% surface area reduction). Reduction in BET surface area might be because of the Cu species dispersed in the external and internal surface of ZSM-5 that interferes with N_2 adsorption during BET measurement [92, 95], or due to the partial blockage of pores by copper species [96] and/or to the destruction of micropores during copper loading due to aluminum leaching by acid attack [38].

Regarding the SAPO-34 catalysts, the BET surface area decreased by about 50% after the ion exchange with copper. Woo et al. [97] points out that it is generally accepted that the BET surface of Cu/SAPO-34 catalysts decreases during ion-exchange [98, 99] or impregnation [97] due to their irreversible hydrolysis. Gao et al. [98] found that BET area of H-SAPO-34 decreased from 549 m^2/g to 236 m^2/g in Cu-SAPO-34 and Frache et al. [99] reported a Cu-SAPO-34 with 21 m^2/g of BET area. The high decrease in surface could be occasioned because ion exchanging H-SAPO-34 with metal is a difficult process that need to be improved, for that reason, authors are looking for new procedures to maintain the surface area, stability, and to reduce synthesis costs in the preparation of Cu-SAPO-34. One of these methods is the one-pot method [100], which allows to synthesize the SAPO-34 and ion exchange with copper in a single vessel.

Table 2.1: BET area of catalysts.

Catalyst	BET area /m^2/g
H-ZSM-5	386
1.2Cu-ZSM-5	374
1.2Cu/ZSM-5	370
2.0Cu-ZSM-5	363
H-SAPO-34	550
Cu-SAPO34	291

2.3.1.4 SEM

SEM micrographs of Cu-based ZSM-5 catalysts (Figures 2.4a–2.4c) reveal that they are formed of agglomerates of small crystallites [101]. The agglomerates in the impregnated samples are more significant than in the ion-exchanged sample. However, they did not show any appreciable difference in the size of the agglomerate in the impregnated samples with different copper loading. This result agrees with the decrease in the BET area because larger agglomerates would decrease surface area.

Respect to 2.6Cu-SAPO-34, Figure 2.4d shows that cubic crystals with smooth surface and small particles between the cubes or on the surface compose the 2.6Cu-SAPO-34, as reported by Zhao et al. [102].

Figures B.1–B.4 show that the elements were evenly distributed and confirm the presence of Cu in all the catalysts. Table B.1 shows the results for copper from the EDS. Those results agree with the expected amount of copper in the catalysts.

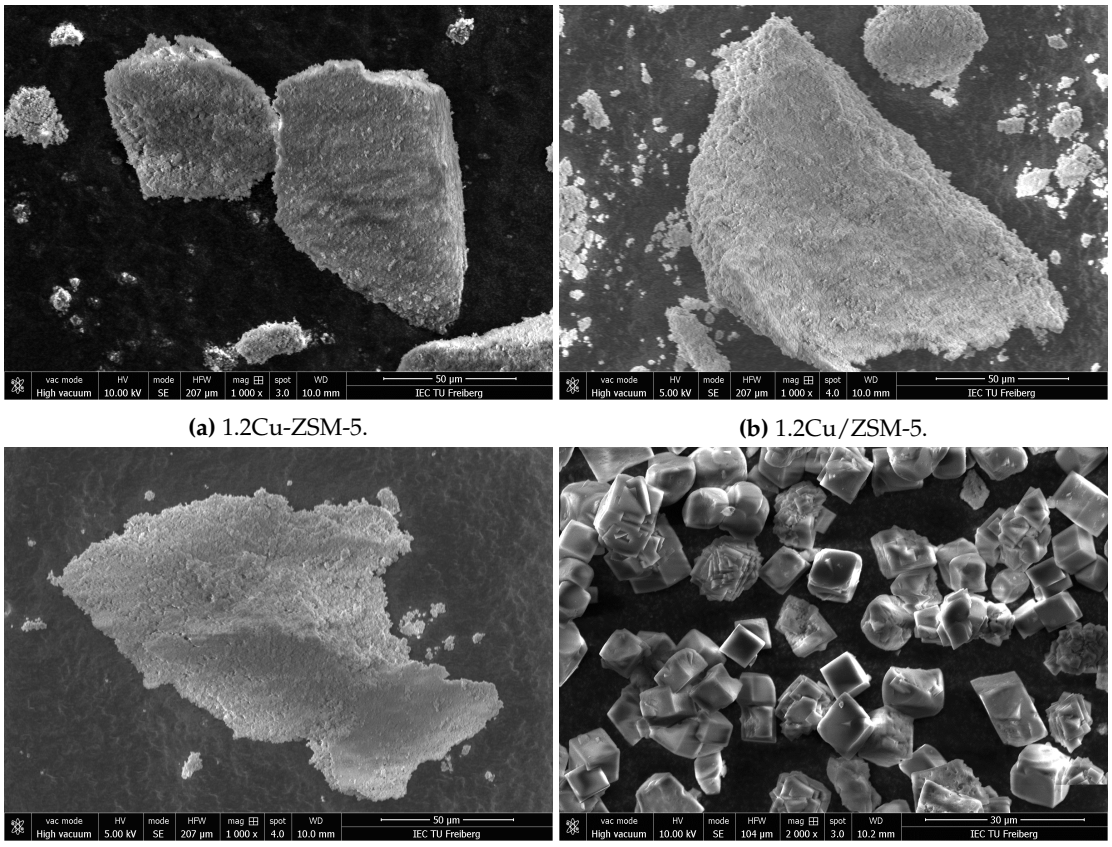

(a) 1.2Cu-ZSM-5. **(b)** 1.2Cu/ZSM-5.

(c) 2.0Cu/ZSM-5. **(d)** 2.6Cu-SAPO-34.

Figure 2.4: SEM micrographs of the catalysts.

2.3.1.5 OH-DRIFTS

Figures 2.5a–2.5c show three characteristic bands: at 3610 cm^{-1} for OH stretching vibration of acidic Si(OH)Al bridging hydroxyl groups, at 3745 cm^{-1} for isolated terminal or extra-zeolitic Si–OH, and a shoulder at 3661 cm^{-1} for the OH stretching vibration of Al–OH or $[Cu^{2+}(O^{-})]^{+}$ groups [103]. All the bands decreased respect to the bare zeolite, suggesting that Cu^{2+} exchanged the protons in Brønsted acid sites [92, 104]. This decrease was more pronounce in the ion-exchange sample than that of the impregnated ones. Comparing the samples synthesized by incipient wetness impregnation (1.2Cu/ZSM-5 and 2.0Cu/ZSM-5), the band's area of the one with 1.2% copper

decreased less than that of the one with 2% copper. It entails that impregnated samples also ion-exchange the H-ZSM-5, and agrees with UV-VIS, which showed that the band regarding d-d transitions of Cu^{2+} was higher for the ion exchange sample, decreased for the 1.2% impregnated and increased for the 2% copper Cu/ZSM-5.

Regarding the SAPO-34 based catalysts (Figure 2.5d), the band around 3625 cm^{-1} regards to the stretching mode of bridge OH groups Al–(OH)–Si, the bands at 3674 and 3745 cm^{-1} to P–OH and Si–OH species located on the external surface of the sample particles, respectively [76]. Again, the intensity of the Cu-containing sample of SAPO-34 decreased concerning the bare catalyst, which might indicate the ion exchange in the sample.

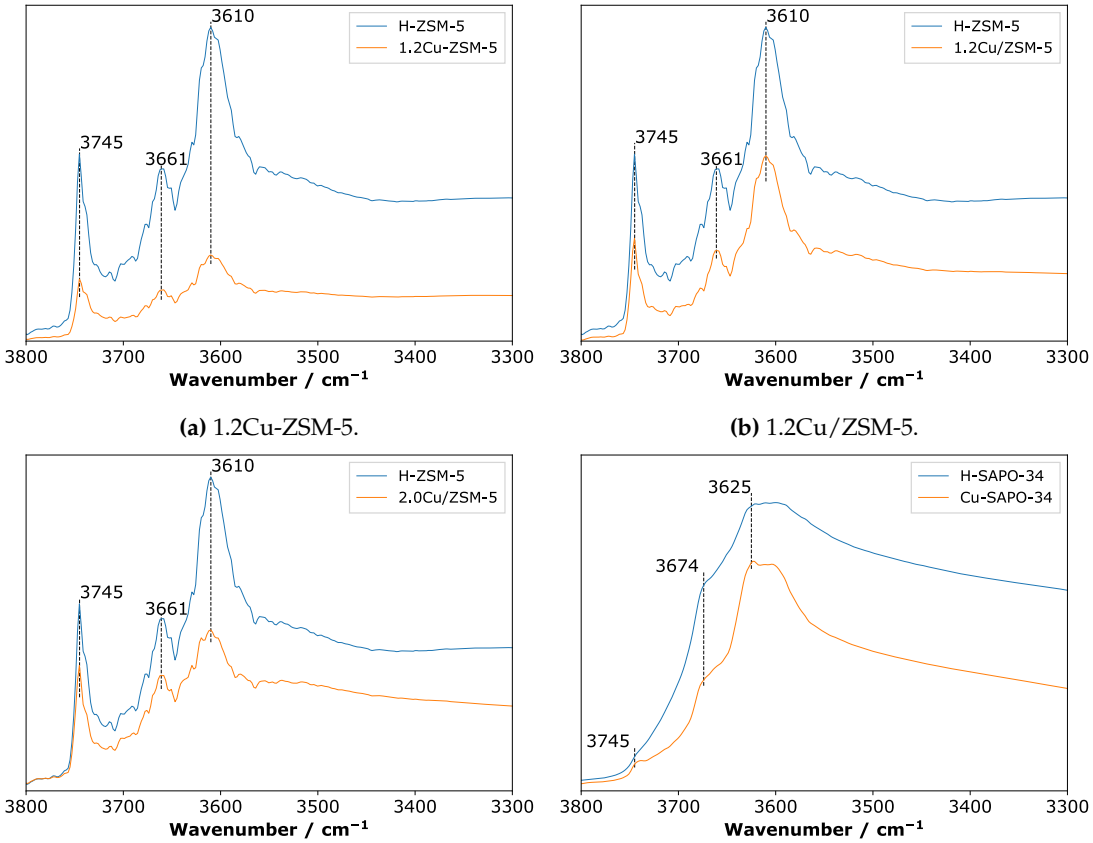

(a) 1.2Cu-ZSM-5.

(b) 1.2Cu/ZSM-5.

(c) 2.0Cu/ZSM-5.

(d) 2.6Cu-SAPO-34.

Figure 2.5: Comparison of OH-DRIFT spectra at 50 °C of Cu-based zeolites with their corresponding bare zeolites.

2.3.2 SCR experiments

The bare zeolites did not show conversions higher than 5% in the whole temperature range (data not show here). Figure 2.6 shows that without C_3H_6, 1.2Cu-ZSM-5 reached maximum conversion for both NO and NH_3 at 400 °C and then decreased for NO, but

remained the same for NH_3. With 500 ppm C_3H_6, the NO conversion decreased about 50% in the whole temperature range, while the NH_3 conversion decreased up to 30% below 400 °C and remained the same above 400 °C. Figure 2.7 shows the C_3H_6 reduced the catalytic activity of 1.2Cu/ZSM-5 in the NH_3-SCR reaction. However, it did not depend on the concentration of C_3H_6. The NO conversion decreased by 25% in the range 350–500 °C, while the NH_3 conversion decreased a little in the between 150–350 °C, and remained almost the same above 350 °C. Figure 2.8 shows that the catalytic activity of 2.0Cu/ZSM-5 decreased and increased depending on the amount of C_3H_6 and the temperature of the reaction. Without C_3H_6, the NO conversion increased in the whole temperature range until reaching 100% conversion at 450 °C and then decreased a little at 500 °C due to NH_3 oxidation. With 200 ppm C_3H_6, the NO conversion was higher than the reaction without C_3H_6 from 250–400 °C, but at 500 °C and 550 °C the conversion was lower. With 500 ppm of C_3H_6, the NO conversion was lower in the whole temperature range concerning the reaction without C_3H_6 and with 200 ppm of C_3H_6. The presence of C_3H_6 increased the NH_3 conversion because of a possible ammoxidation (Reaction 2.13) between NH_3 and C_3H_6 as Heo et al. reported [46]. However, the increase was more notorious, with 200 ppm of C_3H_6 at temperatures below 350 °C. These results agree with [20, 48, 52, 75], in which propylene also reduced the NO conversion in Cu-beta, Cu-SPZ, Cu-SSZ-13, and Cu-ZSM-5.

$$CH_2{=}CHCH_3 + NH_3 + \frac{3}{2}O_2 \longrightarrow CH_2{=}CHCN + 3\,H_2O \tag{2.13}$$

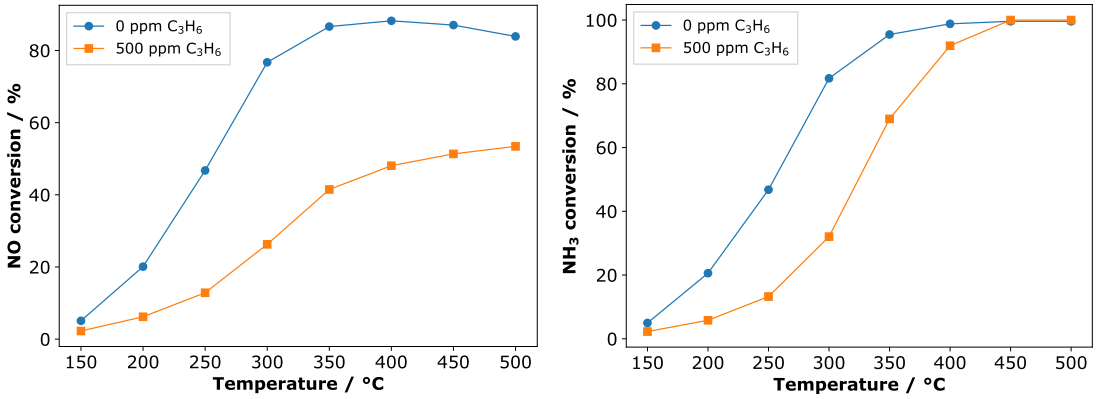

(a) NO conversion. **(b)** NH_3 conversion.

Figure 2.6: NO and NH_3 conversions in the SCR reaction with 1.2Cu-ZSM-5. Reaction conditions: 500 ppm NO_X, 500 ppm NH_3, 5% O_2, 10% H_2O, balance argon; total flow 1 L/min.; 200 mg of catalyst; GHSV = 150000 h^{-1}.

Figure 2.9 shows a different behavior in the effect of C_3H_6 on the NH_3-SCR of NO over 2.6Cu-SAPO-34. Without C_3H_6, the maximum NO conversion of 80% was reached at 350 °C and started decreased at 400 °C, while the NH_3 conversion increased in the whole temperature range until reaching its maximum of 90%. With 200 ppm C_3H_6, the

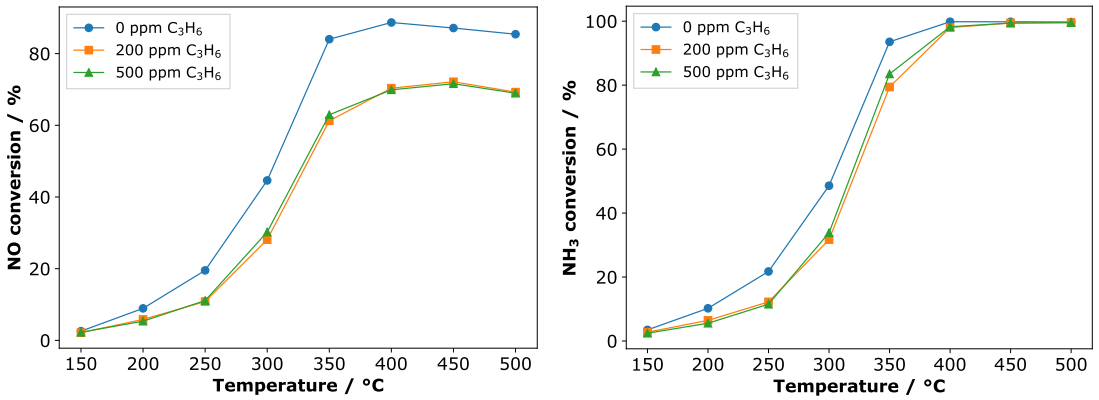

(a) NO conversion. **(b)** NH_3 conversion.

Figure 2.7: NO and NH_3 conversions in the SCR reaction with 1.2Cu/ZSM-5. Reaction conditions: 500 ppm NO_X, 500 ppm NH_3, 5% O_2, 10% H_2O, balance argon; total flow 1 L/min.; 200 mg of catalyst; GHSV = 150000 h^{-1}.

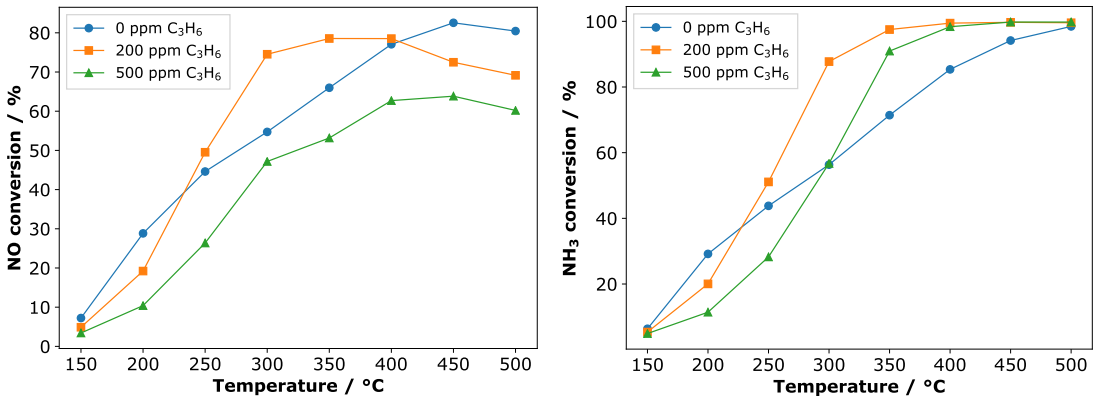

(a) NO conversion. **(b)** NH_3 conversion.

Figure 2.8: NO and NH_3 conversions in the SCR reaction with 2.0Cu/ZSM-5. Reaction conditions: 500 ppm NO_X, 500 ppm NH_3, 5% O_2, 10% H_2O, balance argon; total flow 1 L/min.; 200 mg of catalyst; GHSV = 150000 h^{-1}.

NO conversion increased about 10% in the whole temperature range and remained the same with 500 ppm C_3H_6. The same behavior was obtained for the NH_3 conversion. This result might indicate that low concentrations (around 200 ppm) of C_3H_6 improves the catalytic activity of 2.6Cu-SAPO-34 in the NH_3-SCR of NO, but bigger concentrations (about 500 ppm) might cause a detrimental effect on the catalytic activity. On the other hand, despite the maximum conversion of 2.6Cu-SAPO-34 was lower than the Cu-ZSM-5 catalyst, it present higher resistant to C_3H_6 than the Cu-ZSM-5 catalysts. This different in C_3H_6 effect could be attributed to the pore size of the zeolites (2.6Cu-SAPO-34 has a CHA framework, its pore size is about 3.8 Å and the pore size of the ZSM-5 is about 5.5 Å). This result agrees with the obtained by Ye et al [20] who state that the medium-pore size and cages in the Cu-ZSM-5 led to hydrocarbon deposits [20].

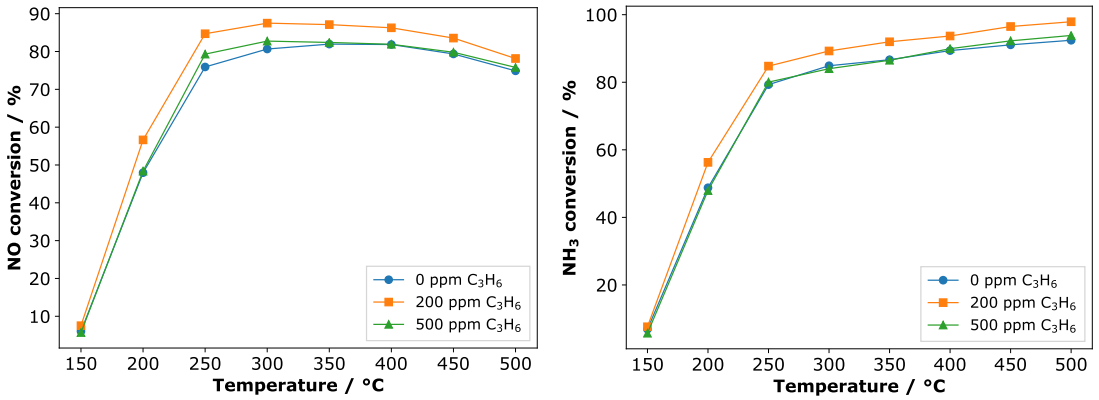

(a) NO conversion. **(b)** NH_3 conversion.

Figure 2.9: NO and NH_3 conversions in the SCR reaction with 2.0Cu/ZSM-5. Reaction conditions: 500 ppm NO_X, 500 ppm NH_3, 5% O_2, 10% H_2O, balance argon; total flow 1 L/min.; 200 mg of catalyst; GHSV = 150000 h^{-1}.

2.3.3 NH_3 adsorption/desorption

2.3.3.1 NH_3-TPD profiles of ZSM-5 based catalysts

Figure 2.10a shows that, at a temperature of adsorption of 50 °C, H-ZSM-5 desorbed NH_3 at two peaks around 170 °C and 375 °C. The low-temperature peak regards weakly bound NH_3 [105], including Lewis acid sites (e.g. extra-framework Al) [106] or NH_3 molecules solvating NH_4^+ ions [107, 108], and the high-temperature peak regards to strongly bound NH_3 on Brønsted acid sites [109, 110], probably on NH_4^+ [106].

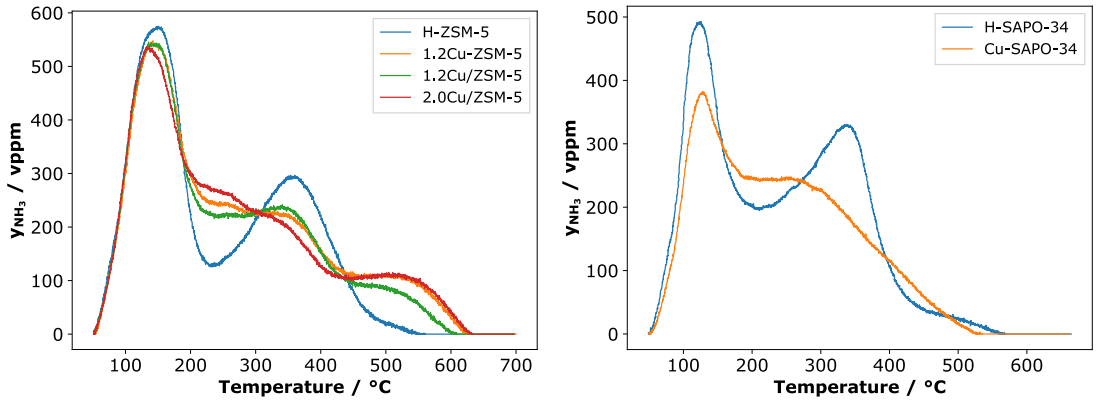

(a) ZSM-5 based catalysts. **(b)** SAPO-34 based catalysts.

Figure 2.10: Comparison NH_3-TPD profiles of the catalysts at a temperature of adsorption of 50 °C.

Incorporating copper into H-ZSM-5 by either incipient wetness impregnation or

by ion exchange reduced the peak around 375 °C because copper ions replace protons on Brønsted acid sites [106] as FTIR in the OH region showed. A new peak appeared around 250 °C, which might correspond to Lewis acid sites introduced by copper species [106], probably on Cu^{2+} sites as Lezcano-Gonzalez et al. suggest [107]. The new peak around 550 °C is difficult to assign but Lezcano-Gonzalez et al. propose that this peak is due to a higher acid strength of the remaining Brønsted acid sites [107]. Comparing the impregnated samples, the higher the copper loading, the higher the reduction of the peak around 360 °C. The peak around 250 °C increased as the copper loading was increased. Comparing the samples with the same copper loading but different synthesis method, the peak at 550 °C did not depend on the synthesis method but the peak at 350 °C did.

Table 2.2 shows that the total amount of NH_3 desorbed increased after copper incorporation respect to the bare zeolites. The catalyst 1.2Cu-ZSM-5 increased the total amount of NH_3 desorbed by 10%, while 1.2Cu/ZSM-5 and 2.0Cu/ZSM-5 increased by 5% and 9%, respectively. Figure 2.11 shows that the number of peaks of NH_3 desorption depends on the temperature at which NH_3 was adsorbed. Thus, H-ZSM-5, at a temperature of adsorption of 50 °C, desorbed NH_3 at two peaks; however, at a temperature of adsorption of 200 °C, H-ZSM-5 only desorbed NH_3 at one peak. The Cu-based ZSM-5 presented the same behavior with two and three peaks. This result suggests that the weakly bound NH_3 did not adsorb at temperatures above 150 °C.

Table 2.2: Amount of NH_3 desorbed in μmol / g at several temperatures of adsorption (T_{ads}) from the NH_3-TPD on fresh catalysts.

	T_{ads} / °C			
Catalyst	50	100	150	200
H-ZSM-5	1188	774	664	561
1.2Cu-ZSM-5	1311	930	772	613
1.2Cu/ZSM-5	1246	863	679	559
2.0Cu/ZSM-5	1300	926	764	583
H-SAPO-34	1070	-	-	485
2.6Cu-SAPO-34	954	720	533	387

2.3.3.2 NH_3-TPD profiles of SAPO-34 based catalysts

Figure 2.10b shows that H-SAPO-34 desorbed NH_3 at two peaks at around 130 °C and 350 °C, the first assigned to weak acid sites from surface hydroxyl groups (Si–OH and P–OH) and the second to moderate and strong structural Brønsted acid sites of SAPO-34 [97]. The 2.6Cu-SAPO-34 had an additional peak around 220 °C, attributed to Lewis acid sites generated by copper Cu^{2+} [97, 111]. The 2.6Cu-SAPO-34 desorbed 10% less NH_3 than the bare SAPO-34 (Table 2.2) differing from the ZSM-5 based catalysts, in which the NH_3 desorbed increased as copper loading increased. This reduction of acidity of

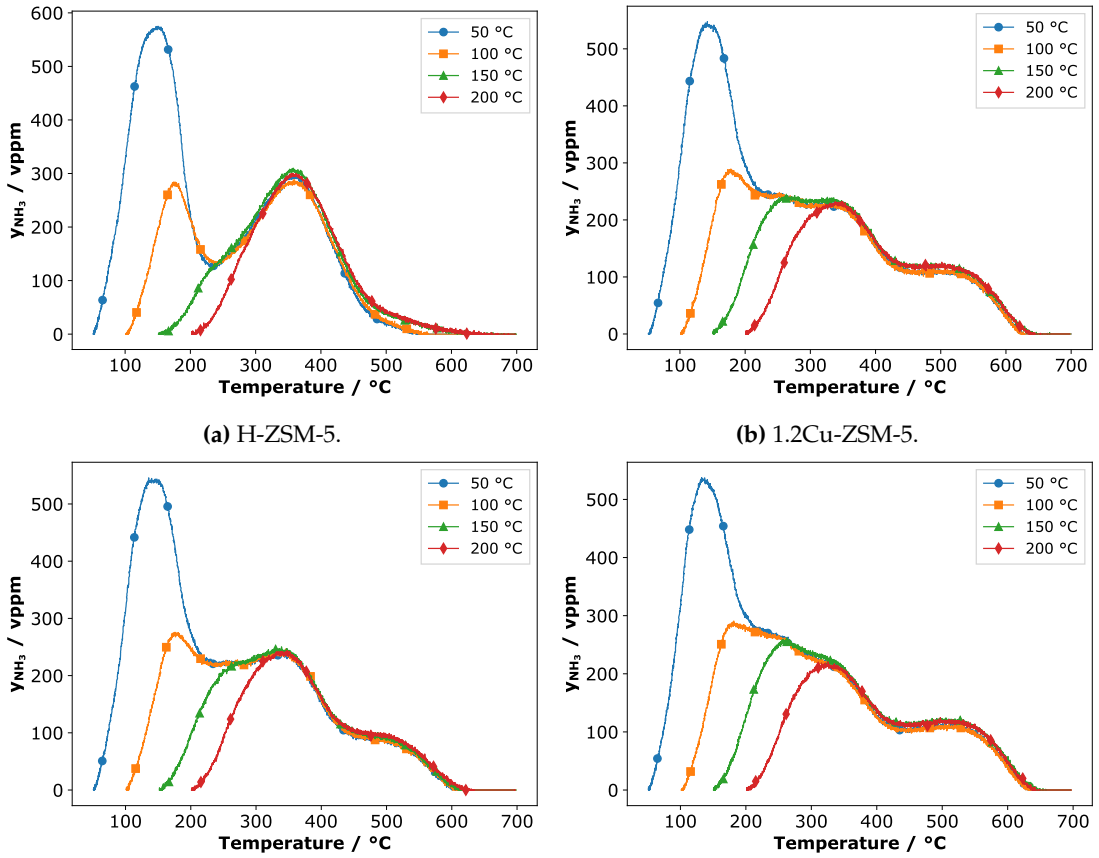

(a) H-ZSM-5.

(b) 1.2Cu-ZSM-5.

(c) 1.2Cu/ZSM-5.

(d) 2.0Cu/ZSM-5.

Figure 2.11: NH_3-TPD profiles of ZSM-5 based catalyst at several temperatures of adsorption.

the bare zeolite might be because Cu^{2+} species substitute the proton (Si–OH–Al) of H-SAPO-34 supports [111] as N_2-DRIFTS also showed or maybe because of the irreversible hydrolysis of the SAPO-34 after the synthesis that also caused the loss of surface area and destroyed Brønsted acid sites.

As in the case of the ZSM-5 based catalysts, performing the NH_3-TPD at several temperatures of adsorption, changed the number of desorption peaks in the TPD profiles. Adsorbing NH_3 in H-SAPO-34 showed two peaks, while it showed one peak adsorbing at 200 °C; 2.6Cu-SAPO-34 behaved similarly. It was an expected result since the capacity of adsorption of the materials decrease with the temperature of adsorption.

2.3.3.3 IR spectra of ZSM-5 based catalysts with adsorbed NH_3

IR spectra of H-ZSM-5 after NH_3 adsorption at 50 °C (Figure 2.13) shows characteristics bands of NH_3 interacting with their acid sites, even after increasing the temperature to 200 °C. In the OH stretching region, the negative bands arose from the consumption of OH bands referring to surface silanol (Si–OH) at 3750 cm^{-1} [112], to extra-framework aluminum (Al–OH) at 3665 cm^{-1} [113]; and to structural hydroxyl groups (Si–OH–Al)

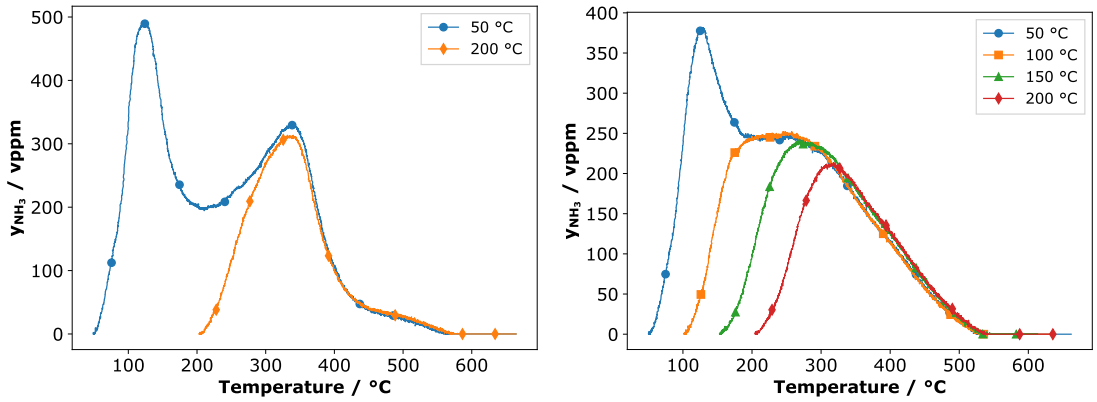

(a) H-SAPO-34. **(b)** 2.6Cu-SAPO-34.

Figure 2.12: NH_3-TPD profiles of SAPO-34 based catalyst at several temperatures of adsorption.

at 3609 cm^{-1} [113]. In the N–H stretching region, the bands at 3370 and 3280 cm^{-1} correspond to ammonium ions bonded to Brønsted acid sites [113]. In the N–H deformation region, the bands at 1480 and 1335 cm^{-1} correspond to the bending vibration of NH_4^+ on the Brønsted acid sites [113, 114].

New bands appeared in the IR spectra of Cu-containing ZSM-5 after NH_3 adsorption (Figures 2.14, B.5, and B.6). The band around 1617 cm^{-1}, which regards to bending vibration of the N–H bonds in the NH_3 coordinate to Lewis acid sites [76, 114], and the band around 3186 cm^{-1}, which regards to NH_3-Cu^+ species on the exchange sites [76].

In all the IR spectra, the negative bands start increasing at 50 °C, indicating that NH_3 is desorbing from the surface. The band at 1617 cm^{-1} remained almost constant until 150 °C and just increased at 200 °C; this might suggest that Lewis acid sites from copper sties start desorbing at 200 °C.

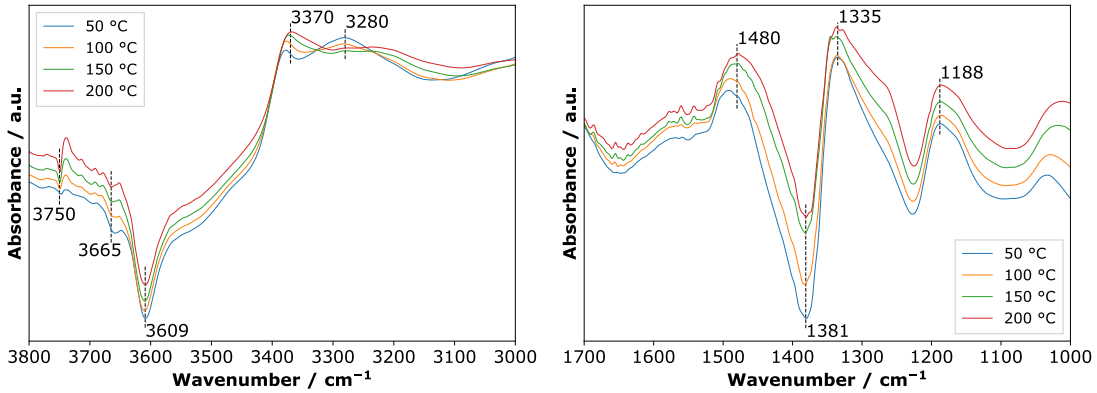

Figure 2.13: NH_3-DRIFT spectra of H-ZSM-5 in absorbance mode.

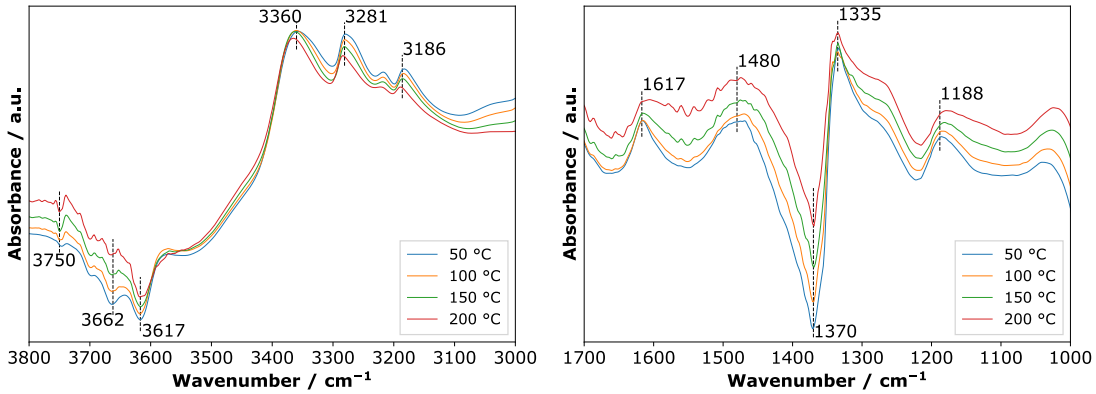

Figure 2.14: NH_3-DRIFT spectra of 1.2Cu-ZSM-5 in absorbance mode.

2.3.3.4 IR spectra of SAPO-34 based catalysts with adsorbed NH_3

FTIR spectra of H-SAPO-34 with adsorbed NH_3 (Figure 2.15) shows negative bands in the OH stretching region at 3745, 3676, 3625 cm^{-1} because NH_3 occupied Si–OH, P–OH, and Si–OH-Al [112]. In the N–H stretching region, the band at 3285 cm^{-1} is assigned to NH_4^+ groups [112]. In the N–H deformation region, the bands at 1465 and 1365 cm^{-1} are assigned to NH_4^+ species [112]. As the temperature increased, the bands in the stretching region increased, showing that NH_3 desorbed from the catalysts. In the N–H stretching region, the bands decreased up to 150 °C, which could mean that all the NH_3 desorbed at 200 °C. In the N–H deformation region, the band at 1465 cm^{-1} could be assigned to strong acid sites because the intensity changes little with temperature, but the remaining sites desorbed NH_3 from 50 to 200 °C. The FTIR spectra of 2.6Cu-SAPO-34 with adsorbed NH_3(Figure 2.16) shows in the OH stretching region, similar behavior to H-SAPO-34; in the N–H stretching region, bands at 3370 cm^{-1} and 3280 cm^{-1} regarding to NH_3 molecules and NH_4^+ groups [112]. Regarding the change with respect to temperature, the bands behaved similarly to H-SAPO-34 except for the band at 1620 cm^{-1}, which shows that this band decreased above 50 °C, but it remains the same at 100, 150, and 200 °C. The first desorption at 50 °C could be related with weakly bound NH_3, but above 200 °C, there could exist stronger Lewis acid sites, which might desorb at a higher temperature.

2.3.4 Effect of pre-adsorbing C_3H_6 on the NH_3 adsorption/desorption

2.3.4.1 NH_3-TPD profiles of C_3H_6-saturated catalysts

ZSM-5 based catalysts

All the catalysts tested adsorbed less NH_3 when performing the NH_3-TPD experiments when saturated with C_3H_6 (Table 2.3, Figures 2.17, 2.18, B.7, and B.8). The TPD profiles

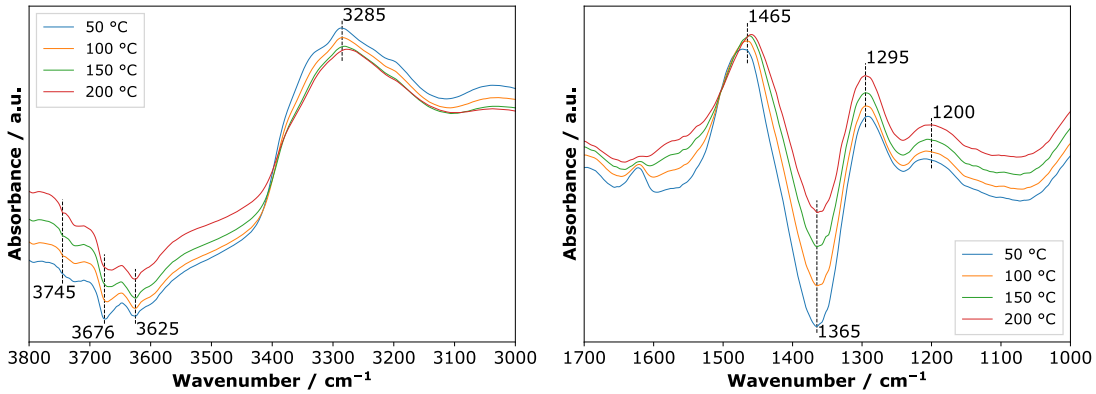

Figure 2.15: NH_3-DRIFT spectra of H-SAPO-34 in absorbance mode.

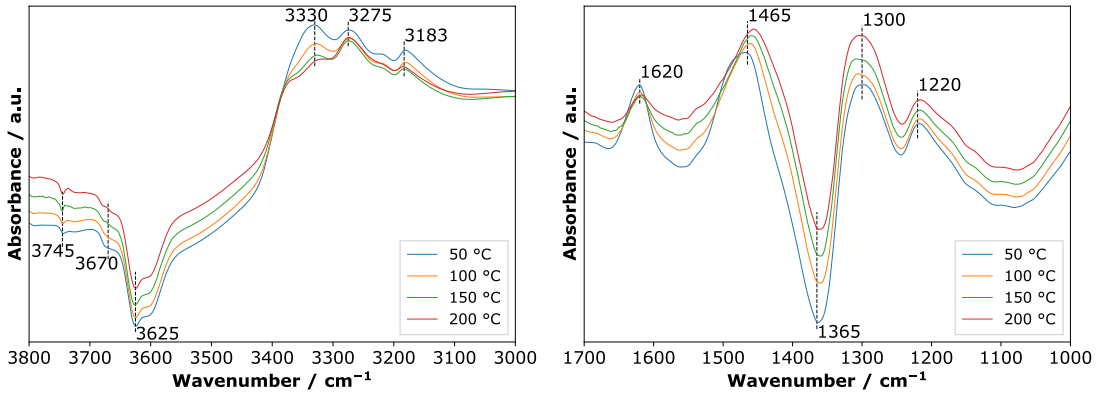

Figure 2.16: NH_3-DRIFT spectra of 2.6Cu-SAPO-34 in absorbance mode.

show that C_3H_6 might be adsorbed on the same acid sites of the NH_3 in all the evaluated catalysts, decreasing their capacity to adsorb NH_3.

By deconvolution of the TPD profiles to corresponding peaks and finding the amount of NH_3 desorbed from each peak, it indicates that adsorbing at 50 °C, the weakly bound NH_3 decreased by about 85% in H-ZSM-5 (Figure 2.17a), 60% in 1.2Cu-ZSM-5 (Figure 2.18a), 75% in 1.2Cu/ZSM-5 (Figure B.7a), and 50% in 2.0Cu/ZSM-5 (Figure B.8a); the strongly bound NH_3 decreased by about 35% in H-ZSM-5 (Figure 2.17a), 84% in 1.2Cu-ZSM-5 (Figure 2.18a), 89% in 1.2Cu/ZSM-5 (Figure B.7a), and 72% in 2.0Cu/ZSM-5 (Figure B.8a). At the adsorption temperature of 200 °C, the strongly bound NH_3 decreased by about 33% in H-ZSM-5 (Figure 2.17b), and by about 36% in all the Cu-based ZSM-5 (Figures 2.18, B.7, B.8). The peak around 250 °C was affected depending on the method of synthesis and copper content. The amount of NH_3 decreased less in the ion-exchanged sample than the impregnated ones, and the higher the content of copper, the smaller the decrease in NH_3 desorbed. The peak around 550 °C, which was only present in the Cu-containing ZSM-5, was not affected by the C_3H_6 at an adsorption temperature of 50 °C and was slightly decreased at an adsorption temperature of 200 °C. These results suggest that C_3H_6 adsorb more on weakly or moderate acid sites

than strongly acid sites and more in the bare H-ZSM-5 than the Cu-containing ZSM-5.

Table 2.3: C_3H_6 desorbed in μmol / g from the NH_3-TPD with pre-adsorbed C_3H_6. The adsorption temperatures were 50 and 200 °C.

	T_{ads} / °C	
Catalysts	50	200
H-ZSM-5	408	332
1.2Cu-ZSM-5	398	78
1.2Cu/ZSM-5	532	342
2.0Cu/ZSM-5	655	364
H-SAPO-34	24	-
2.6Cu-SAPO-34	878	383

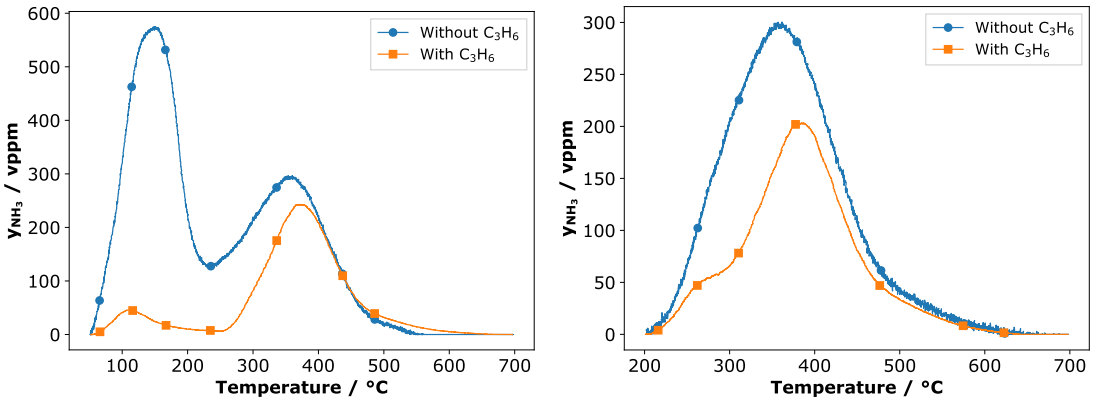

(a) 50 °C. **(b)** 200 °C.

Figure 2.17: Effect of pre-adsorbed C_3H_6 on the NH_3-TPD over H-ZSM-5.

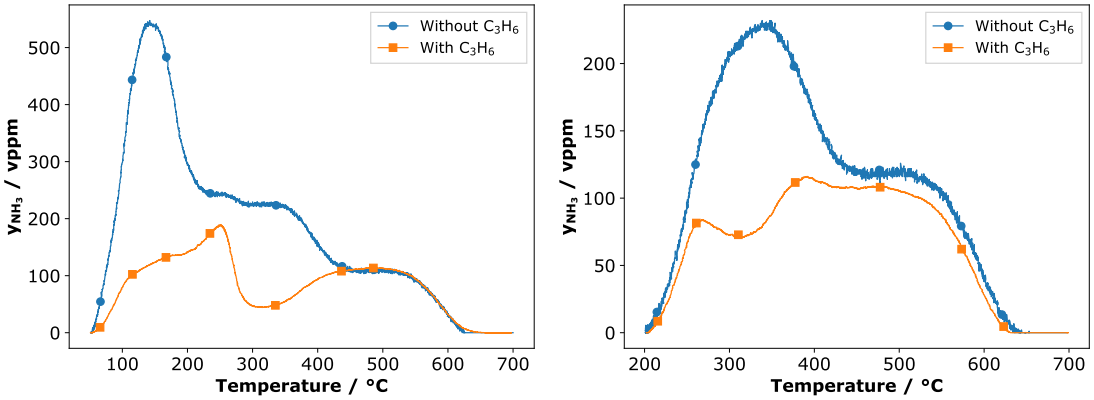

(a) 50 °C. **(b)** 200 °C.

Figure 2.18: Effect of pre-adsorbed C_3H_6 on the NH_3-TPD over 1.2Cu-ZSM-5.

SAPO-34 based catalysts

Figure 2.19 shows that after adsorbing C_3H_6 on the 2.6Cu-SAPO-34, at 50 °C, the amount of NH_3 desorbed was less; while at 200 °C it was almost the same. Comparing Table 2.2 and Table 2.3 we found that adsorbing C_3H_6 at 50 °C reduced the adsorption of NH_3 by 8% mainly due to the decreased of the peak at 150 °C, which corresponds to weakly bound NH_3.

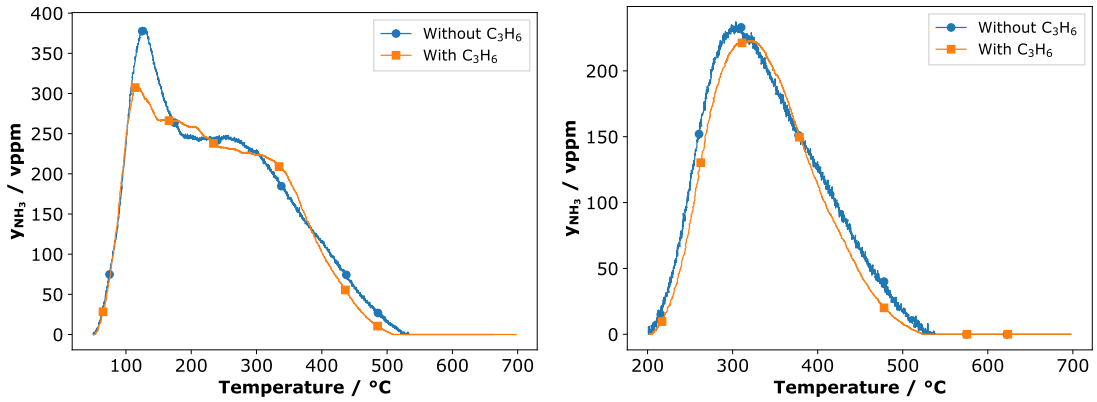

(a) 50 °C. **(b)** 200 °C.

Figure 2.19: Effect of pre-adsorbed C_3H_6 on the NH_3-TPD over 2.6Cu-SAPO-34.

2.3.4.2 IR spectra of C_3H_6-saturated catalysts

ZSM-5 based catalysts

Figure 2.20 shows that H-ZSM-5 adsorbed C_3H_6 at 3745, 3662, and 3611 cm^{-1} in the OH stretching vibration region; at 1469, 1305, and 1188 cm^{-1} in the N–H deformation region, which correspond to bending vibration of NH_4^+ on the Brønsted acid sites [113, 114]. H-ZSM-5 did not adsorb C_3H_6 on the sites in the N–H stretching vibration region but presented bands at 2936 and 2861 cm^{-1} (not present in the IR spectra of samples adsorbed with NH_3), which correspond to asymmetric vibration of $–CH_2–$ and to symmetric vibration of $–CH_3–$, respectively [115]. After saturating with NH_3, the bands in the OH vibration region increased a little, evidencing that propylene strongly adsorbed on H-ZSM-5 but NH_3 can adsorb on the same acid sites. In the N–H stretching vibration region, the band at 3315 cm^{-1} appeared. This band was different from the one in the IR spectra of catalysts saturated with NH_3 and may suggest that C_3H_6 forms compounds that affect the sites in which NH_3 is adsorbed [49]. Krishna and Makkee reported that C_3H_6 can form condensed aromatic rings (coke) [116]. Regarding the Cu-containing ZSM-5 samples, Figures 2.21, B.9, and B.10 show that the C_3H_6-saturated catalysts did not exhibit bands in the N–H stretching vibration region. Still, a band around 1548 cm^{-1},

which corresponds to C–C stretching vibration of adsorbed hydrocarbons [52]. However, after adding NH_3, the bands at 3350, 3279, and 3184 cm^{-1} arose, which as said in the NH_3-saturated IR of fresh samples, correspond to ammonium ions bonded to Brønsted acid sites. The band at 1610 cm^{-1} appeared, evidencing that C_3H_6 did not adsorb on the Lewis acid sites regarding Cu in the Cu-based ZSM-5 catalysts, which can correlate the peak in the NH_3-TPD profile at 550 °C.

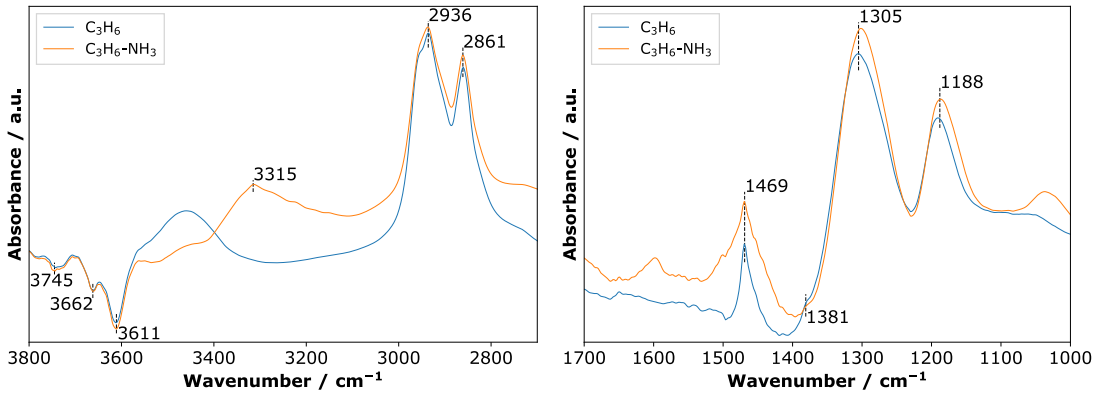

Figure 2.20: NH_3-DRIFT spectra in absorbance mode of C_3H_6-saturated H-ZSM-5 at 50 °C.

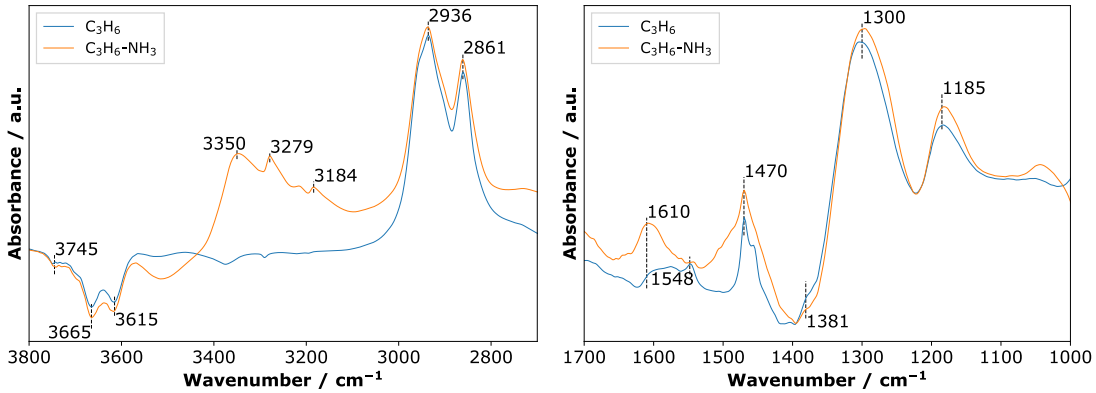

Figure 2.21: NH_3-DRIFT spectra in absorbance mode of C_3H_6-saturated 1.2Cu-ZSM-5 at 50 °C.

SAPO-34 based catalyst

Figure 2.22 shows that the bands of C_3H_6-saturated 2.6Cu-SAPO-34 are weak. The band at 3665 cm^{-1} correspond to C_3H_6 adsorbed on the OH bands, and the bands at 2960 cm^{-1} and 2861 cm^{-1} corresponds to asymmetric vibration of $–CH_2–$ and to symmetric vibration of $–CH_3–$, respectively [115]. The bands in the N–H deformation region correspond to C_3H_6 adsorbed on Brønsted acid sites [117]. After introducing NH_3, the bands highly increased, evidencing again that C_3H_6 hardly adsorbed on the 2.6Cu-SAPO-34 catalyst. The bands in the OH bands switch to negatives indicating that NH_3 might replace the C_3H_6 previously adsorbed [112]. The bands in both the N–H stretching vibration and

the N–H deformation regions appeared, indicating the less capacity of 2.6Cu-SAPO-34 to adsorb C_3H_6. Also, the band at 1625 cm^{-1} appeared, indicating that C_3H_6 did not adsorb on the Lewis acid sites.

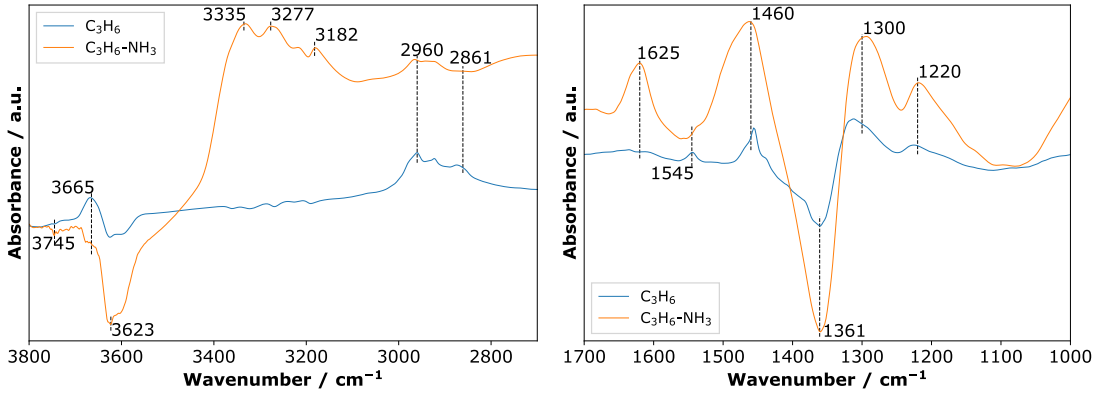

Figure 2.22: NH_3-DRIFT spectra in absorbance mode of C_3H_6-saturated 2.6Cu-SAPO-34 at 50 °C.

2.3.4.3 Py-DRIFTS

Figure 2.23 shows that C_3H_6 affects the adsorption of pyridine on H-ZSM-5 drastically. At temperatures below 250 °C, the bands at 1599 cm^{-1} and 1449 cm^{-1} might appear due to hydrogen-bonded pyridine and could distort the results; the inset plots show the DRIFT spectra to temperatures above 250 °C to avoid distorted results [118]. The bands at 1545 cm^{-1} and 1647 cm^{-1} correspond to Brønsted acid sites [119, 120] and the band at 1449 cm^{-1} to Lewis acid sites regarding unsaturated Al^{3+} [119]. When increasing the temperature (see inset Figure 2.23), both bands, at 1545 cm^{-1} and 1449 cm^{-1} remained up to 350 °C because these two bands are associated with strong acid sites. In the spectra of the C_3H_6-saturated H-ZSM-5, the bands at 1545 cm^{-1} and 1449 cm^{-1} did not appear (even in the inset), it confirms that in H-ZSM-5 catalyst, C_3H_6 affects both Brønsted and Lewis acid sites drastically.

For the Cu-containing catalysts (Figures 2.24–2.26), the bound around 1449 cm^{-1} shifted to lower bands around 1420 cm^{-1} attributed to the weaker interaction of the Cu^{2+} cation with pyridine [119]. The band in the Cu-containing samples around 1447 cm^{-1} corresponds to Lewis acid sites.

For the case of 1.2Cu-ZSM-5 (Figure 2.24), the Lewis acid sites remained in a major proportion than the Brønsted in the C_3H_6-saturated catalysts. It might indicate that C_3H_6 affected more Brønsted acid sites, confirming NH_3-DRIFTS results. Generally, for the copper-containing ZSM-5 catalysts, C_3H_6 decreased the intensity of the bands regarding both Brønsted and Lewis acid sites. For the case of 1.2Cu/ZSM-5 (Figure 2.25), the C_3H_6-saturated samples had similar intensity in the bands regarding Brønsted and Lewis acid sites (inset Figure 2.25), probably because this catalyst was synthesized by

impregnation, so it has a significant availability of Brønsted acid sites that are partially affected by C_3H_6. For the case of 2.0Cu/ZSM-5, since it had a lower number of Brønsted acid sites, as OH-DRIFTS (Figure 2.5) and NH_3-TPD (Figure 2.10a) show, they completely disappeared in the spectra of the C_3H_6-saturated sample (Figure 2.26).

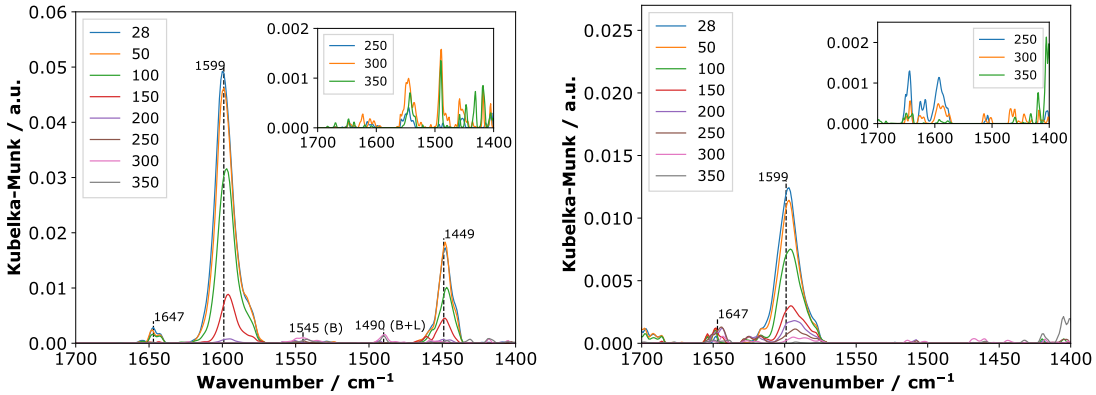

(a) Fresh H-ZSM-5. **(b)** C_3H_6-saturated H-ZSM-5

Figure 2.23: Py-DRIFT spectra of H-ZSM-5.

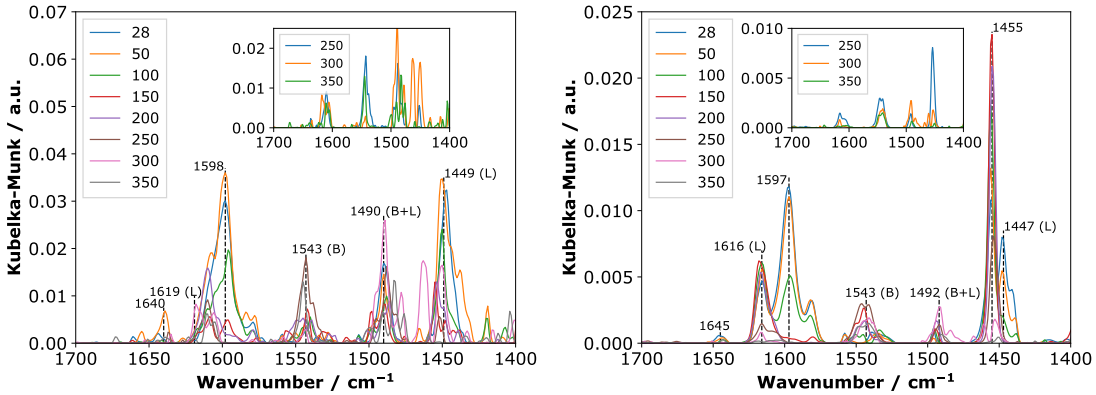

(a) Fresh 1.2Cu-ZSM-5. **(b)** C_3H_6-saturated 1.2Cu-ZSM-5

Figure 2.24: Py-DRIFT spectra of 1.2Cu-ZSM-5.

2.3.5 Modeling and simulation

2.3.5.1 NH_3 adsorption/desorption kinetic of fresh samples

The calculated adsorption capacities Equations 2.10 and 2.11 for the fitting were in the same order of magnitude for all the catalysts (Table 2.4). The adsorption capacities of the Z–OH site were smaller than the ones of the S site except for H-ZSM-5 because samples with Cu have less Brønsted acid sites, as NH_3-TPD and NH_3-DRIFTS showed. The initial coverage (θ) of the NH_4^+ site was lower than the NH_3 site for all the catalysts, indicating that, for this model, the acid sites represented by Brønsted acid sites desorbed

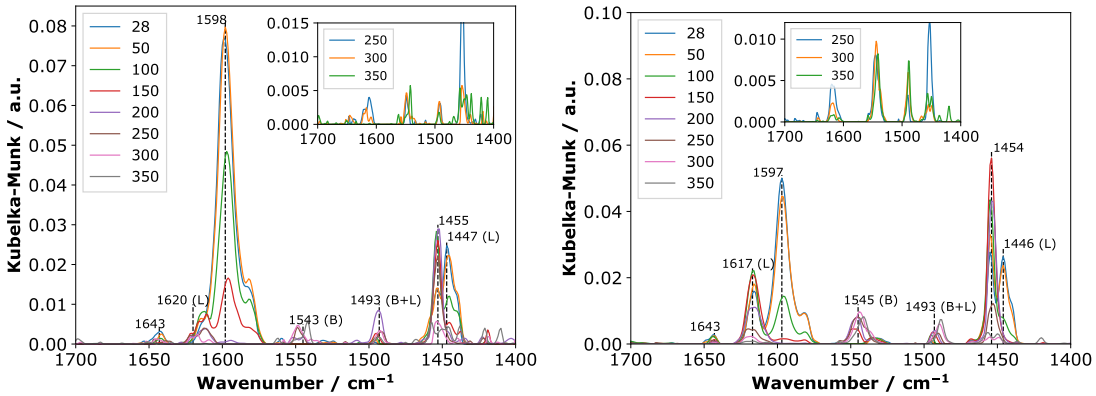

(a) Fresh 1.2Cu/ZSM-5. **(b)** C_3H_6-saturated 1.2Cu/ZSM-5

Figure 2.25: Py-DRIFT spectra of 1.2Cu/ZSM-5.

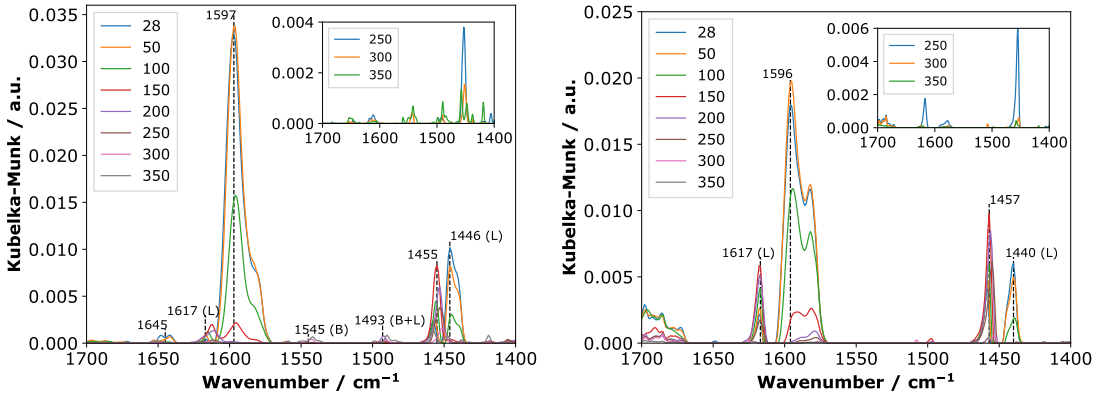

(a) Fresh 2.0Cu/ZSM-5. **(b)** C_3H_6-saturated 2.0Cu/ZSM-5

Figure 2.26: Py-DRIFT spectra of 2.0Cu/ZSM-5.

faster from the surface. Figure 2.27 shows that, for HZSM-5, the model fits well the TPD profile as demonstrated for the R^2 value near to 1.0 and small X^2. Figure B.13 validates the kinetic model at other adsorption temperatures (100, 150, and 200 °C) showing R^2 values near to 1.0 and small X^2. Regarding the Cu-containing samples, the kinetic reasonably simulate the TPD profiles for 1.2Cu-ZSM-5 and 1.2Cu/ZSM-5 (Figure 2.28, Figure B.11); and acceptably fits for 2.0Cu/ZSM-5 (Figure B.12). In general, the models sub-estimates the NH_3-TPD profiles for the Cu-containing samples as Figures B.14–B.16 probably because more than two sites could be involved, and the model needs to be expanded to a minimum of three sites. The same applied for the 2.6Cu-SAPO-34 sample Figures 2.29 and B.17.

The parameters obtained in the fitting of the desorption of NH_3 on the catalysts (Table 2.5) agree with the reported in the literature for Fe/BEA [78]. The pre-exponential factors of the low-temperature peak (which corresponds to site Z–OH in the kinetic model) are higher than the high-temperature peak (which corresponds to site S in the

Table 2.4: NH_3 adsorption capacity (Γ) in μmol/m^2 at 50 °C and initial coverages (θ) fitted for the kinetic of the desorption of fresh and C_3H_6-saturated catalysts.

	Γ_{Z-OH}		Γ_S		$\theta_{NH_4^+}$		θ_{NH_3}	
Catalyst	w/o.	w/	w/o.	w/	w/o.	w/	w/o.	w/
H-ZSM-5	1.6	0.1	1.4	0.9	0.9	0.7	1.0	1.0
1.2Cu-ZSM-5	1.2	0.9	2.3	0.7	0.8	0.8	1.0	1.0
1.2Cu/ZSM-5	1.3	0.6	2.1	0.8	0.7	0.9	1.0	1.0
2.0Cu/ZSM-5	1.1	1.2	2.5	0.6	0.8	0.9	0.9	1.0
2.6Cu-SAPO-34	0.7	0.7	2.5	2.3	0.8	0.6	1.0	1.0

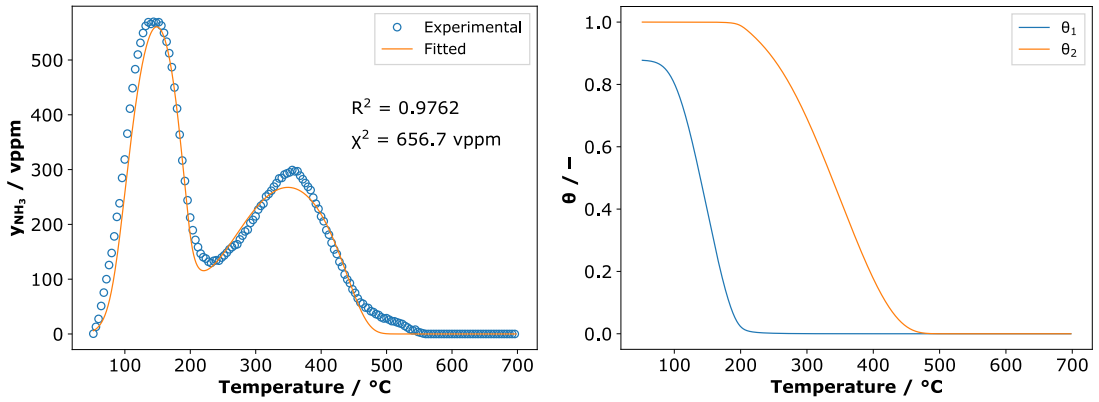

(a) NH_3 content. **(b)** Surface coverages.

Figure 2.27: Fitting of the NH_3-TPD profiles of H-ZSM-5 at an adsorption temperature of 50 °C. Fitting of the NH_3-TPD profiles of H-ZSM-5 at an adsorption temperature of 50 °C. θ_1 and θ_2 corresponds to $\theta_{NH_4^+}$ and θ_{NH_3}.

kinetic model). At the same time, the activation energies and the coverage dependence of the activation energy are smaller than the S site. Analyzing the presence of copper, samples with copper had less activation energy and coverage dependence of the activation energy the site Z–OH than the sample without copper. The pre-exponential factors of the site Z–OH tended to decrease with the incorporation of copper but did not depend on the incorporation method of copper. The pre-exponential factors of site S had different behavior. It was lower in 1.2Cu-ZSM-5 than the bare zeolite, but it was similar for the 1.2Cu/ZSM-5 and increased in the 2.0Cu/ZSM-5. These results agree with the NH_3-TPD, in which we concluded that the high-temperature peak was the most affected, and the fitting parameters of the high-temperature peaks changed more than the low-temperature peaks. Increasing the copper content did not change the site Z–OH peak (Table 2.5), as NH_3-TPD showed that the peak at 120 °C remained unchanged. However, it changed the peak of the site S drastically as both, the activation energy and coverage dependence decreased and increased, respectively.

The 2.6Cu-SAPO-34 sample values in the same order of magnitude than the ZSM-5 samples. However, the activation energy of site S are lower than the Cu-based ZSM-5.

We did not fit the parameters of the H-SAPO-34 because it was unstable, and we considered the simulation would depend on the time we performed the NH_3-TPD. For this catalyst, the difference in the activation energy and coverage dependence of the activation of both sites was not so notorious as in the case of the ZSM-5 based samples. This is probably because in the NH_3-TPD profiles, the maximum concentration of the two peaks of desorption is similar, while in the ZSM-5 based catalysts the maximum concentration of NH_3 of the low-temperature peak doubles the one of the high-temperature peak.

Table 2.5: Parameters of the kinetic of adsorption/desorption of the fresh catalysts obtained from the fitting in Matlab® at a desorption temperature of 50 °C.

	Catalyst				
Parameter	H-ZSM-5	1.2Cu-ZSM-5	1.2Cu/ZSM-5	2.0Cu/ZSM-5	2.6Cu-SAPO-34
A_2 / mol/m^2/s	$(2.0 \pm 0.9)\cdot10^{10}$	$(1.6 \pm 0.8)\cdot10^{9}$	$(1.7 \pm 1.8)\cdot10^{9}$	$(2.6 \pm 2.0)\cdot10^{9}$	$(1.3 \pm 1.4)\cdot10^{10}$
E_2 / kJ/mol	100.4 ± 1.7	88.4 ± 3.9	87.3 ± 3.3	89.3 ± 1.0	89.3 ± 3.2
$\alpha_{NH_4^+}$ / kJ/mol	9.0 ± 0.4	5.9 ± 0.9	7.6 ± 0.8	6.8 ± 2.4	5.8 ± 6.7
A_4 / mol/m^2/s	$(6.5 \pm 1.5)\cdot10^{6}$	$(2.3 \pm 0.9)\cdot10^{5}$	$(5.6 \pm 3.4)\cdot10^{6}$	$(7.5 \pm 9.8)\cdot10^{8}$	$(9.0 \pm 4.1)\cdot10^{5}$
E_4 / kJ/mol	113.2 ± 1.3	124.0 ± 0.4	121.0 ± 0.3	114.0 ± 7.0	98.9 ± 0.2
α_{NH_3} / kJ/mol	12.3 ± 0.3	55.7 ± 0.2	50.8 ± 0.2	59.1 ± 0.4	32.6 ± 0.1

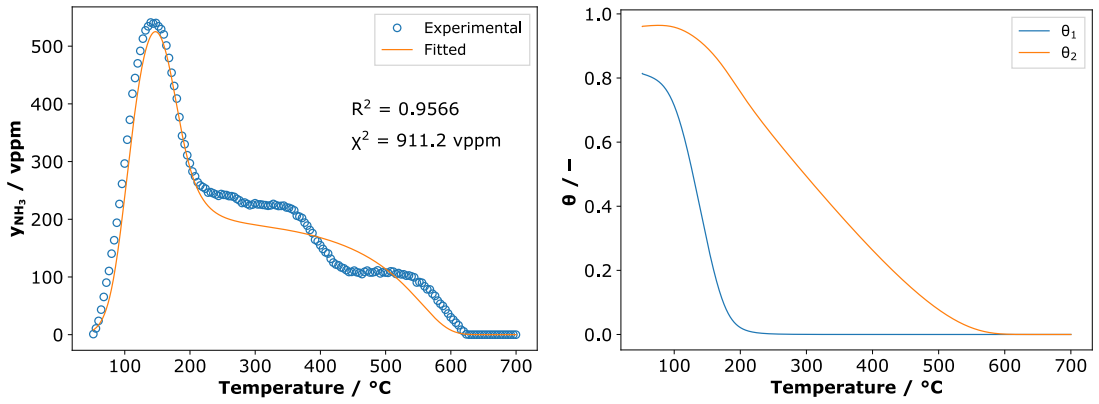

(a) NH_3 content. **(b)** Surface coverages.

Figure 2.28: Fitting of the NH_3-TPD profiles of 1.2Cu-ZSM-5 at an adsorption temperature of 50 °C.

2.3.5.2 NH_3 adsorption/desorption kinetic with three sites

To evaluate the kinetic model with another site, we expanded the model to three sites and obtained the results of Figure 2.30. We obtained that the model to three acid sites fitted better than the model with two acid sites. However, the computation time was so high, and for now we continued the kinetic with two acid sites to see the effect of the hydrocarbons in the NH_3-SCR of NO_X. We tried to perform the fitting of the C_3H_6-saturated catalysts, but the model has not converged so far.

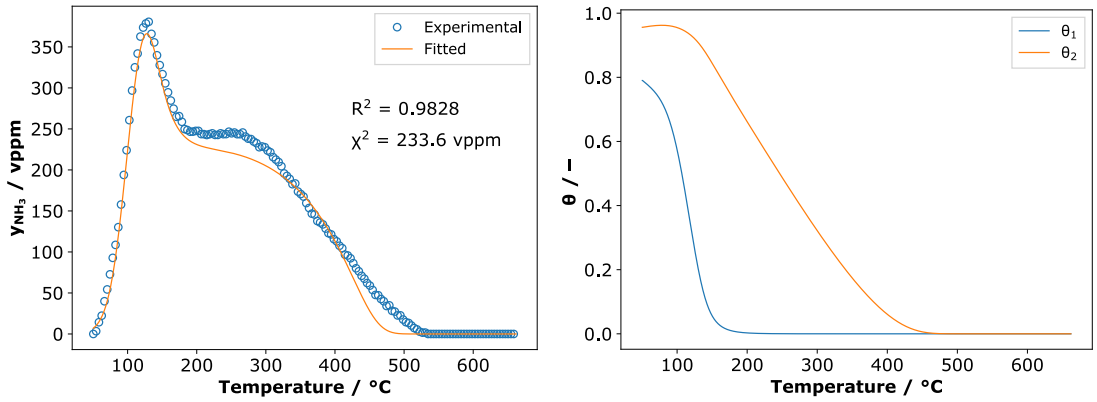

(a) NH_3 content. **(b)** Surface coverages.

Figure 2.29: Fitting of the NH_3-TPD profiles of 2.6Cu-SAPO-34 at an adsorption temperature of 50 °C.

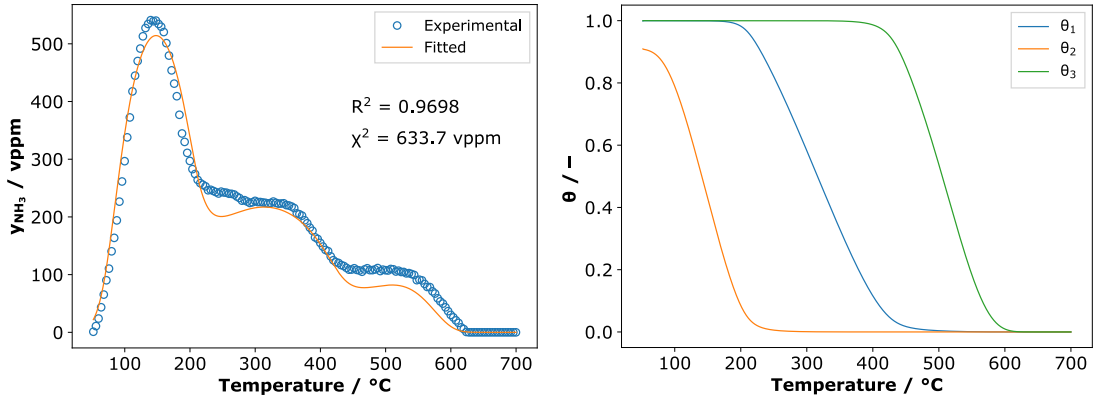

(a) NH_3 content. **(b)** Surface coverages.

Figure 2.30: Fitting of the NH_3-TPD profiles of 1.2Cu-ZSM-5 at an adsorption temperature of 50 °C with a kinetic model concerning three sites.

2.3.5.3 NH_3 adsorption/desorption kinetic of C_3H_6-saturated samples

We used the same procedure for fitting the NH_3-TPD profiles of C_3H_6-saturated samples, but in this case, only the data of the temperature of adsorption of 200 °C were used to validate the results. The simulation seed values of the parameters were obtained in the NH_3-TPD profiles of fresh samples. Figure B.18 shows the fitting of H-ZSM-5 at the adsorption temperature of 50 °C and its simulation at a temperature of adsorption of 200 °C. It shows that the fitting was proper and that these parameters can simulate the TPD profile at a temperature of adsorption of 200 °C. For the Cu-containing samples (Figures B.19, B.20, and B.21) despite the proper values of R^2 and X^2, the simulation was not so well, probably because the kinetic modeling needs to be expanded to three sites as reported in some Cu-based zeolites [64].

The adsorption capacities of the samples saturated with C_3H_6 were lower than that of the fresh samples (Table 2.4). However, the decreased was more pronounce in the

Table 2.6: Parameters of the kinetic of adsorption/desorption of the C_3H_6-saturated catalysts obtained from the fitting in Matlab® at a desorption temperature of 50 °C.

	Catalyst				
Parameter	H-ZSM-5	1.2Cu-ZSM-5	1.2Cu/ZSM-5	2.0Cu/ZSM-5	2.6Cu-SAPO-34
A_2 / mol/m^2/s	$(1.1 \pm 0.5)\cdot10^{10}$	$(1.2 \pm 1.8)\cdot10^{7}$	$(1.9 \pm 4.8)\cdot10^{7}$	$(3.9 \pm 4.8)\cdot10^{9}$	$(8.3 \pm 11)\cdot10^{10}$
E_2 / kJ/mol	99.4 ± 1.2	93.1 ± 5.3	94.0 ± 7.3	118.0 ± 4.4	96.2 ± 3.8
$\alpha_{NH_4^+}$ / kJ/mol	12.8 ± 0.2	24.1 ± 2.0	20.7 ± 3.0	39.6 ± 2.0	6.4 ± 0.9
A_4 / mol/m^2/s	$(1.8 \pm 1.1)\cdot10^{7}$	$(8.9 \pm 12)\cdot10^{7}$	$(3.9 \pm 10)\cdot10^{7}$	$(3.8 \pm 4.6)\cdot10^{7}$	$(1.8 \pm 1.0)\cdot10^{7}$
E_4 / kJ/mol	121.1 ± 3.6	146.0 ± 8.2	141.0 ± 12.1	158.6 ± 7.3	113.4 ± 3.0
α_{NH_3} / kJ/mol	3.3 ± 1.0	16.9 ± 2.5	17.6 ± 3.6	16.2 ± 1.9	34.1 ± 1.2

Γ_S value. The surface coverages of both sites decreased to a minor extent for the fresh samples. The kinetic parameters of the fresh samples were unsatisfactory in simulating the NH_3-TPD profiles of the C_3H_6-saturated samples (figures not shown here). It could indicate that adsorbing C_3H_6 changes the kinetic the adsorption/desorption of NH_3. To prove that, Table 2.6 shows new parameters fitted using the data of the NH_3-TPD profiles of the C_3H_6-saturated samples. In general, the new parameters presented the same tendency for the case of the fresh samples. However, the parameters from fresh and C_3H_6-saturated samples have noteworthy differences.

For the Z–OH site, the pre-exponential factor, and the activation energy in H-ZSM-5 remained the same. However, for the Cu-containing catalysts, the pre-exponential factor decreased by two orders of magnitude, while the activation energies increased by 6%. For the case of the coverage dependence of the activation energy of the site Z–OH, it increased by 40% in the H-ZSM-5, four times for the 1.2Cu-ZSM-5 sample, and three times for 1.2Cu/ZSM-5 and 2.0Cu/ZSM-5. As the NH_3-TPD shows, in the H-ZSM-5 sample, the C_3H_6 affected more the low-temperature peak, which corresponds to the Z–OH site. Those results might indicate that in the H-ZSM-5 catalyst, the C_3H_6 changes the kinetics of the NH_3 adsorption by changing the dependence of the activation energy. It means that the change in activation energy with temperature depends more on the surface coverage. For the Cu-containing samples, the C_3H_6 affected all the parameters of the Z–OH site indicating that C_3H_6 affected more drastically the kinetics of the adsorption/desorption of NH_3 than in the case of H-ZSM-5.

For the site S, the pre-exponential factor increased by one order of magnitude in H-ZSM-5 and 1.2Cu-ZSM-5, but it remained almost the same in the 1.2Cu/ZSM-5 and 2.0Cu/ZSM-5 catalysts; the activation energy increased about 7% in H-ZSM-5, 18% in 1.2Cu-ZSM-5 16% in 2.0Cu/ZSM-5, and 23% in 2.0Cu/ZSM-5; the coverage dependence of the activation energy decreased around 70% in all the catalysts. Since C_3H_6 affected the parameters of the S site, it shows that the kinetics of the adsorption/desorption of NH_3 is also affected. Although the NH_3-TPD profiles indicated that the amount of NH_3 is less affected in this site, the kinetic changed utterly. Summarizing, C_3H_6 affects the kinetics of the adsorption/desorption of NH_3 in Cu-based ZSM-5

catalysts drastically, in addition to the SCR activity. It is a remarkable result because when proposing detailed kinetic models of the NH_3-SCR of ZSM-5 based catalysts, it must consider the adsorption of NH_3, which should have parameters that include the effect of possible hydrocarbons in the gas exhaust.

2.4 Partial conclusions

Three Cu-based ZSM-5 catalysts were synthesized, one by ion exchange and two by incipient wetness impregnation. XRD revealed that the MFI framework was retained after the synthesis, UV-Vis showed characteristic bands of zeolites with Cu referred to charge transfer from O to Cu^+/Cu^{2+} and d–d transitions of isolated Cu^{2+}. BET surface area decreased after the synthesis, and SEM micrographs showed agglomeration of the catalysts as the copper content increased. OH-DRIFTS showed a reduction in the bands in the OH region, due to the ion exchange that reduced the amount of Brønsted acid sites. NH_3-TPD showed two peaks corresponding to the weakly bound NH_3 and NH_3 adsorbed on Brønsted acid sites. The Cu-containing catalysts were active in the NH_3-SCR reaction, but adsorbing C_3H_6 before the reaction decreased both the NO and NH_3 conversions. NH_3-TPD results showed that pre-adsorbing C_3H_6 on the samples decreased the amount of NH_3 adsorbed. IR spectra of samples after adsorption with NH_3 showed that C_3H_6 affected to a major extent the Brønsted acid sites, while the Lewis acid sites corresponding to Cu were less affected. The elementary mean-field model fitted the NH_3-TPD profiles. When the catalysts were pre-adsorbed with C_3H_6, it changed the parameters of the model. It suggests that when simulating the NH_3-SCR of NO over Cu-containing ZSM-5 catalysts, the parameters of the NH_3 adsorption should take the effect of hydrocarbons into account. Computing the ratios of effective reaction rates of desorption and SCR reactions, suggested that the C_3H_6 could affect more the SCR reaction in the ion-exchanged samples and the adsorption of NH_3 in the impregnated samples.

Chapter 3

Effect of dodecane on the NH_3-SCR over Cu-SSZ-13

This chapter studies the effect of dodecane, which can be a surrogate for diesel due to its high molecular weight, but few reports exist about how it affects the NH_3-SCR of NO_X. We synthesized by ion exchange Cu-ZSM-5 starting from a commercial NH_4-ZSM-5, and Cu-SSZ-13 starting from a synthesized H-SSZ-13. We adapted a reaction system with gas washing bottles to introduce water and $C_{12}H_{26}$ into the gas stream to evaluate the effect of $C_{12}H_{26}$ on the NH_3-SCR of NO, NH_3 oxidation, and NO oxidation at three different GHSV. We found that $C_{12}H_{26}$ reduced the catalytic activity of both Cu-ZSM-5 and Cu-SSZ-13 catalysts, but affected more the Cu-ZSM-5. Also, we found that the higher the GHSV, the higher the decrease in NO conversion in the NH_3-SCR and NH_3 oxidation over Cu-SSZ-13. We also synthesized a monolith catalyst by coating a cordierite honeycomb-type material with a slurry of Cu-ZSM-5. However, despite their excellent thermal and mechanical resistance, its activity in the NH_3-SCR of NO reaction was low. We concluded that despite $C_{12}H_{26}$ being a long-chain hydrocarbon, it might affect a small-pore zeolite, and for that reason, these kinds of studies should be considered when designing NH_3-SCR systems.

3.1 Introduction

Using diesel engines—which are more efficient and consume less fuel than the gasoline ones [121]—is an alternative for reducing cost in transportation, but they produce more CO_2 and NO_X. NH_3-SCR of NO is the most efficient technique for NO_X abatement from diesel engines, however, diesel fuel is a blend of several hydrocarbons (HCs) that, if unburned, can affect the catalyst performance.

Focus on real driving conditions increases studies about the effect of HCs in the NH_3-SCR of NO. For example, propylene (C_3H_6), a short-chain hydrocarbon, affected zeolites with medium to large pore such as Fe/MOR [50], Fe/Beta [45, 50], Cu/Beta [48, 49], Fe/ZSM-5 [13, 20, 46, 50], and Cu/ZSM-5 [20, 46]. In the same way, decane ($C_{10}H_{22}$), a long-chain hydrocarbon affected Cu/MOR [122] and Cu/ZSM-5 [122]. Regarding small-pore zeolites—the most promising catalyst for SCR—, C_3H_6 also affected them [48, 51, 53, 55], but the effect of long-chain hydrocarbons is not clear. Kumar et al. [51] report that even small-pore zeolite catalysts can store quantities of long-chain hydrocarbons such as n-dodecane ($C_{12}H_{26}$) and Selleri et al. [55] report that $C_{12}H_{26}$ does not affect the activity of a small-pore zeolite in the NH_3-SCR of NO. Also, in the literature, we did not find reports concerning durability tests (reactions for long times) on zeolites subject to hydrocarbons—a vital parameter for the use of catalysts on diesel engines—, since they can run for several hours.

This work aims to elucidate the effect of $C_{12}H_{26}$ on Cu-SSZ-13 in the NH_3-SCR of NO; and NO and NH_3 oxidation at several conditions and analyze the production of NO_2, N_2O, CO, and CO_2. Also, to perform durability tests on the catalysts by submitting them to a reaction with and without $C_{12}H_{26}$.

3.2 Experimental

3.2.1 Catalysts synthesis and characterization

Cu-based zeolites were synthesized by ion exchange starting from NH_4-ZSM-5 (Si:Al = 15) and H-SSZ-13 (Si:Al = 25). NH_4-ZSM-5 was purchased from Zeolyst International (CBV 3024E), and H-SSZ-13 was donated by Juan Miguel González Martínez, who synthesized it at Purdue University, as a task of a cooperative project. NH_4-ZSM-5 was calcined at 550 °C for 5 h to obtain the H-ZSM-5 form. Then, 12 g of catalyst were refluxed with 1.5 L of copper acetate solution with 160 ppm of Cu at 65 °C for 24 h. The final solution was filtrated, washed several times with deionized water, dried in air at 100 °C overnight and calcined at 550 °C for 4 h with a heating rate of 5 °C/min. H-SSZ-13 was ion-exchanged with 100 mL of $Cu(NO_3)_2$) 0.6 M solution per gram of catalyst at 80 °C for 8 h. The final solution was washed with deionized water, separated by centrifugation, dried at 120 °C overnight and calcined at 560 °C for 12 h with a 2 K min^{-1}.

XRD patterns were recorded in a PANalytical Empyrean diffractometer in the range of 5–60° with CuKα wavelength 0.179 nm, in 0.032°/min steps. Copper content was obtained by atomic absorption.

3.2.2 Monolith preparation and testing

Cordierite 6x6x12 mm monolith blocks were pretreated in nitric acid solution 30% v/v for 5 hours, washed with deionized water until reaching neutral pH, immersed in acetone for 2 h, dried at 100 °C for 3 h, and calcined at 600 °C for 2 h with a heating rate of 2.5 °C/min. The slurry consisted of 30% catalyst (Cu-ZSM-5 sieved to $<$ 80 mesh size), 8% binder (boehmite Catapal), 62% solvent (water), and 12 mL of acetic acid for adjusting the pH to 3.5. It was stirred and then milled at 200 rpm for 16 h in a planetary mill Retsch PM 100. Water was added to the slurry for obtaining 35% of solids, and the resulting mixture was dispersed in a mechanical homogenizer Ultraturrax at 3000 rpm for 10 min. Each monolith side was immersed into the slurry for 1 min; the excess of the coating was removed by blowing compressed air. They were dried at 120 °C for 1 h, and the process was repeated until obtaining 15% mass increase. Finally, they were calcined at 500 °C for 5 h with a heating rate of 0.4 °C/min to avoid cracks. The monoliths were tested by registering the mass change when submitting them to several conditions. For the mechanical test, they were submitted to ultrasonic bath in deionized water for 30 min; and for thermal resistance, they were submitted to 10 temperatures changes for 10 min at 500 °C and at room temperature. Loss of mass was calculated with Equation 3.1 and Equation 3.2, in which MML represents the percentage of monolith loss of mass; M_i, and M_f are the initial and final mass of the monolith; CML represents the percentage of coating loss of mass; C_i, and C_f are the initial and final mass of the coating.

$$MML = \left(\frac{M_i - M_f}{M_i}\right) \cdot 100\% \tag{3.1}$$

$$CML = \left(\frac{C_i - C_f}{C_i}\right) \cdot 100\% \tag{3.2}$$

3.2.3 Reaction facilities

The bench reactor (Figure 3.1) consisted of gas bottles (NO, Linde Gas, 4850 ppm in helium; NH_3, Cryogas, 3000 ppm in helium; O_2 Oxígenos de Colombia, grade 2.7, 99.7%; Argon, Cryogas, 99.999%). Flows were controlled via BROOKS 5850E and OMEGA mass flow controllers. Water and $C_{12}H_{26}$ were entered into the feed by passing argon through gas washing bottles at 48 °C to obtain the required concentrations. NO, O_2, water, $C_{12}H_{26}$ when used, and argon as balance were mixed with NH_3 at the entrance of the

reactor for avoiding homogeneous reactions. The reactor was a borosilicate glass tube (10 mm O.D.) heated by an electric furnace controlled by a PID ANAFAZE 8LS temperature controller. The catalyst was held on a quartz frit, between two pieces of glass wool, and with some quartz wool above the bed to pre-mix the gases. Tubing from the exit of the reactor to the inlet of the FT-IR spectrometer was heated to 150 °C to avoid water condensation. Concentrations were analyzed by an Antaris IGS FT-IR spectrometer with 200 mL, 2 m cell at 150 °C with the methods explained in Appendix A.

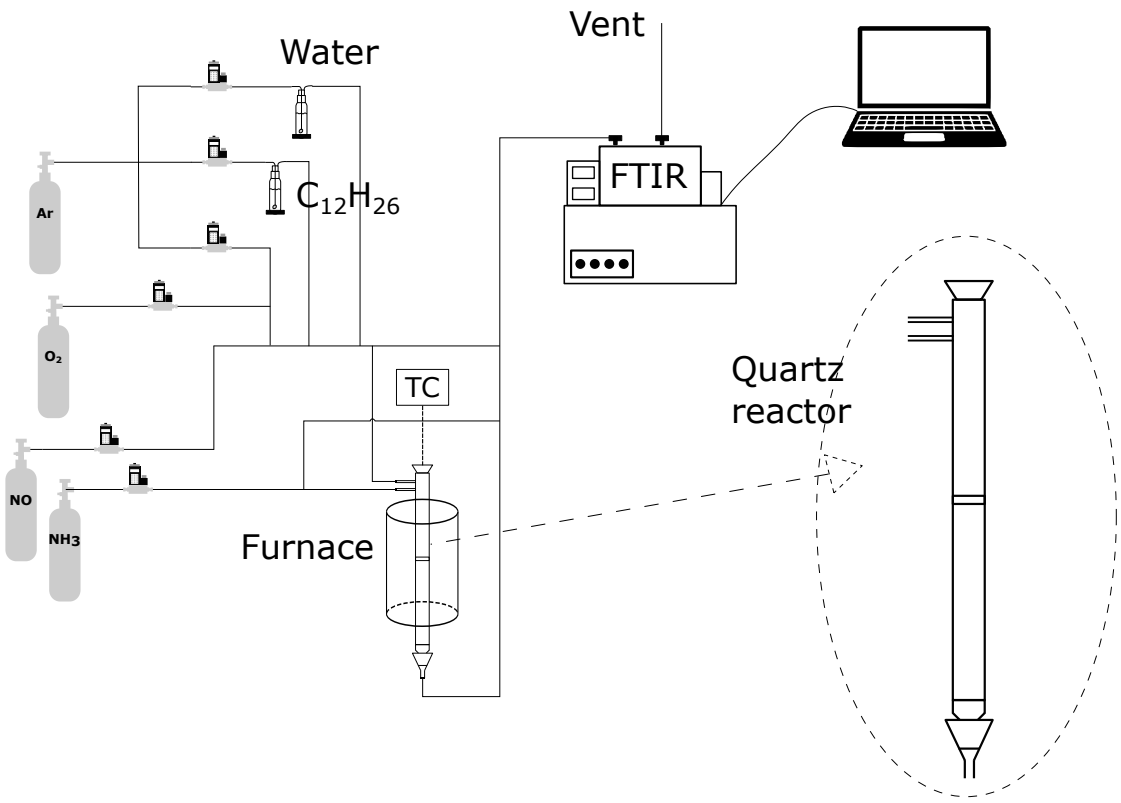

Figure 3.1: Bench reactor for the study of NH_3-SCR of NO.

3.2.4 Catalytic activity

Reactions were performed in a fixed-bed glass reactor at atmospheric pressure (Figure 3.1). The reaction conditions were 400 ppm NO, 400 ppm NH_3, 8% O_2, 5% H_2O, 300 ppm $C_{12}H_{26}$ when used, and balance argon. Temperature range was 150–550 °C at 50 °C intervals. Typically, 100 mg of catalyst (sieved 30–40 mesh) were loaded to the reactor. The catalyst was treated in 100 mL/min oxygen at 400 °C for 6 h and then letting to cool to room temperature by convection. Initial concentrations of the reactants were measured after stabilizing the flow for 3 h when NH_3 was in the stream or 2 h without NH_3. The gas flow was directed to the catalyst and left to stabilize for 3 h when having NH_3 or 2 h without it. At each reaction temperature, the gas flow was let to stabilize

for 2 or 1 h if having NH_3 or not. Conversion of NO and NH_3 was calculated according to Equation 3.3, in which, X is the conversion, c_{in} is the inlet concentration at room temperature and c_{out} is the outlet concentrations at the reaction temperature. The Gas Hourly Space Velocity (GHSV) was calculated by Equation 3.4, where F is the gas flow through the catalyst, ρ is the apparent density (assumed to be 500 kg/m^3), and M is the catalyst mass. N_2 concentration and selectivity were calculated using Equation 3.5, and Equation 3.6, respectively [123].

The GHSV was varied by changing the gas flow while maintaining the catalyst mass constant. The stability tests were performed at the same reaction condition at a fixed temperature for 30 h with and without $C_{12}H_{26}$.

$$X = \left(\frac{c_{in} - c_{out}}{c_{in}}\right) \cdot 100\% \tag{3.3}$$

$$GHSV = \frac{F \cdot \rho}{M} \tag{3.4}$$

$$[N_2]_{out} = \frac{[NH_3]_{in} - [NH_3]_{out} + [NO_X]_{in} - [NO_X]_{out} - 2[N_2O]_{out}}{2} \tag{3.5}$$

$$N_2\ selectivity = \left(\frac{2[N_2]_{out}}{2[N_2]_{out} + 2[N_2O]_{out} + [NO_2]_{out}}\right) \cdot 100\% \tag{3.6}$$

3.3 Results and discussion

3.3.1 Catalyst characterization

Figure 3.2 shows that the XRD patterns of the Cu-SSZ-13 and Cu-ZSM-5 agreed with their corresponding bare catalyst [110], indicating that the framework of the starting material remained after the ion exchange. We did not see any appreciable peaks corresponding to copper oxides that appeared around 35.5° and 38.7° [72, 90]. Copper loading of Cu-SSZ-13 and Cu-ZSM-5 obtained by atomic absorption were 1.4% and 1.2%, respectively.

3.3.2 Effect of temperature on the NH_3-SCR of NO over Cu-based zeolite catalysts

Figure 3.3 shows the catalytic activity of 1.2Cu-ZSM-5 with and without hydrocarbons. 1.2Cu-ZSM-5 attained maximum conversion NO and NH_3 at 250 °C without hydrocarbons. The NO conversion started decreasing at 450 °C due to the non-selective oxidation of NH_3, while the NH_3 conversion remained the same up to 550 °C. With $C_{12}H_{26}$, the

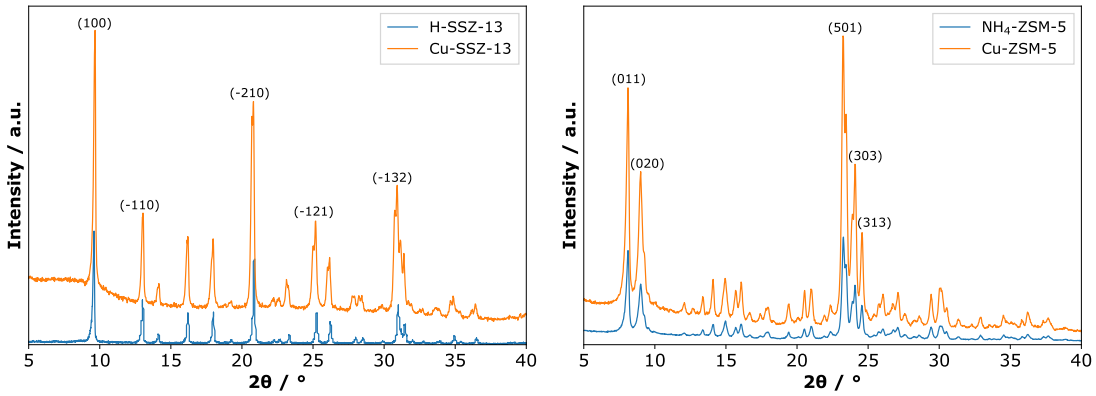

(a) SSZ-13 based catalysts, Si:Al = 25. **(b)** ZSM-5 based catalysts, Si:Al = 15.

Figure 3.2: XRD patterns of Cu-based zeolite catalysts.

maximum NO and NH_3 conversions were also attained at 250 °C, but the NO conversion decreased little from 300 °C and 500 °C, while the NH_3 conversion just decreased a little at temperatures above 500 °C. With C_3H_6, the NO conversion had an s-shaped behavior and was decreased about 50% at the temperature with maximum conversion, which could be related to the competitive adsorption on the catalyst in the surface as Heo et al. [46] pointed out. This competitive adsorption might reduce NO conversion at temperatures below 350 °C, but at higher temperatures the NO conversion started to increase due to C_3H_6-SCR reaction [53]. In fact, Fig. 3.3 shows that the C_3H_6-SCR reaction starts at 300 °C to a maximum conversion at 400 °C.

For the case of the 1.4Cu-SSZ-13, Figure 3.4 shows a similar behavior than the 1.2Cu-ZSM-5 catalyst. C_3H_6 affect the NO conversion in a s-shaped manner and reduce it about 10% at 350 °C, and $C_{12}H_{26}$ decreased the NO conversion. C_3H_6 and $C_{12}H_{26}$ decreased the NH_3 conversion at low temperature but the effect is minor at temperatures above 450 °C.

These results demonstrated that $C_{12}H_{26}$ affected both 1.4Cu-SSZ-13 and 1.2Cu-ZSM-5. From now, we selected the 1.4Cu-SSZ-13 catalyst to perform a series of experiments. 1.4Cu-SSZ-13 is the most promising catalyst for the NH_3-SCR of NO_X and its resistance to hydrocarbons needs to be studied deeply.

3.3.3 GHSV effect on the catalytic activity of Cu-SSZ-13 in the NH_3-SCR of NO

Increasing the GHSV from 60000 to 150000 h^{-1} reduced both NO and NH_3 conversions (Figures 3.5 and 3.6). Without $C_{12}H_{26}$ and below 250 °C, NO and NH_3 conversions decreased as the GHSV increased because the residence time is higher, inducing more contact time between the catalyst and the gas. Above 250 °C, reduction in conversion was less notable for all GHSV, probably because the consumption rate is faster than the

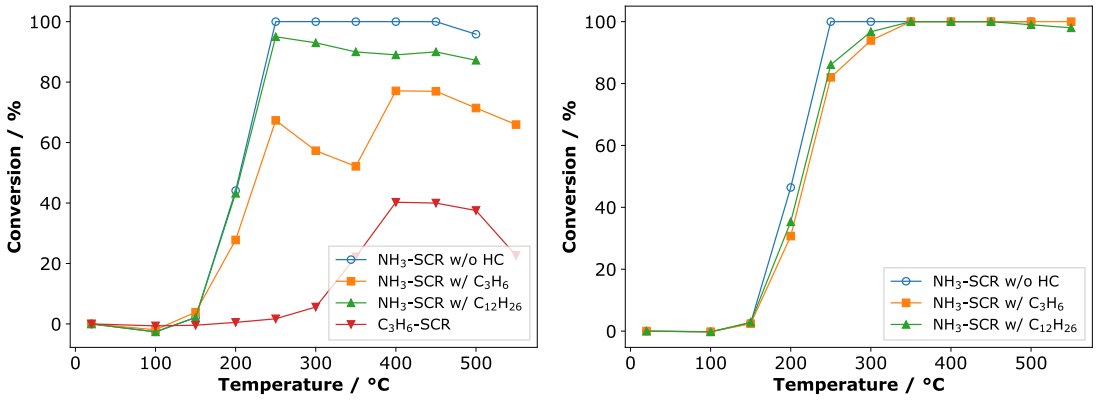

(a) NO conversion. **(b)** NH_3 conversion.

Figure 3.3: Effect of hydrocarbons on the catalytic activity of 1.2Cu-ZSM-5. Reaction conditions: 400 ppm NO, 400 ppm NH_3, 8% O_2, 5% H_2O, 300 ppm $C_{12}H_{26}$ when used, balance argon. GHSV = 90000 h^{-1}.

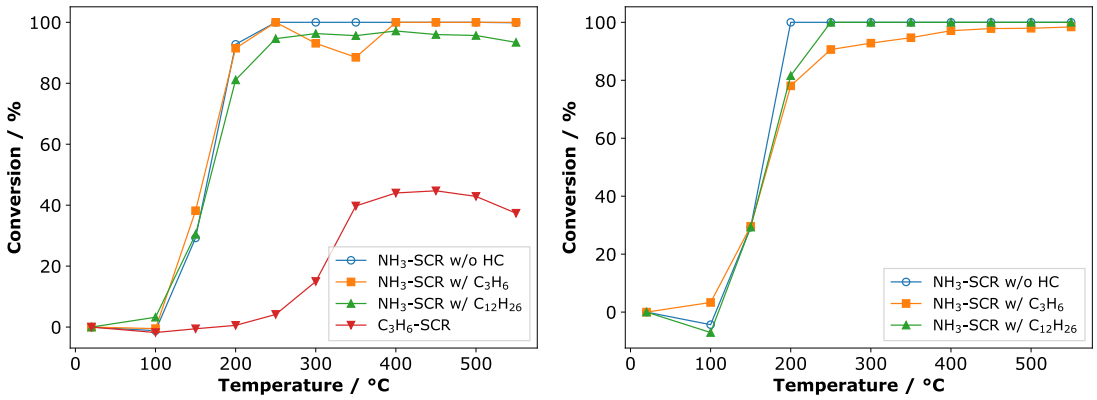

(a) NO conversion. **(b)** NH_3 conversion.

Figure 3.4: Effect of hydrocarbons on the catalytic activity of 1.4Cu-SSZ-13. Reaction conditions: 400 ppm NO, 400 ppm NH_3, 8% O_2, 5% H_2O, 300 ppm $C_{12}H_{26}$ when used, balance argon. GHSV = 90000 h^{-1}.

residence time. At 90000 and 150000 h^{-1}, $C_{12}H_{26}$ reduced NO conversion in the whole temperature range (Figure 3.5a and Figure 3.5b). At 60000 h^{-1}, the $C_{12}H_{26}$ reduced the NO conversion at temperatures below 250 °C. $C_{12}H_{26}$ decreased the NH_3 conversion in the whole temperature range at all GHSV studied. However, it was more notable at 150000 h^{-1}. $C_{12}H_{26}$ induced the production of carbon monoxide (CO) (Figure C.1a). CO is a product of the partial oxidation of $C_{12}H_{26}$ that could affect NH_3-SCR of NO by the reduction of nitrates to nitrites that then react with N_2O releasing NO [53]. We saw that after the reaction with $C_{12}H_{26}$, the catalysts turned gray, evidencing some carbonaceous deposits. Those results agree with Kumar et al. [51], who pointed out that both short- or long-chain hydrocarbons can be stored on small-pore zeolites. Also, Zheng et al. [53] report that Cu-SSZ-13 can store significant amounts of carbonaceous deposits via an oxygen-dependent, thermally-activated storage process, which reduces NO and

NH_3 conversions in the NH_3-SCR of NO. Without $C_{12}H_{26}$, nitrogen selectivity was almost 100% at temperatures above 150 °C for all the GHSV tested (Figure C.3). $C_{12}H_{26}$ reduced N_2 selectivity at 200 °C about 10% and about 25% at 150 °C at 150000 h^{-1} (Figure C.3). The concentration of NO_2 without $C_{12}H_{26}$ decreased as the temperature increased (Figure C.2b) and the higher the GHSV, the higher the concentration of NO_2. For the case of the reaction with $C_{12}H_{26}$ the NO_2 concentration was higher for GHSV of 150000 h^{-1}. This result agrees with the reduction in N_2 selectivity, which decreased with the inclusion of $C_{12}H_{26}$ to produce nitrogen oxides compounds. The concentration of N_2O behaved similarly to the concentration of NO_2. The major production of N_2O was obtained in the presence of $C_{12}H_{26}$ at a GHSV of 150000 h^{-1}. It shows that $C_{12}H_{26}$ could affect both NO conversion and N_2 selectivity in NH_3-SCR of NO.

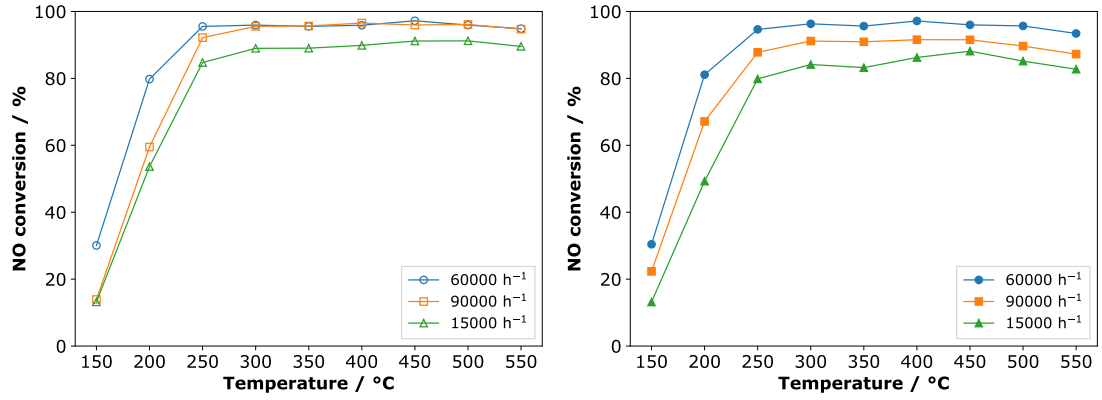

(a) Without $C_{12}H_{26}$. **(b)** With $C_{12}H_{26}$.

Figure 3.5: Effect of GHSV on the NO conversion in the NH_3-SCR of NO over Cu-SSZ-13. Reaction conditions: 400 ppm NO, 400 ppm NH_3, 8% O_2, 5% H_2O, 300 ppm $C_{12}H_{26}$ when used, balance argon.

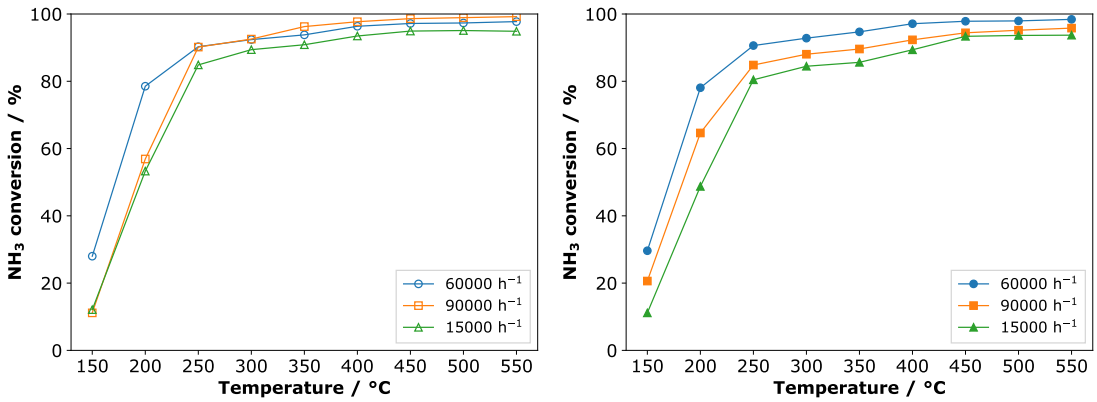

(a) Without $C_{12}H_{26}$. **(b)** With $C_{12}H_{26}$.

Figure 3.6: Effect of GHSV on the NH_3 conversion in the NH_3-SCR of NO over Cu-SSZ-13. Reaction conditions: 400 ppm NO, 400 ppm NH_3, 8% O_2, 5% H_2O, 300 ppm $C_{12}H_{26}$ when used, balance argon.

3.3.4 GHSV effect on the catalytic activity of Cu-SSZ-13 in the oxidation of ammonia

NH_3 oxidation experiments (Figure 3.7) showed better conversions at low GHSV. $C_{12}H_{26}$ reduced NH_3 conversion below 500 °C and increased it at 500 °C and 550 °C and produced CO_2 (Figure C.1b) and CO (Figure C.1a) at temperatures above 350 °C. Again, the catalyst turned gray after the reaction with $C_{12}H_{26}$. This confirms that $C_{12}H_{26}$ can form carbonaceous in the total or partial compounds combustion that may interfere in the NH_3-SCR of NO as Kumar et al. reports [51] at temperature below 450 °C or it may react with $C_{12}H_{26}$ as Heo et al. [46] reports.

Regarding the production of NO_2 and N_2O (Figure C.2a and Figure C.2b), and the N_2 selectivity; the $C_{12}H_{26}$ did not have any effect of them. This may suggests that despite it reduces the conversion of NH_3, it may formed other compounds from reaction like ammoxidation (Equation 3.7) [46] (this need to be confirmed by FT-IR)

$$CH_2{=}CHCH_3 + NH_3 + \frac{3}{2}O_2 \longrightarrow CH_2{=}CHCN + 3\,H_2O \tag{3.7}$$

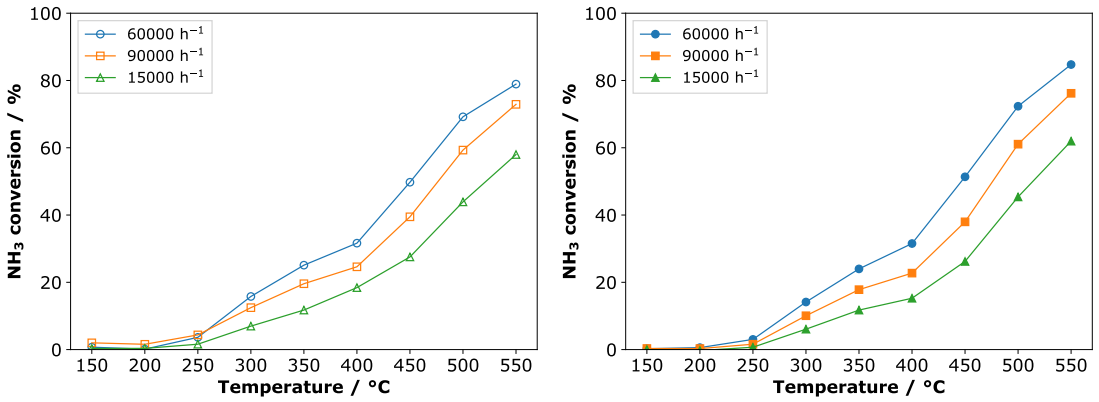

(a) Without $C_{12}H_{26}$. **(b)** With $C_{12}H_{26}$.

Figure 3.7: Effect of the GHSV on the oxidation of NH_3 over Cu-SSZ-13. Reaction conditions: 400 ppm NH_3, 8% O_2, 5% H_2O, 300 ppm $C_{12}H_{26}$ when used, balance argon.

3.3.5 GHSV effect on the catalytic activity of Cu-SSZ-13 in the oxidation of NO

Figure 3.8 shows that NO conversion was below 6% in the whole temperature range and that the presence of $C_{12}H_{26}$ unaffected the NO conversion. Leistner et al. [37] obtained NO conversions in the NO oxidation over Cu/SSZ-13 up to 6%, which agree with our results. Figure C.7a shows that the presence of $C_{12}H_{26}$ produced CO_2 and CO, probably due to complete or partial of $C_{12}H_{26}$.

The concentration of CO was higher in the NO oxidation than in the NH_3 oxidation (Figure C.4a and Figure C.7a). It also suggests that $C_{12}H_{26}$ may react with NH_3 at high temperatures; however, in the NO oxidation reaction, $C_{12}H_{26}$ may suffer partial oxidation instead of reacting with NO.

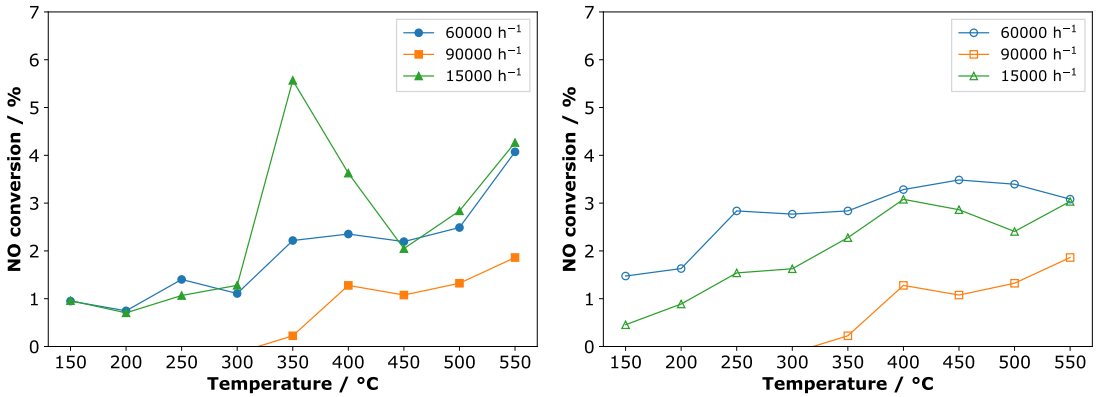

(a) Without $C_{12}H_{26}$. **(b)** With $C_{12}H_{26}$.

Figure 3.8: Effect of the GHSV on the NO oxidation over Cu-SSZ-13. Reaction conditions: 400 ppm NO, 8% O_2, 5% H_2O, 300 ppm $C_{12}H_{26}$ when used, balance argon.

3.3.6 Stability tests

Stability tests (Figure 3.9 and Figure 3.10) shows that at 500 °C, $C_{12}H_{26}$ neither affect NO nor NH_3 conversion, however, at 250 °C, NH_3 conversion started decreased after 20 h of reaction. Since the SCR systems tends to operate at low temperatures, hydrocarbons might affect more the catalysts at low temperatures.

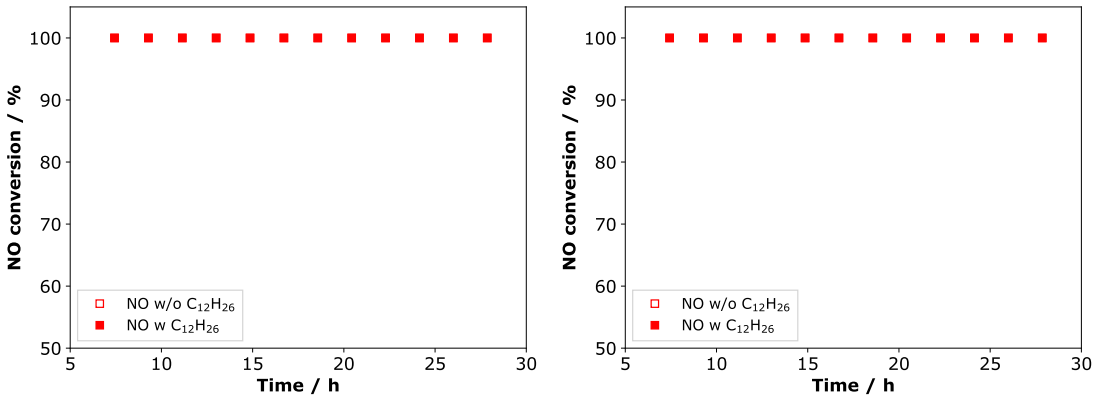

(a) 250 °C. **(b)** 500 °C.

Figure 3.9: Effect of $C_{12}H_{26}$ on the NO conversion in the stability test over Cu-SSZ-13. Reaction conditions: 400 ppm NO, 400 ppm NH_3, 8% O_2, 5% H_2O, 300 ppm $C_{12}H_{26}$ when used, and balance argon. Total flow: 300 mL/min. GHSV = 90000 h^{-1}.

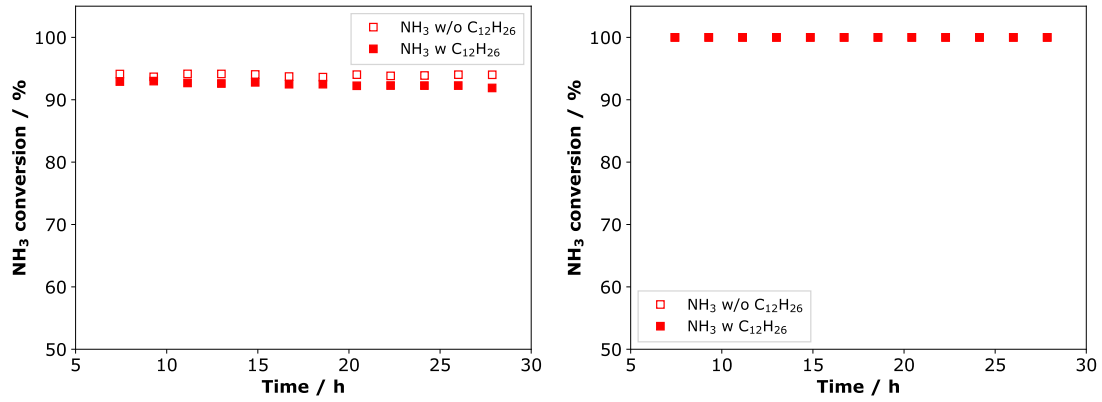

(a) 250 °C **(b)** 500 °C.

Figure 3.10: Effect of $C_{12}H_{26}$ on the NH_3 conversion in the stability test over Cu-SSZ-13. Reaction conditions: 400 ppm NO, 400 ppm NH_3, 8% O_2, 5% H_2O, 300 ppm $C_{12}H_{26}$ when used, and balance argon. Total flow: 300 mL/min. GHSV = 90000 h^{-1}.

3.3.7 Monolith testing

Table 3.1 shows that the monoliths had low mechanical resistance, because, the ultrasound test removed 26.3% of the coating; they resisted temperature changes since the coating mass loss was less than 3%. The monolith we synthesized can resist the changes in temperature that occur in a diesel engine (e.g., when turning on the engine), however, if the engine suffers abrupt movements, it can cause detaching the coating from the surface. Regarding the catalytic activity, Figure 3.11 shows that the monolith hadlittle activity in the NH_3-SCR of NO reaction, probably because of the low amount of coating, which represents a low availability of active sites for the reaction. So far, we did not perform any other experiments to improve the synthesis of the monolith and focused on working with powder studying other conditions to understand better the effect of HC on the catalysts. For improving the catalytic activity of the monolith, more tests such as changing the binder, the amount of catalyst, the amount of coating in the monolith or the copper loading in the catalyst should be performed to find the best conditions that represent in a better catalytic activity of the monolith.

Table 3.1: Monolith mass loss in the mechanical and thermal test.

Test	Mass loss respect to coating / %	Mass loss respect to monolith / %
Mechanical	26.3	5.2
Thermal	2.2	0.3

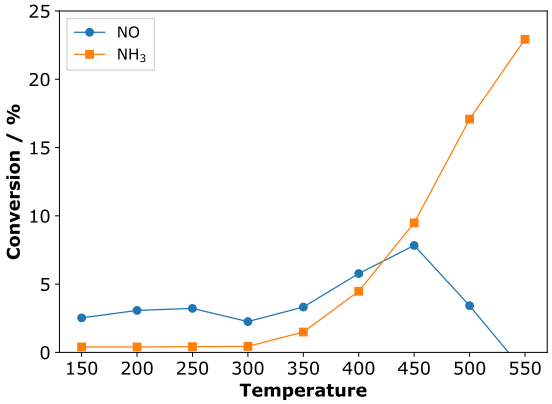

Figure 3.11: Conversion of NO and NH_3 in the NH_3-SCR of NO of the 1.2Cu-ZSM-5 monolith. Reaction conditions: 400 ppm NO, 400 ppm NH_3, 8% O_2, 5% H_2O, balance argon. GHSV = 60000 h^{-1}.

3.4 Partial conclusions

We synthesized Cu-ZSM-5 and Cu-SSZ-13 catalysts and found that $C_{12}H_{26}$ reduced the conversion of both NO and NH_3 in both catalysts. Since Cu-SSZ-13 is the most promising catalyst for using in the NH_3-SCR of NO_X we performed a series of experiments for understanding the effect of $C_{12}H_{26}$ on several reactions. We concluded that $C_{12}H_{26}$ affects the catalytic activity of Cu-SSZ-13 in the NH_3-SCR of NO and the NH_3 oxidation. Our results suggested that NH_3 and $C_{12}H_{26}$ may react at high temperature and reduce NH_3 to selectively reacts with NO. We also observed that the effect is more notable at the highest GHSV studied (150000 h^{-1}).

Chapter 4

Effect of HCs on the kinetic of NH_3-SCR over Cu-based zeolites

In this chapter, we studied the effect of a short- and long-chain hydrocarbon (C_3H_6 and $C_{12}H_{26}$) on the catalytic activity, NH_3 adsorption, stability, and kinetics in a small- and a medium-por zeolites (Cu-ZSM-5 and Cu-SSZ-13). Performing temperature programmed desorption experiments of NH_3 together with hydrocarbons, C_3H_6 reduced more the amount of NH_3 desorbed in the TPD compared with the NH_3-TPD alone. Also, C_3H_6 reduced more the catalytic activity of the catalysts around 350 °C. Finally, the kinetics experiments showed that both hydrocarbons, $C_{12}H_{26}$, and C_3H_6, affected the parameters of a power-law reaction rate meanly that HCs can affect the mechanism in the NH_3-SCR of NO on Cu-ZSM-5 and Cu-SSZ-13.

4.1 Introduction

Diesel engines have a wide usage in transportation [58] but emit more nitrogen oxides than their gasoline counterparts [59]. As environmental concerns about the diesel engine emissions are increasing, studying them under more realistic conditions is vital to accomplish the more stringent legislation [124]. Despite the NH_3-SCR of NO_X [19] being the leading technique for the abatement of NO_X, it needs to overcome some problems to work properly.

Including hydrocarbons into the probe exhaust gas makes the process more realistic [54]. Hydrocarbons can be present in the exhaust of a diesel engine if they are unburnt in the cold start or long idling states of the engine [55]. The presence of hydrocarbons in the NH_3-SCR of NO_X system could affect catalyst performance [43]. Reports in the literature that study the effect of hydrocarbons on the catalysts used in the NH_3-SCR of NO_X focused on how they reduced the catalytic activity by measuring conversions [13, 20, 43, 46–50, 53–55, 122] and how they reduced the adsorption of NH_3 by performing temperature-programmed desorption experiments [13, 20, 46, 48, 51, 52, 54, 55, 70]. Studies about the effect of hydrocarbons on the NH_3-SCR of NO kinetics and catalyst durability are still missing. Studies that deal with the NH_3-SCR of NO kinetics over Cu-based zeolites have reported both polynomic [125–128], Langmuir-Hinshelwood [85, 129–132], and Eley-Rideal [133, 134] approaches. However, as mentioned before, those studies do not include hydrocarbons in their analysis.

This chapter aimed to study two catalysts—Cu-ZSM-5 and Cu-SSZ-13—under the presence of hydrocarbons—C_3H_6 and $C_{12}H_{26}$—in the NH_3-SCR of NO by evaluating their adsorption of NH_3 in TPD experiments, their catalytic activity, orders of reaction of a polynomial kinetics, and stability tests.

4.2 Materials and methods

4.2.1 Catalyst synthesis and characterization

The Cu-ZSM-5 catalysts was synthesized by the ion-exchange as in Subsection 2.2.1.1 and the Cu-SSZ-13 as in Subsection 3.2.1.

XRD patterns were recorded in a PANalytical Empyrean diffractometer in the range of 5–60° with CuKα wavelength 0.179 nm, in 0.032°/min steps. Copper content was obtained by atomic absorption.

4.2.2 Bench reactor

Subsection 3.2.3 depicts the bench reactor used for determining the kinetic parameters of the catalysts in the NH_3-SCR of NO with and without C_3H_6 and $C_{12}H_{26}$, adsorption/desorption and durability experiments.

4.2.3 Adsorption/desorption experiments

The sample (previously pelletized, grinded, and granulated to sieve 80–120) was pretreated at 450 °C for 1.5 h in 500 mL/min 20% O_2/Argon. It was cooled to 50 °C to saturate it with either 1000 ppm NH_3, 1000 ppm C_3H_6, or 1000 ppm NH_3 + 1000 ppm C_3H_6 for 3 hours. When using $C_{12}H_{26}$, the catalyst was first saturated with 150 ppm $C_{12}H_{26}$ for 4 h, and then with 1000 ppm NH_3 for 3 h. After saturating the catalyst, it was flushed with 200 mL/min Ar for 4 h to perform the TPD at a heating rate of 10 °C/min to 700 °C. The amount of the compounds desorbed from the surface was calculated using Equation 2.1, but the flow of argon replaces the flow of nitrogen.

4.2.4 Catalytic activity

The catalysts were pelletized at 15000 lb for 15 min, crushed in a ceramic mortar with a pestle, and sieved to mesh size 30–40 (420–595 μm). Typically, 100 mg of catalyst was pretreated at 450 °C in 500 mL/min of synthetic air (20% O_2/N_2) for 1 h with a heating rate of 10 °C/min. It was cooled down to room temperature to start the reaction. The gases mixture flow was 200 mL/min (400 ppm NO, 400 ppm, 8% O_2, 5% H_2O, 300 ppm C_3H_6 or 200 ppm $C_{12}H_{26}$ (when used), and balance argon). The gas flow stabilized for 4 h, and the temperature was increased in steps of 50 °C from room temperature to 550 °C with a stabilization time of 2 h at each temperature. The concentrations were measured by FTIR spectroscopy in an Antaris IGS with a 200 mL and 2 m cell at 150 °C, and a cooled MCT detector. Conversions were calculated by Equation 3.3.

4.2.5 Stability experiments

Chapter 3 presents the NH_3-SCR of NO in the catalysts up to 30 h when subjected to $C_{12}H_{26}$ and show that it reduced the NO conversion of Cu-ZSM-5, but it unaffected that of the Cu-SSZ-13. The stability results section report the stability of the catalysts in the NH_3-SCR of NO reaction when subjected to C_3H_6 up to 35 h and compare to the stability results obtained in Chapter 3.

4.2.5.1 Mass transfer limitations

We studied the external mass transfer limitations by measuring the reaction rate, maintaining the flow to the mass of catalyst ratio constant, and the internal mass transfer

limitations by measuring the reaction rate at several particle sizes. We diluted the catalyst with SiC (silicon carbide)—an inert material previously tested in our laboratory with no activity in the SCR reaction— to dispersed the sample over the reactor to avoid axial gradients of concentration and temperature spots. We also assured differential conditions, working at conversions less than 15%. The regime without changes in reaction rate with respect to the GHSV and the particle size assures working at free mass transfer limitations. Equations 4.1–4.14 are the set of equations to calculate the reaction rates at each condition. ML is the metal loading, MC is the metal composition, and m is the catalyst mass, TMS is the total metal surface, N_{NOx} is the nitrogen lost from NO_X, N_{NH_3} is the nitrogen lost from NH_3, NO_C is the NO converted, $NH_{3,\,C}$ is the NH_3 converted, $NO_{2,\,C}$ is the NO_2 converted, $N_{2,\,NO}$ is the nitrogen from NO, $N_{2,\,NH_3}$ is the nitrogen from NH_3, X_{NO} is the NO conversion, X_{NH_3} is the NH_3 conversion, S_{N_2O} is the N_2O selectivity, $F_{N_{2,\,in}}$ is the flow of nitrogen at the inlet, r_M is the rate measured, and TOR is the turnover rate.

$$ML = \frac{MC \cdot m}{100} \tag{4.1}$$

$$TMS = \frac{m \cdot *D}{100 \cdot MW_{Cu}} \tag{4.2}$$

$$N_{NOx} = [\mathrm{NO}]_{\mathrm{in}} + [\mathrm{NO_2}]_{\mathrm{in}} - [\mathrm{NO}]_{\mathrm{out}} - [\mathrm{NO_2}]_{\mathrm{out}} \tag{4.3}$$

$$N_{NH_3} = [\mathrm{NH_3}]_{\mathrm{in}} - [\mathrm{NH_3}]_{\mathrm{out}} \tag{4.4}$$

$$NO_C = [\mathrm{NO}]_{\mathrm{in}} - [\mathrm{NO}]_{\mathrm{out}} \tag{4.5}$$

$$NH_{3,\,C} = [\mathrm{NH_3}]_{\mathrm{in}} - [\mathrm{NH_3}]_{\mathrm{out}} \tag{4.6}$$

$$NO_{2,\,C} = [\mathrm{NO_2}]_{\mathrm{in}} - [\mathrm{NO_2}]_{\mathrm{out}} \tag{4.7}$$

$$N_{2,\,NO} = NO_C - NO_{2,\,C} \tag{4.8}$$

$$N_{2,\,NH_3} = NH_{3,\,C} - 2 \cdot NO_{2,\,C} \tag{4.9}$$

$$X_{NO} = \frac{NO_C}{[\mathrm{NO}]_{\mathrm{in}}} \cdot 100\% \tag{4.10}$$

$$X_{NH_3} = \frac{NH_3,\ C}{[\mathrm{NH_3}]_{\mathrm{in}}} \cdot 100\% \tag{4.11}$$

$$S_{N_2O} = \left(\frac{[\mathrm{N_2O}]_{\mathrm{out}} - [\mathrm{N_2O}]_{\mathrm{in}}}{N_{NOx}} \right) \cdot 100\% \tag{4.12}$$

$$F_{N_{2,\ in}} = \frac{N_{2,\ NO} \cdot F}{1 \cdot 10^6} \tag{4.13}$$

$$r_M = \frac{F_{N_{2,\ in}} \cdot 101.325kPa}{\frac{60s}{min} \cdot 1000 \cdot 8.314 \frac{J}{mol \cdot K} \cdot 298K \cdot ML} \tag{4.14}$$

4.2.6 kinetic studies

The TOR (turnover rates) method helps to find the kinetic parameters. Equation 4.15 defines how to calculate the TOR: it considers all the active sites identical and allows data comparison with different catalysts in different laboratories [135]. Equation 4.16 calculates the TOR from the reaction measured (r_M) and total metal surface values (TMS).

$$TOR = \frac{(\text{Number of molecules reacted})}{(\text{Number of sites}) \cdot (\text{time})} \tag{4.15}$$

$$TOR = \frac{r_M}{TMS} \tag{4.16}$$

4.2.6.1 Apparent activation energy

We obtained the apparent activation energy by measuring the TOR at the reaction conditions (avoiding mass transfer limitations) of 400 ppm NO, 400 ppm NH_3, 8% O_2, 5% H_2O, argon as balance, and 300 ppm $C_{12}H_{26}$ or 300 ppm C_3H_6. The temperatures ranged around 250 °C for Cu-SSZ-13 and 400 °C for Cu-ZSM-5, and the slope of the plot of $\ln(TOR)$ vs. T^{-1} gives the apparent activation energy according to Equation 4.17.

$$E_a = -slope \cdot R \tag{4.17}$$

4.2.6.2 Kinetic equation

The reaction rate of the NH_3-SCR of NO used in this thesis was a power-law model according to Equation 4.18, where R_{SCR} is the reaction rate of NO; [NO], [NH_3], and [O_2] are the concentrations of NO, NH_3, and O_2, respectively; α, β, and γ are the power-dependency of NO, NH_3, and O_2, respectively; and E_a is the apparent activation energy. This power-law rate equation has been studied in other works [125, 133, 136] as a way

to determine a global dependency of the reaction rate with the concentration of the reactants without taking into account the mechanism, which could include hundreds or even thousands of reactions.

$$-R_{SCR} = A_0 \exp\left(\frac{-E_a}{RT}\right) \cdot [NO]^{\alpha}[NH_3]^{\beta}[O_2]^{\gamma} \tag{4.18}$$

We calculated the orders of the reaction by changing the initial concentrations of the compound of interest, maintaining the others constant. The concentration of NH_3 and NO were varied from 200–600 ppm and the concentrations for O_2 were varied from 2–20%. The slope of the plot of $\ln(TOR)$ vs. $\ln(\text{concentration})$ gives the order of the reaction. We performed the reaction at 400 °C and 250 °C for Cu-ZSM-5 and Cu-SSZ-13, respectively, which yields conversions less than 20%.

4.3 Results and discussion

4.3.1 Catalyst characterization

Subsection 3.3.1 shows the results of the XRD patterns and the Cu content for the Cu-SSZ-13 and Subsection 2.2.1.1 the one of the Cu-ZSM-5.

4.3.2 Adsorption/desorption experiments

The TPD profiles of the Cu-ZSM-5 (Figure 4.1) show that the NH_3 alone adsorbed onto three acid sites: at around 200 °C, which regards to weak acid sites, including Lewis acid sites [106], at around 270 °C, which corresponds to Lewis acid sites from Cu [106], and around 390 °C, which regards to strongly bound NH_3 probably on Brønsted acid sites [109, 110]. When performing the adsorption with HCs, the peak around 200 °C decreased by the presence of both C_3H_6 and $C_{12}H_{26}$, however the peak around 390 °C was only affected by C_3H_6. When performing the TPD with a mixture of NH_3 and C_3H_6, the peak at 270 °C was narrower, probably due to a competitive adsorption between NH_3 and C_3H_6. Table 4.1 shows that C_3H_6 and $C_{12}H_{26}$ reduced the amount of NH_3 desorbed from Cu-ZSM-5 by 23 and 9%, respectively, suggesting that a short-chain hydrocarbon affects more the adsorption of NH_3 than a long-chain hydrocarbon. Heo et al [46] obtained a decreased in the desorption of NH_3 in the presence of C_3H_6, those values differs probably because the copper content, Heo et al. used a 3.2% Cu and this work used 1.4% Cu in the Cu-ZSM-5 catalyst. Figure 4.1b shows that in the TPD with HC, the Cu-ZSZM-5 catalyst desorbed more $C_{12}H_{26}$ than C_3H_6 probably because $C_{12}H_{26}$ can adsorb on the surface of the catalyst on a different site with respect to NH_3 and C_3H_6. Another possibility is that $C_{12}H_{26}$ which is a liquid at ambient conditions, could condensate if it enters the pores of the Cu-ZSM-5 catalyst at the temperature of adsorption

of 50 °C in a major amount that the C_3H_6, which is a gas. The boiling point of $C_{12}H_{26}$ is 216.2 °C; $C_{12}H_{26}$-TPD profiles (Figure 4.1b), which could be attributed to the evaporation of $C_{12}H_{26}$ from the surface of the catalyst. This result agrees with that of Luo et al. [48] who point out that $C_{12}H_{26}$ could condensate on the surface of a Cu/Beta catalyst. Table 4.1 shows that Cu-ZSM-5 desorbed about 7% more than C_3H_6, but the NH_3 reduced the amount of C_3H_6 at the half, while almost nothing to the $C_{12}H_{26}$.

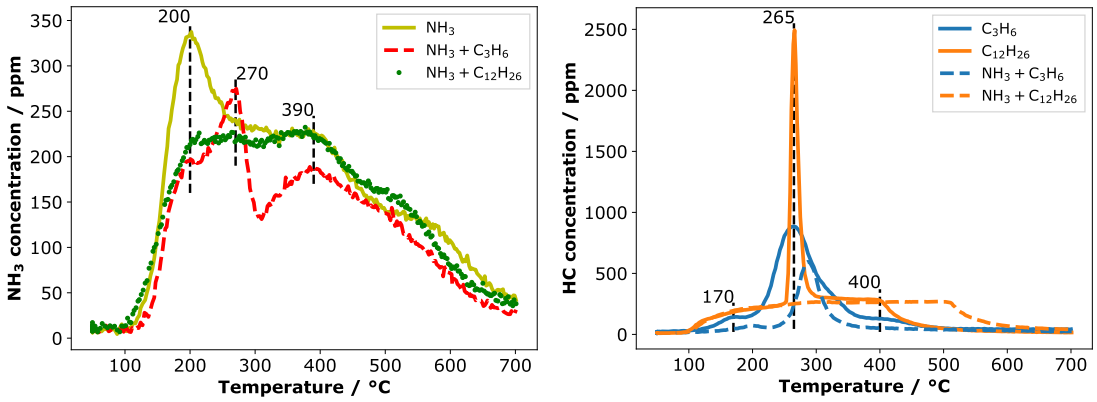

(a) NH_3-TPD **(b)** HC-NH_3-TPD

Figure 4.1: TPD profiles obtained for Cu-ZSM-5.

Table 4.1: Amount desorbed of each compounds from TPD experiments in μmol/g

	NH_3-TPD			C_3H_6-TPD		$C_{12}H_{26}$-TPD	
Catalyst	w/o HC	w/ C_3H_6	w/	w/o NH_3	w/ NH_3	w/o NH_3	w/ NH_3
Cu-ZSM-5	909	696	825	988	449	1059	1003
Cu-SSZ-13	1145	993	1087	942	384	248	218

Regarding the Cu-SSZ-13, Figure 4.2a shows that NH_3 alone desorbed from the catalyst at three peaks: around 190 °C, which corresponds to physically adsorbed NH_3 [52] or weakly bound NH_3 on Lewis acid sites [76], around 320 °C, to medium bound NH_3 probably on Lewis and Brønsted acid sites [52], and around 450 °C, to strongly bound NH_3 probably on Brønsted acid sites [52]. Figure 4.2a shows that $C_{12}H_{26}$ hardly affected the NH_3-TPD profile and C_3H_6 only affected the weakly bound NH_3. Table 4.1 shows that C_3H_6 and $C_{12}H_{26}$ reduced the amount desorbed of NH_3 by 13 and 5%. Those values were lower than the obtained with Cu-ZSM-5 and suggest that the HC affect in major extent the medium-pore size zeolite than the small-pore zeolite. Figure 4.2b shows that C_3H_6 desorbed at three temperatures: around 160 °C, which corresponds to weakly bound C_3H_6 probably on Lewis acid sites [70]: around 280 °C and 350 °C, which could regard to the desorption of C_3H_6 from Cu sites [70]. When NH_3 was on the TPD experiments, the profile of C_3H_6 was affected while the $C_{12}H_{26}$ remained the same. It suggests that C_3H_6 and NH_3 might compete for the same acid sites. Table 4.1 shows that NH_3

reduced the amount of C_3H_6 desorbed from Cu-SSZ-13 by about 60%, while it reduced the amount of $C_{12}H_{26}$ by about 12%.

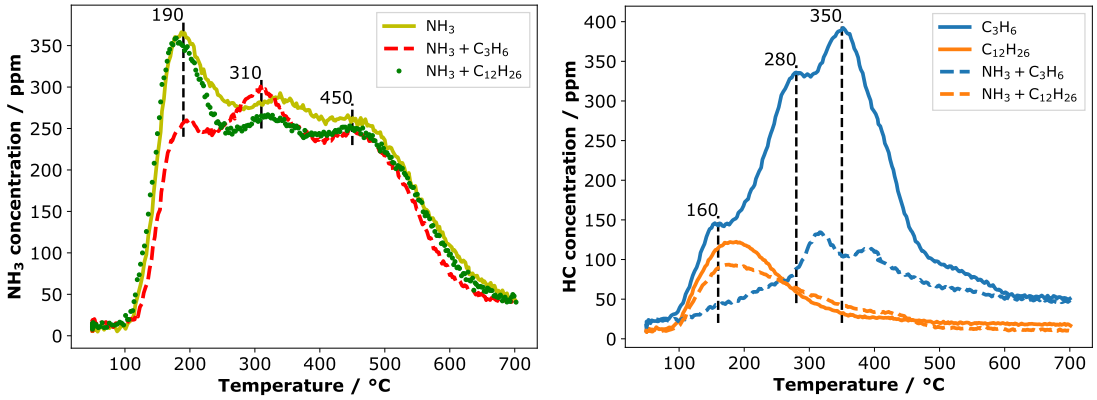

(a) NH_3-TPD **(b)** HC-NH_3-TPD

Figure 4.2: TPD profiles obtained for Cu-SSZ-13.

4.3.3 Catalytic activity

Both Cu-ZSM-5 and Cu-SSZ-13 had similar behavior in the NH_3-SCR of NO without C_3H_6 (Figure 4.3). Both catalysts reached largest NO conversion at 250 °C despite at 200 °C, Cu-SSZ-13 already doubled the NO conversion of Cu-ZSM-5. With Cu-ZSM-5, the NO conversion started decreasing at 500 °C, while Cu-SSZ-13 conversion remained at 100% even at 550 °C. In the C_3H_6-SCR (Figure 4.3), both catalysts behaved similarly: they attained a maximum NO conversion of 40% from 400–450 °C, but at a higher temperature, the conversion decreased more in the Cu-ZSM-5 than in the Cu-SSZ-13. Those results confirmed that both catalysts are effective in reducing NO_X, being Cu-SSZ-13 more active at 200 °C up to 550 °C. Studies in the literature report that the structure of the zeolite is fundamental [110, 137] in the activity for the NH_3-SCR.

Both catalysts presented an s-shaped figure when performing the NH_3-SCR of NO in the presence of C_3H_6, which is related to the competitive adsorption on the catalyst surface as Heo et al. reported [46] and was obtained in the TPD of this work. This competitive adsorption might reduce NO conversion at temperatures below 350 °C, but at higher temperatures the NO conversion started increasing due to C_3H_6-SCR reaction [53]. Figure 4.3 shows that the C_3H_6-SCR reaction starts at 300 °C to a maximum conversion at 400 °C and that $C_{12}H_{26}$ reduced the NO conversion in minor extent than the C_3H_6. This result indicates that long-chain hydrocarbons affect less the NO conversion than a small-chain hydrocarbon and that it affected more a medium-pore zeolite than a large-pore zeolite; the reduction in NO conversion in Cu-SSZ-13 was about 5% and should not be neglected.

$C_{12}H_{26}$ unaffected the NH_3 conversion of both Cu-ZSM-5 and Cu-SSZ-13 in the NH_3-SCR of NO (Figure 4.4). NH_3 could also react with oxygen to produce NO or nitrogen, or react with $C_{12}H_{26}$ to produce ammoxidation products [46]. However, C_3H_6 affects little the NH_3 probably because it can take part in the C_3H_6-SCR, which avoid of NH_3 reacting with NO at temperatures around 250 °C.

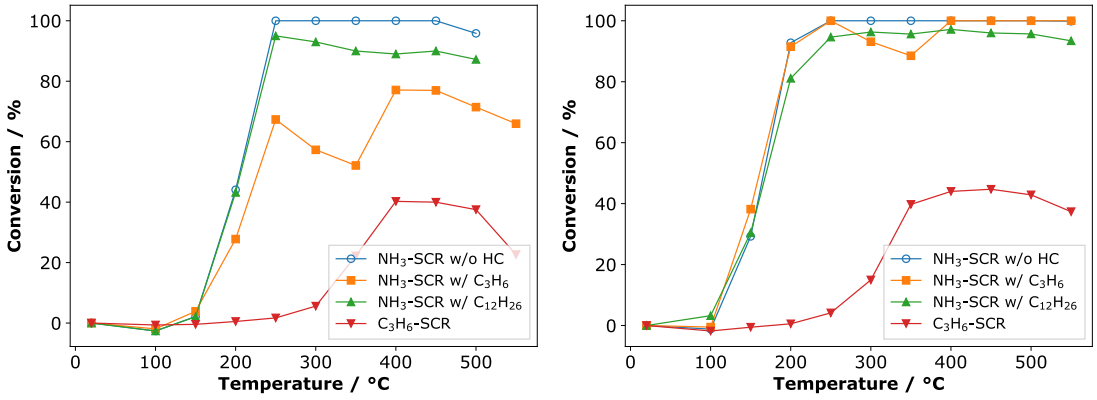

(a) Cu-ZSM-5 **(b)** Cu-SSZ-13

Figure 4.3: Effect of C_3H_6 on the NO conversion of Cu-based zeolites in the NH_3-SCR of NO.

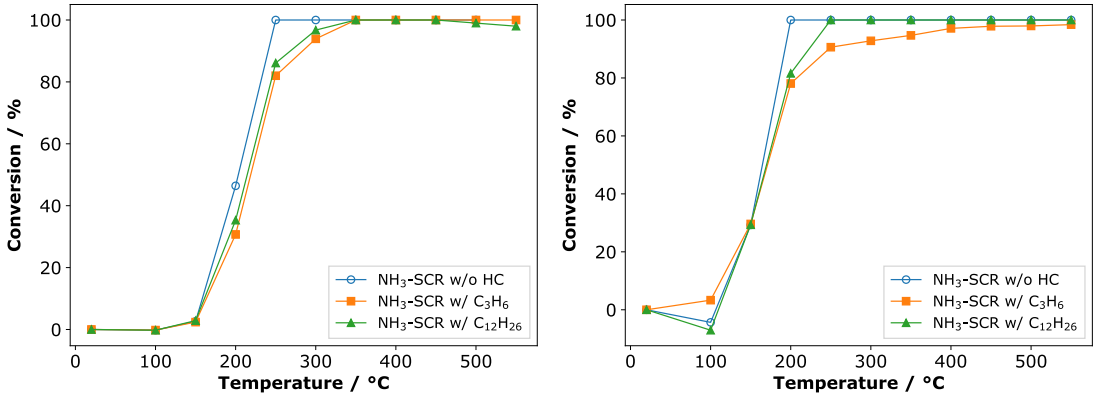

(a) Cu-ZSM-5 **(b)** Cu-SSZ-13

Figure 4.4: Effect of C_3H_6 on the NH_3 conversion of Cu-based zeolites in the NH_3-SCR of NO.

4.3.4 Stability in the presence of C_3H_6 and $C_{12}H_{26}$

Figure 4.5a shows that the NO and NH_3 conversions of Cu-ZSM-5 in the NH_3-SCR of NO in the presence of C_3H_6 decreased by 60 and 75%, respectively and continue decreasing with time. In the presence of $C_{12}H_{26}$ the NO and NH_3 conversions decreased by 30 and 50% and continue decreasing with time. Figure 4.5b shows the NO and NH_3 conversions of Cu-SSZ-13 decreased by 3 and 5% and stayed stable up to 30 h. This result demonstrates that Cu-SSZ-13 is more resistant to HC than Cu-ZSM-5 even for long periods, but in the presence of hydrocarbons for an extended period, it might suffer

deactivation. This problem could occur in a diesel vehicle with an old diesel oxidation catalyst or long idling periods or cold start, in which unburnt hydrocarbons can be present in the catalyst. If the engine runs for extended periods, the catalyst in the NH_3-SCR of NO system could lose activity and release NO_X and NH_3 into the atmosphere. Most of the studies about the effect of HCs do not report stability experiments, which could be a vital parameter since an engine could be run for hours and be subject to hydrocarbon poisoning.

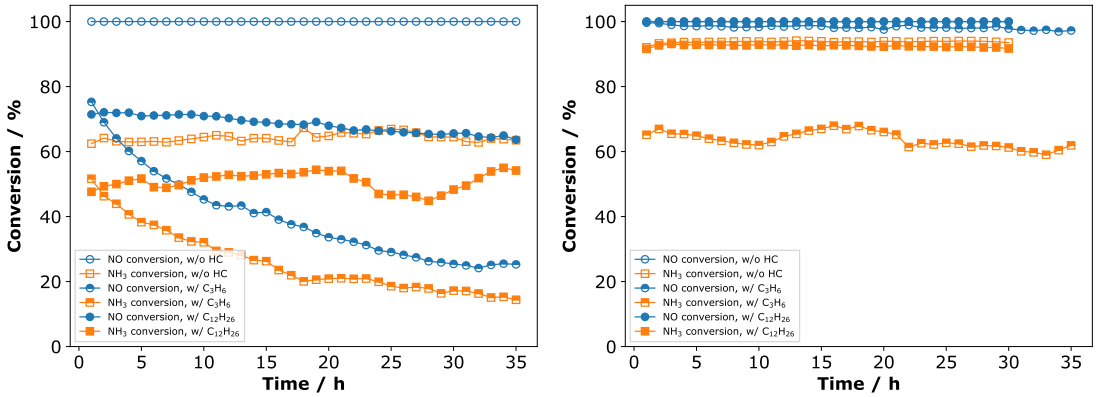

(a) Cu-ZSM-5 **(b)** Cu-SSZ-13

Figure 4.5: Effect of C_3H_6 on the catalytic activity of Cu-ZSM-5 in a reaction up to 35 h. Reaction conditions: 400 ppm NO, 400 ppm NH_3, 8% O_2, 5% H_2O, 300 ppm C_3H_6, and balance argon

4.3.5 Mass transfer limitations

According to Figure 4.6a, for gas flows higher than 450 mL/min let to decreased the external mass transfer limitations since no appreciable changes are observed in the NO reaction rate. Similarly, Figure 4.6b shows that for particle sizes above 194 μm, the reaction rate is almost equal. So, for finding the kinetic parameters, we decided to work under the conditions that Table 4.2 shows, which corresponds to a regime under free mass transfer limitations. These values correspond to GHSV of 9000000 and 4500000 h^{-1}. The higher mass in Cu-SSZ-13 was because it is less dense than Cu-ZSM-5, so we needed to weight more mass to have a good dispersion in the diluent. Table 4.2 also shows the Weisz-Prater number calculated with the equations in Appendix D. The Weisz-Prater numbers below 0.3 confirms that our system is free of internal mass transfer limitation [138].

Table 4.2: Conditions used for each catalyst for determining the kinetic parameters that ensure reactions without mass transfer limitations.

Catalyst	Flow / mL min^{-1}	Mass / mg	T / °C	Particle size / μm	Weisz-Prater number
Cu-ZSM-5	450	1.5	400	151	0.04
Cu-SSZ-13	450	3.0	250	151	0.01

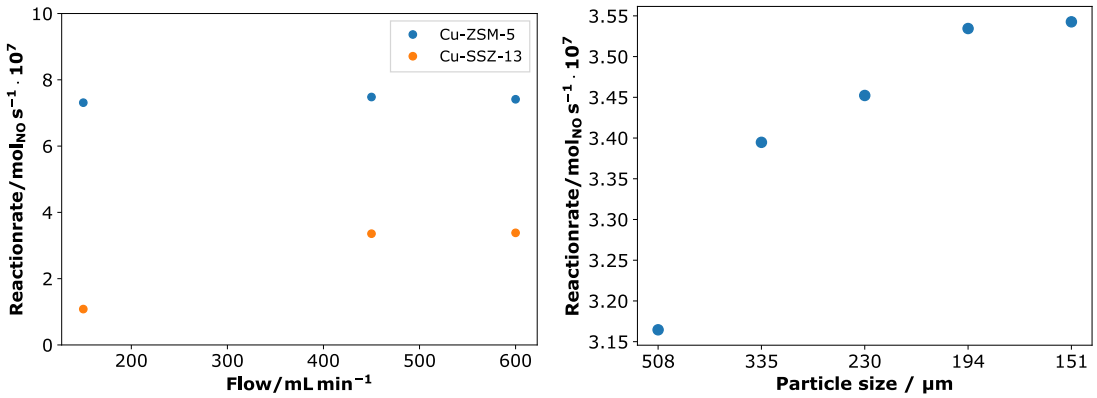

(a) External **(b)** Internal

Figure 4.6: Plots for the study of mass transfer limitations on Cu-based zeolites.

4.3.6 Apparent activation energies

Table 4.3 shows that hydrocarbons changed the apparent activation energies of the catalysts when present in the NH_3-SCR of NO reaction. The higher value of Cu-ZSM-5 is because we measured at a higher temperature than the measured in the Cu-SSZ-13. $C_{12}H_{26}$ reduced the apparent activation energy of Cu-ZSM-5 and Cu-SSZ-13 by 19 and 45%, respectively, while the C_3H_6 reduced the apparent activation energy by 78 and 2%. Interestingly, dodecane reduced more the apparent activation energy in Cu-SSZ-13 than in Cu-ZSM-5, but it influenced little on the adsorption, so it suggest that $C_{12}H_{26}$ might change the mechanism of the NH_3-SCR of NO in both, Cu-ZSM-5 and Cu-SSZ-13 at the studied temperatures. For the case of C_3H_6, at the temperature of 250 °C, the reaction mechanism of the NH_3-SCR of NO could remain the same in Cu-SSZ-13 due to that the apparent activation energy remains unchanged and as Figure 4.3b shows no change in NO conversion at 250 °C with the presence of C_3H_6. C_3H_6 reduced more the apparent activation energy of Cu-ZSM-5 than $C_{12}H_{26}$ due to probable reactions of C_3H_6 with NH_3 at 400 °C, as C_3H_6 reduced more the catalytic activity.

Table 4.3: Apparent activation energy in kJ mol^{-1} of the catalysts.

Catalyst	Parameter	Without HC	With $C_{12}H_{26}$	With C_3H_6
Cu-ZSM-5	E_a	72.9	58.9	16.1
	α	0.5	0.4	0.3
	β	0.0	0.3	0.1
	γ	0.5	0.6	0.5
Cu-SSZ-13	E_a	42.3	22.9	41.3
	α	0.5	0.7	0.4
	β	−0.1	−0.1	0.0
	γ	0.2	0.2	0.3

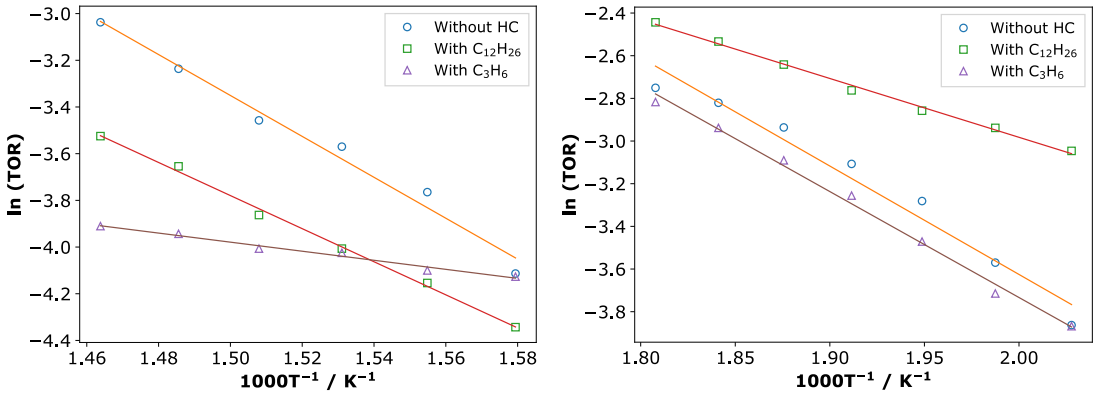

(a) Cu-ZSM-5 **(b)** Cu-SSZ-13

Figure 4.7: Arrhenius plots of the effect of HCs on the apparent activation energy of Cu-based zeolites.

4.3.7 Orders of reaction

The orders of reaction of the Cu-ZSM-5 and Cu-SSZ-13 in the NH_3-SCR of NO reaction showed several behaviors (Figures 4.8–4.10). The orders or reaction with respect to NO were from 0.3–0.7, reports in the literature for Cu-based zeolites range from 0.7–1.0 [125, 133, 136]. The low values obtained could be due to the high GHSVs or an imperfect contact between the reactants and the catalyst. According to Table 4.3, $C_{12}H_{26}$ decreased the order of reaction of NO in Cu-ZSM-5, but the change considering the $C_{12}H_{26}$ was not significant and could stay in the experimental error; C_3H_6, reduced the order of NO, which confirms that more C_3H_6 might cause more reactions in the mechanism and for that reason decreased the NO order of reaction. Regarding the Cu-SSZ-13, the $C_{12}H_{26}$ increased the NO order of reaction, and C_3H_6 decreased it. It means that $C_{12}H_{26}$ increased the rate of the reaction quickly in the NH_3-SCR of NO and $C_{12}H_{26}$ can influence a reaction that favor the production of N_2.

The orders of reaction concerning NH_3 ranged from slightly negative to zero, as reported in the literature [125, 133, 136]. We obtained comparable results for the catalysts in the NH_3-SCR of NO, but they changed in the presence of hydrocarbons. For the case of the ZSM-5, $C_{12}H_{26}$ increased the NH_3 order of reaction due to an increase of NH_3 coverage as Delahay [133] reported. It could confirm a reaction of NH_3 that may produce N_2 and increase the reaction rate. Regarding the Cu-SSZ-13, the orders of reaction for NH_3 remained unchanged, which confirms that C_3H_6 did not affect the catalytic activity of the Cu-SSZ-13 in the NH_3-SCR of NO reaction at 250 °C.

Other kinetics of SCR reaction, such as the reported by Stevenson et al. [129] (4.19) and Delahay et al. [133] (Eq. 4.20), fit acceptably to data of the Cu-ZSM-5.

$$r_{N_2} = \frac{k_{SCR}[NO][O_2]}{1 + K_a[NH_3]} + \frac{k_{ox}K_a[NH_3]}{1 + K_a[NH_3]} + k_O[NO] \tag{4.19}$$

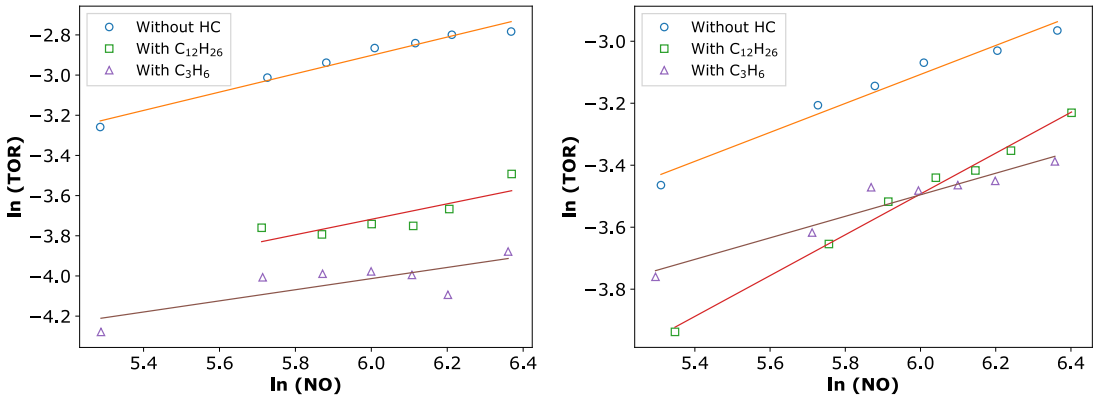

(a) Cu-ZSM-5 **(b)** Cu-SSZ-13

Figure 4.8: Plots for determining the order of reaction respect to NO for Cu-based zeolites on the NH_3-SCR of NO.

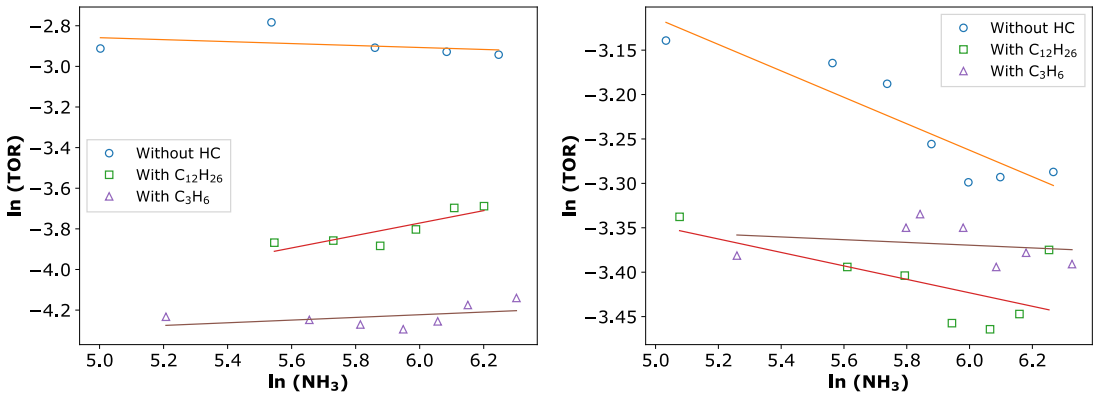

(a) Cu-ZSM-5 **(b)** Cu-SSZ-13

Figure 4.9: Plots for determining the order of reaction respect to NH_3 for Cu-based zeolites on the NH_3-SCR of NO.

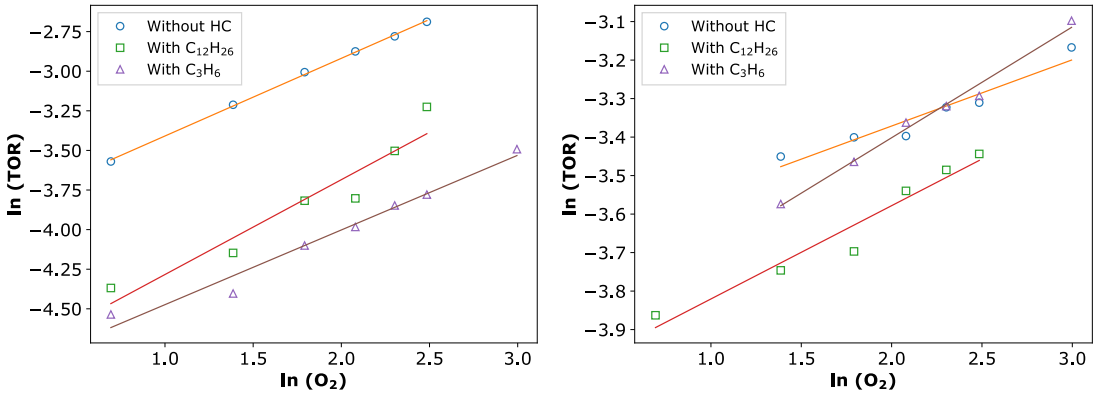

(a) Cu-ZSM-5 **(b)** Cu-SSZ-13

Figure 4.10: Plots for determining the order of reaction respect to O_2 for Cu-based zeolites on the NH_3-SCR of NO.

$$r = k_2\theta_2 P_{NO} = \frac{4k_1k_2k_3P_{O_2}P_{NO}P_{NH_3}}{k_2k_3P_{NO}P_{NH_3} + 4k_1k_3P_{O_2}P_{NH_3} + 4k_1k_2P_{O_2}P_{NO}} \tag{4.20}$$

4.4 Partial conclusions

We synthesized two Cu-base zeolites—CuZSM-5 and Cu-SSZ-13—to study the effect of a short-chain hydrocarbon (C_3H_6) and a long-chain hydrocarbon ($C_{12}H_{26}$) by performing experiments of catalytic activity, temperature-programmed desorption of NH_3 and determination of the parameters of a power-law kinetics. We concluded that the decreased in catalytic activity in the catalysts could be occasioned by the competitive adsorption of the HC with NH_3, since the C_3H_6 reduced more both, the catalytic activity in the NH_3-SCR of NO reaction and the amount of NH_3 desorbed in the NH_3-TPD. From the kinetics, we concluded that both C_3H_6 and $C_{12}H_{26}$ probably change the mechanism of the NH_3-SCR of NO reaction of Cu-ZSM-5 and Cu-SSZ-13, since the activation energy changed when performing the reaction with the HCs. We propose that NH_3 could react with C_3H_6 or even $C_{12}H_{26}$ at 250 °C and 400 °C for Cu-SSZ-13 and Cu-ZSM-5 because we measured changes in the order of reaction.

Chapter 5

General conclusions, limitations and recommendations

5.1 General conclusions

We studied hydrocarbons (C_3H_6 and $C_{12}H_{26}$), catalysts (Cu-ZSM-5, Cu-SSZ-13, Cu-SAPO-34) that have been used successfully in the NH_3-SCR of NO_X, in various kind of experiments: in Chapter 2 we studied the Cu-based ZSM-5 and Cu-SAPO-34 catalysts to determine how much C_3H_6 affects the adsorption of NH_3 on the catalysts; in Chapter 3 we studied the most promising catalyst—Cu-SSZ-13— to several reactions in the presence of $C_{12}H_{26}$, and finally, in Chapter 4 we studied the kinetic of both, Cu-ZSM-5 and Cu-SSZ-13 in the presence of C_3H_6 and $C_{12}H_{26}$. We found that all the hydrocarbons tested affected in different extents the catalysts we studied. Saturating the Cu-based ZSM-5 and Cu-SAPO-34 catalysts with C_3H_6 reduced the amount of NH_3 adsorbed and changes the parameters of the kinetic of the desorption. We also proved that despite of $C_{12}H_{26}$ being a long-chain hydrocarbon and Cu-SSZ-13 a small-pore zeolite, $C_{12}H_{26}$ reduced the catalytic activity and of Cu-SSZ-13 in NH_3 oxidation and NH_3-SCR of NO reactions at high temperature but it has a decent resistance to $C_{12}H_{26}$ at the temperature with the best NO conversion. Finally, we determine the parameters of a power-law kinetic in the presence of C_3H_6 and $C_{12}H_{26}$ to Cu-ZSM-5 and Cu-SSZ-13 catalysts and found that both can change the apparent activation energy and the orders of reaction with respect to NO and NH_3. From those results, we finally conclude that for designing NH_3-SCR of NO_X systems it is vital to take into account the changes in the kinetic of both the adsorption and reaction of the catalysts. That means, it changes the mechanism of the reaction and for detail kinetics, to take into account the adsorption and desorption kinetic has to evaluate the parameters that affect the final design of reactor.

5.2 Limitations

To develop this thesis, we had several problems that avoid studying more profoundly and in a better way the topics treated. In Chapter 2, we intended to have an idea of how propylene affect the kinetic of the adsorption of Cu-based catalysts with different pore size (ZSM-5 and SAPO-34), however, the SAPO-34 was not stable. We detect a tremendous change in surface area after the ion exchange with copper. We also performed ammonia temperature programmed desorption of ammonia experiments and found changes in one month span of measurements, so for improving the analysis is better idea to study the synthesis of SAPO-34 to obtain a more stable catalyst. Also, we started from a kinetic of desorption that consider ammonia adsorb in two acid sites. Despite we obtained a decent fitting with two sites, we extend the kinetic to three sites and obtained better fit. However, the computation time last about one and a half week for the first fitting in a i5 second generation Windows 10 computer. One of the major contributions of this thesis was to study the effect of n-dodecane but we intended to study an aromatic hydrocarbon (toluene) and longer-chain hydrocarbons (C_{15}–C_{18}) as more realistic surrogate for diesel. We tried to make the experimental setup, but due low or high volatility, it was difficult to carried out the experiments. One of the first objectives, was to work with a monolithic catalyst, however despite the mechanical and thermal tests, had decent results, the catalytic activity was poor. We did not have time to try improving the synthesis or the money to buy a commercial monolith.

5.3 Recommendations

This thesis is a first approach to study the effect of hydrocarbons in the NH_3-SCR of NO, however, we recommend the following to have a better understanding of the whole process:

- Characterizes more the catalysts. For example, Nuclear magnetic resonance will be helpful to determine if treatment with hydrocarbons can change the structure of the Cu zeolites. X-ray absorption spectroscopy to determine how hydrocarbons change the surroundings of the active sites;
- to perform more studies in situ and in operando to, for example, infrared to have an idea of the functional groups on the surface that would let to better proposed a mechanism of the NH_3-SCR of NO reaction in the presence of hydrocarbons;
- extend the kinetic of the desorption of NH_3 on the catalyst to three sites and take the necessary time for the fitting and simulations;
- improve monolith preparation by preparing a better slurry or increase the copper content in the catalyst;

- to determine the effect of HC by more studies, such as, XPS to verify changes in the oxidation state of the catalysts, pyridine FT-IR to verify if hydrocarbons affect more the Lewis of Brønsted acid sites, chemisorption to determine the dispersion of the catalysts and if it has an effect on the way hydrocarbons affect the catalysts, for example, to answer the question if HCs affect more catalysts with better dispersion, this would help to look for alternatives in the synthesis to improve the resulting catalysts;
- test an aromatic surrogate like toluene for performing the experiment delt in this thesis and the proposed in this section;
- to study the Si:Al ratio in the catalysts, since it gives an idea of the acidity of the catalysts, hydrocarbons may affect in different ways catalysts with different Si:Al ratio due to their capacities to adsorb NH_3;
- to include water in the adsorption studies, as it is reported to have an effect on the adsorption of NH_3 on the catalyst [54], it would have an effect on the adsorption of HCs;
- nowadays, with the increasing of data science, it would interesting to formulate an experimental design to evaluate how factors such as Si:Al ratio, Cu content, catalyst synthesis, type of catalyst on the response that would be the amount of NH_3 and HC adsorbed;
- since it is reported that the catalysts can adsorb carbonaceous materials, we recommend to study the adsorption of HC under oxidizing conditions.

Appendix A

Calibration of equipment

A.1 Mass flow controllers calibration

We calibrated the mass flow controllers (MFCs) by registering the flow at several setpoints. We measured the flow by taking the time a soap bubble ascends through a defined volume of a burette with Equation A.1; where F is the flow in mL/min, V is the volume of the burette in mL, and t is the time in seconds. Figure A.1 shows that the flow of the MFC depends linearly on the setpoint as expected. We combined all the functions of the MFCs with the concentrations of the gas cylinders, and temperature of the gas wash bottles for obtaining the flow for ensuring the desired concentrations.

$$F = \frac{60 \cdot V}{t} \tag{A.1}$$

A.2 FT-IR calibration

The FT-IR used was an Antaris IGS FT-IR spectrometer from Thermo Fischer Scientific equipped with a nitrogen cooled MCT detector, a cell with 200 mL of volume and 2 m of pathlength. We calibrated it by taking several spectra of standards via either OMNIC® or Result® software. Each spectrum, which consists of 32 scans, were taken with a 0.5 cm^{-1} resolution. We used the software TQ Analyst® for creating a quantitative method with the spectra taken previously. For methods including compounds without overlapping bands, we used the simple beer's law; for methods including compounds with overlapping bands, we used the PLS (partial least square) analysis type. We ensure performance index of the methods higher than 90%. In some cases, we could not create a methods with all the compounds to measure in the reaction. We created methods of specific compounds and measure the concentrations in the reactions. We save all the spectra of the reaction and reprocess the data with a new method to obtained the concentrations of new compounds. Water was a problem because its spectrum comprehends most of the spectrum range, so we included water in all calibrations to overcome

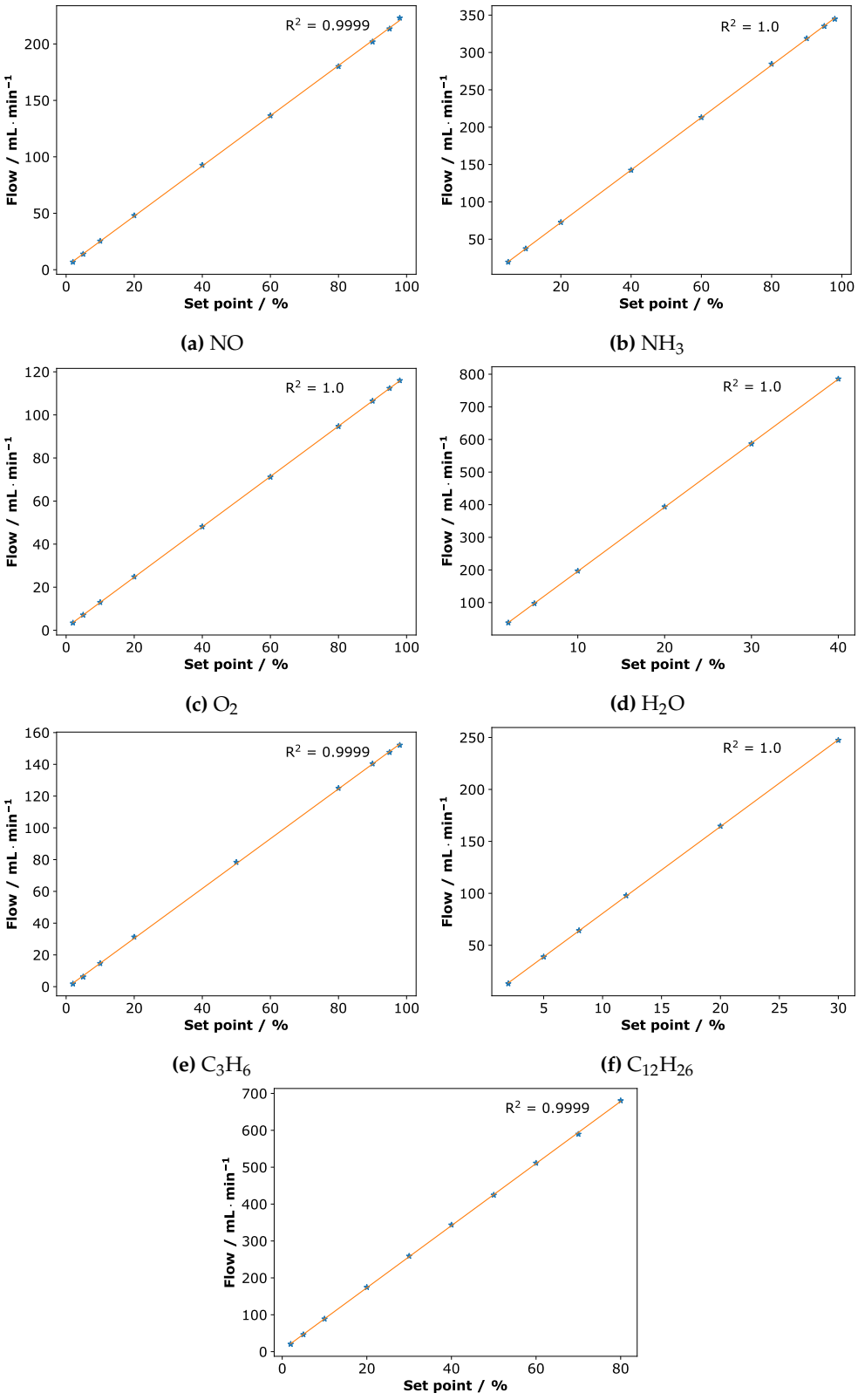

(a) NO **(b)** NH_3

(c) O_2 **(d)** H_2O

(e) C_3H_6 **(f)** $C_{12}H_{26}$

(g) Balance

Figure A.1: Calibration of the mass flow controllers used in the SCR experiments.

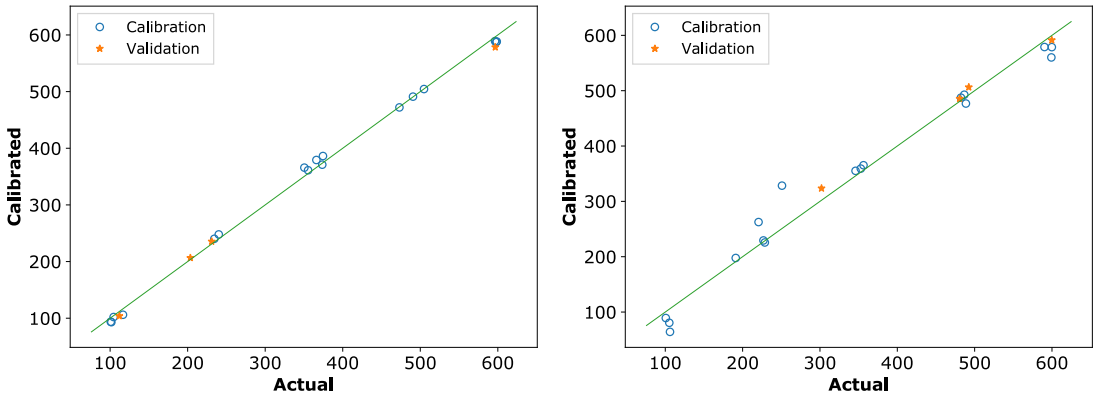

(a) NO **(b)** NH_3

Figure A.2: Example of a plot of the calculated vs. actual values in a FT-IR calibration in TQ Analyst®.

the overlapping of bands with another compounds. If two compounds different from water have an overlapping band, we choose another band to reduce the uncertainties. Figure A.2 shows the good fitting of the NO and NH_3 to the calibration method. For the calibration we used the spectrum range, which is the sum of the intensities of the spectrum in the range selected for each compound in the calibration.

Appendix B

Additional figures for Chapter 2

B.1 Energy Dispersive Spectroscopy (EDS) results

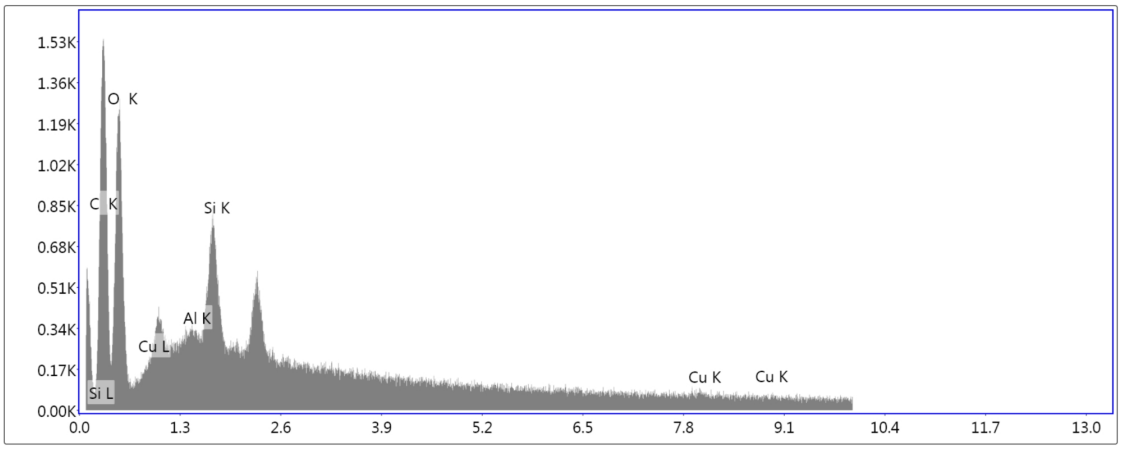

Figure B.1: EDS spectra of 1.2Cu-ZSM-5 catalyst.

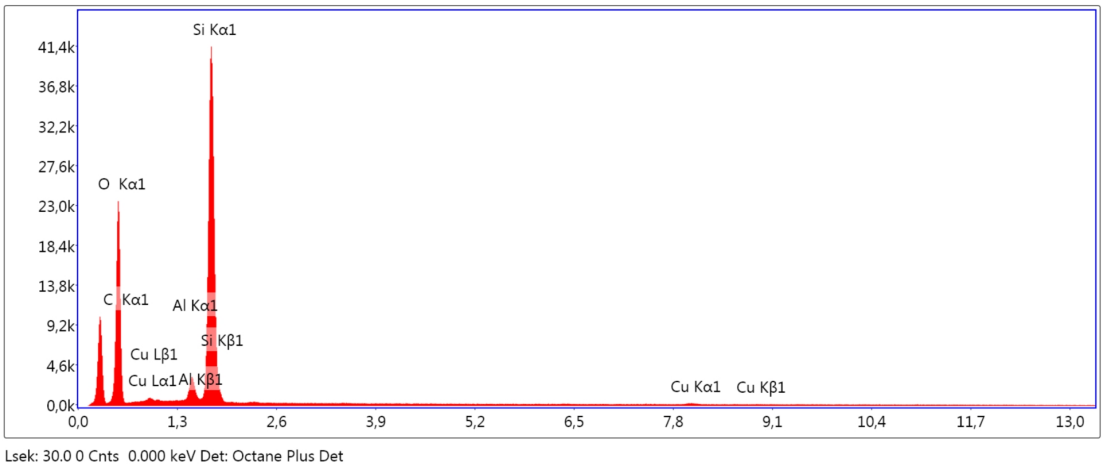

Figure B.2: EDS spectra of 1.2Cu/ZSM-5 catalyst.

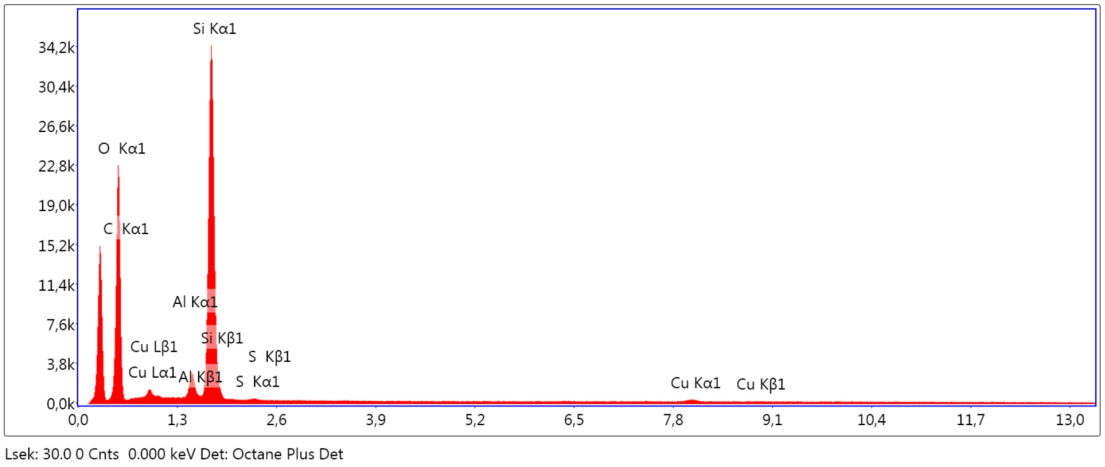

Figure B.3: EDS spectra of 2.0Cu/ZSM-5 catalyst.

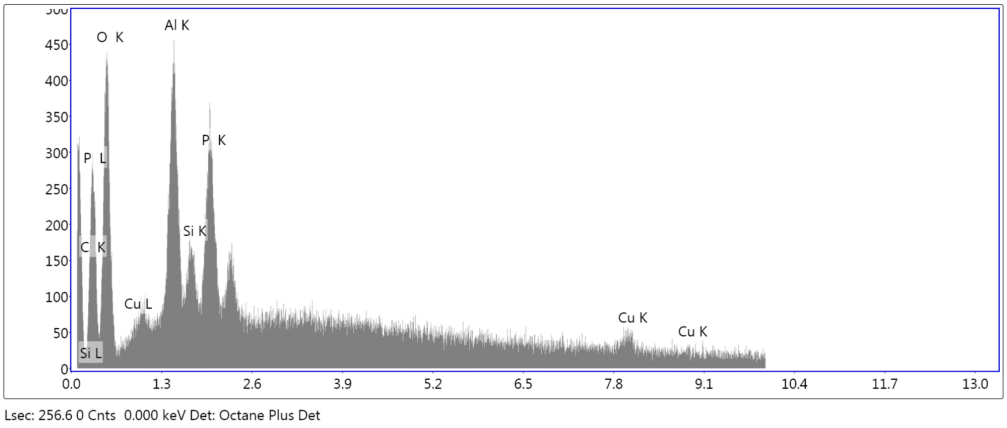

Figure B.4: EDS spectra of 2.6Cu-SAPO-34 catalyst.

Table B.1: Cu content in the catalysts form EDS results.

Catalysts	Cu weight / %	Cu atom ratio / %
1.2Cu-ZSM-5	1.29	0.36
1.2Cu/ZSM-5	1.17	0.29
2.0Cu-ZSM-5	1.66	0.40
Cu-SAPO34	2.36	2.36

B.2 FTIR spectra of catalyst with adsorbed NH_3

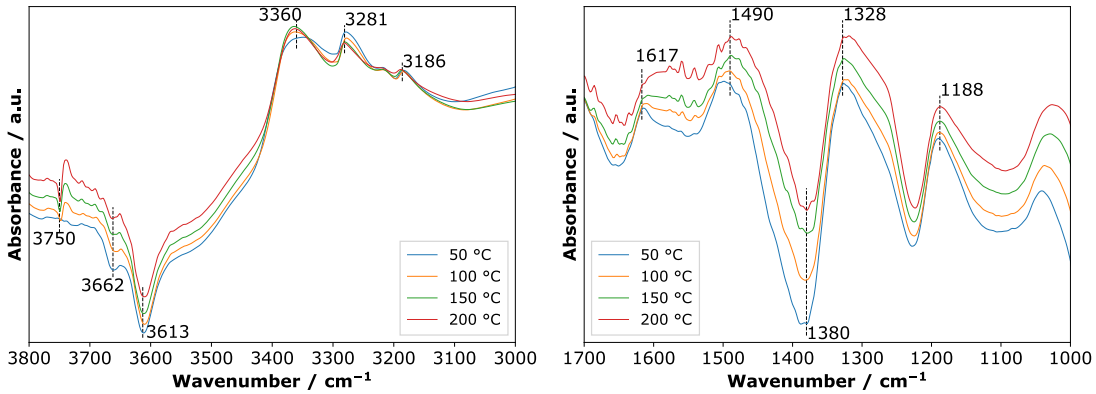

Figure B.5: FTIR spectra of 1.2Cu/ZSM-5 with adsorbed NH_3.

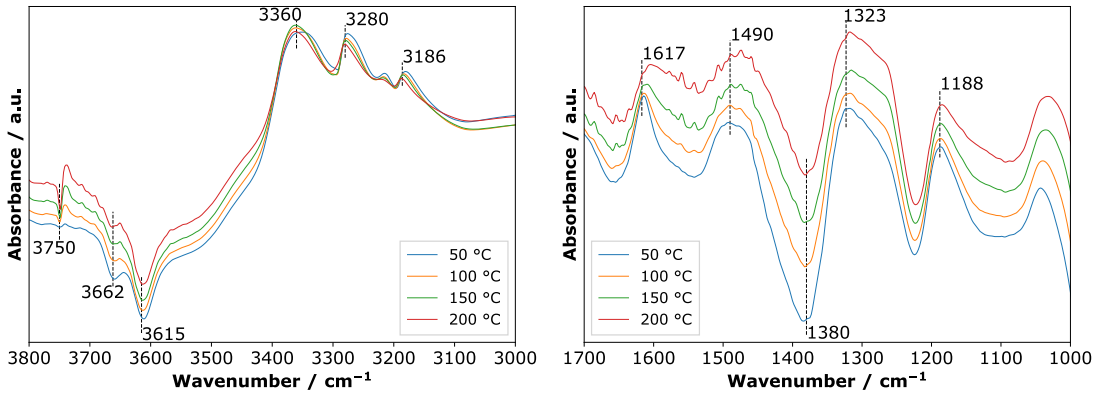

Figure B.6: FTIR spectra of 2.0Cu/ZSM-5 with adsorbed NH_3.

B.3 C_3H_6/NH_3-TPD profiles

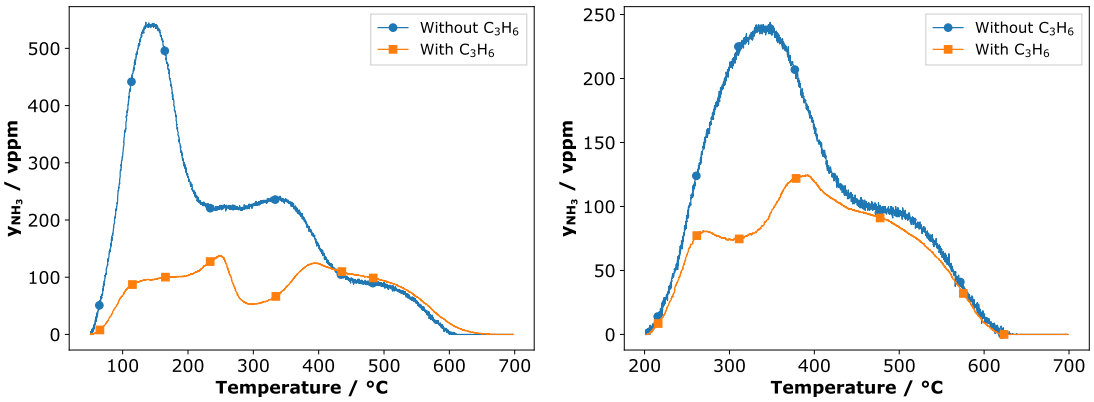

(a) 50 °C. **(b)** 200 °C.

Figure B.7: Effect of adsorbed C_3H_6 on the NH_3-TPD over 1.2Cu/ZSM-5.

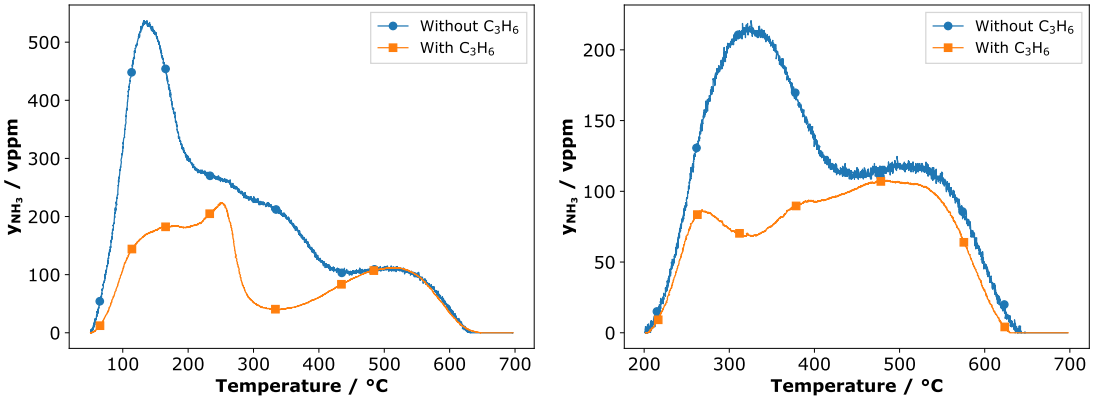

(a) 50 °C. **(b)** 200 °C.

Figure B.8: Effect of adsorbed C_3H_6 on the NH_3-TPD over 2.0Cu/ZSM-5.

B.4 NH_3-DRIFT spectra of C_3H_6-saturated catalysts

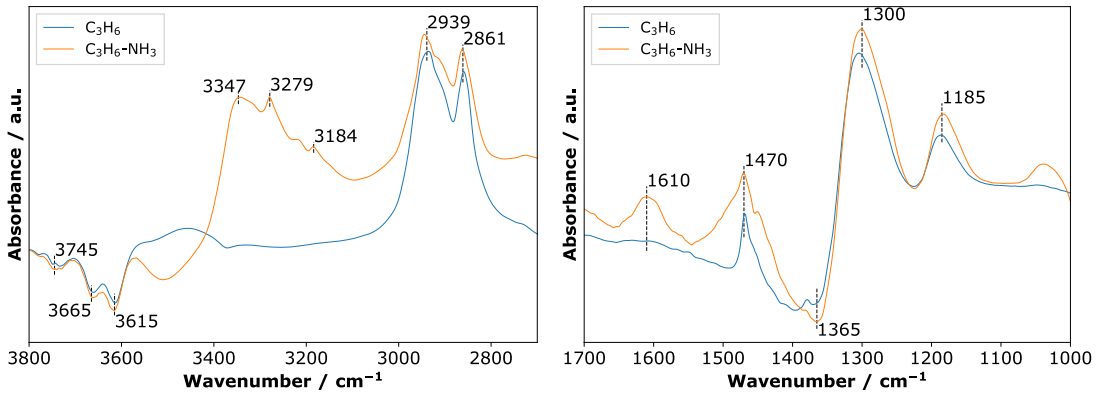

Figure B.9: FTIR spectra of C_3H_6-saturated and with adsorbed NH_3 of 1.2Cu/ZSM-5 at 50 °C.

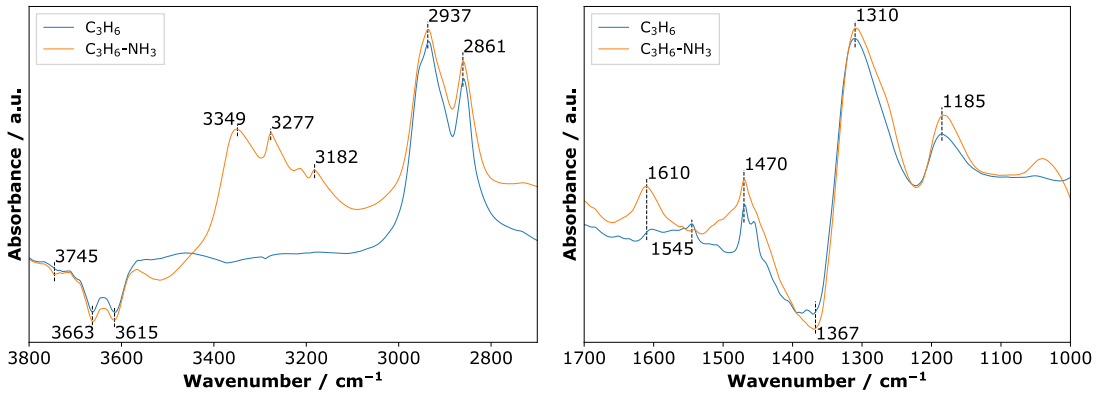

Figure B.10: FTIR spectra of C_3H_6-saturated and adsorbed NH_3 of 2.0Cu/ZSM-5 at 50 °C.

B.5 Fitting results

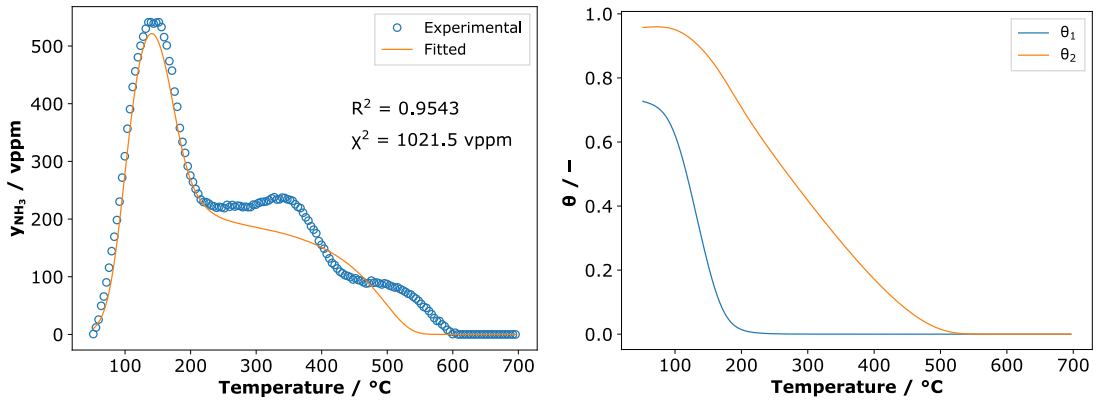

(a) NH_3 content. **(b)** Surface coverages.

Figure B.11: Fitting of the NH_3-TPD profiles of 1.2Cu/ZSM-5 at an adsorption temperature of 50 °C.

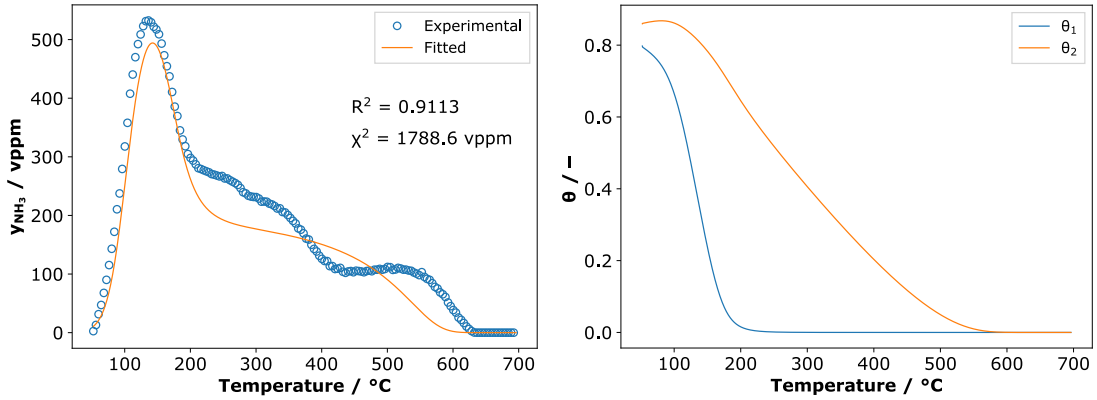

(a) NH_3 content. **(b)** Surface coverages.

Figure B.12: Fitting of the NH_3-TPD profiles of 2.0Cu/ZSM-5 at an adsorption temperature of 50 °C.

B.6 Validation results

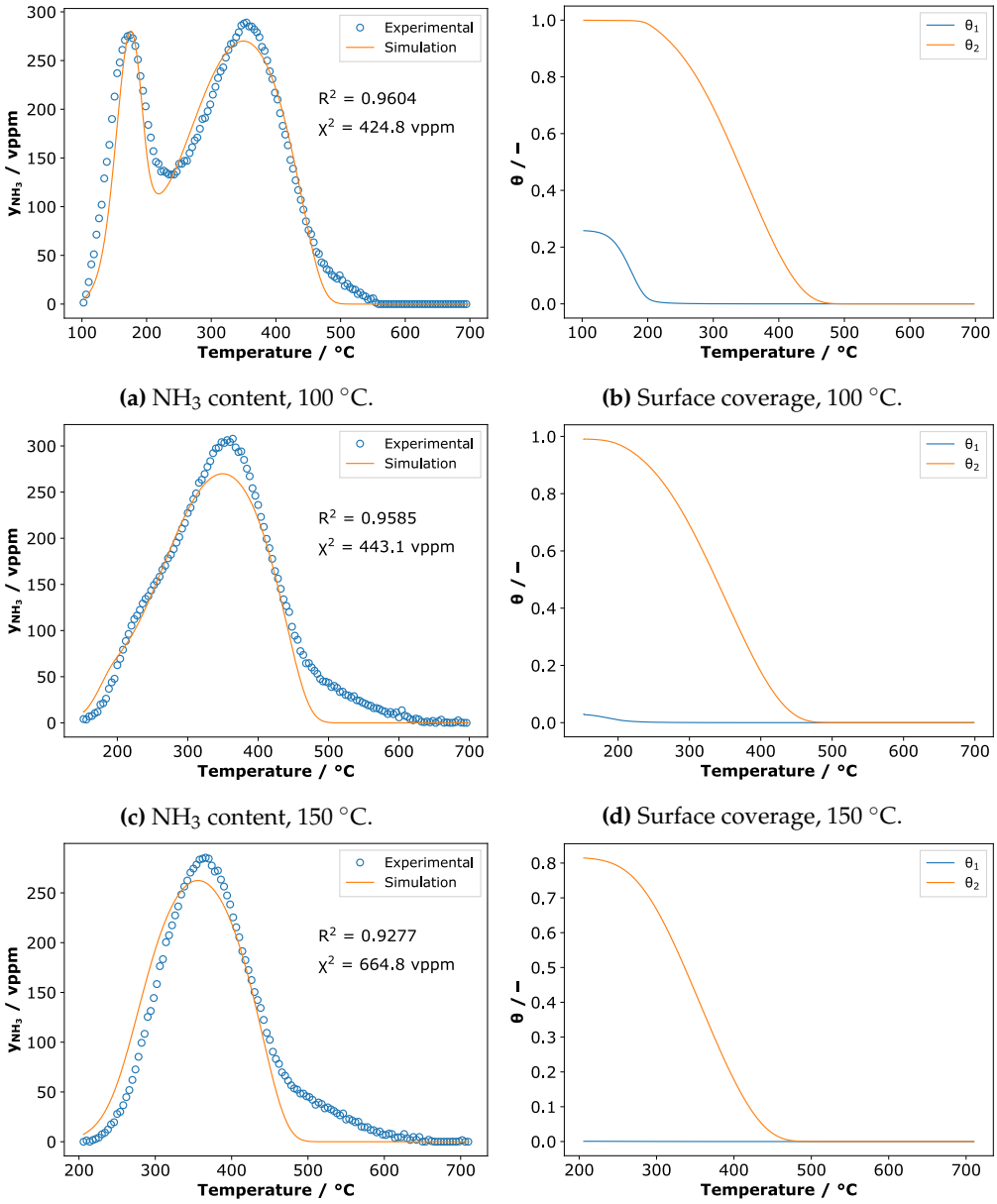

(a) NH_3 content, 100 °C.

(b) Surface coverage, 100 °C.

(c) NH_3 content, 150 °C.

(d) Surface coverage, 150 °C.

(e) NH_3 content, 200 °C.

(f) Surface coverage, 200 °C.

Figure B.13: Validation of the kinetic model for HZSM-5 at several temperatures of adsorption.

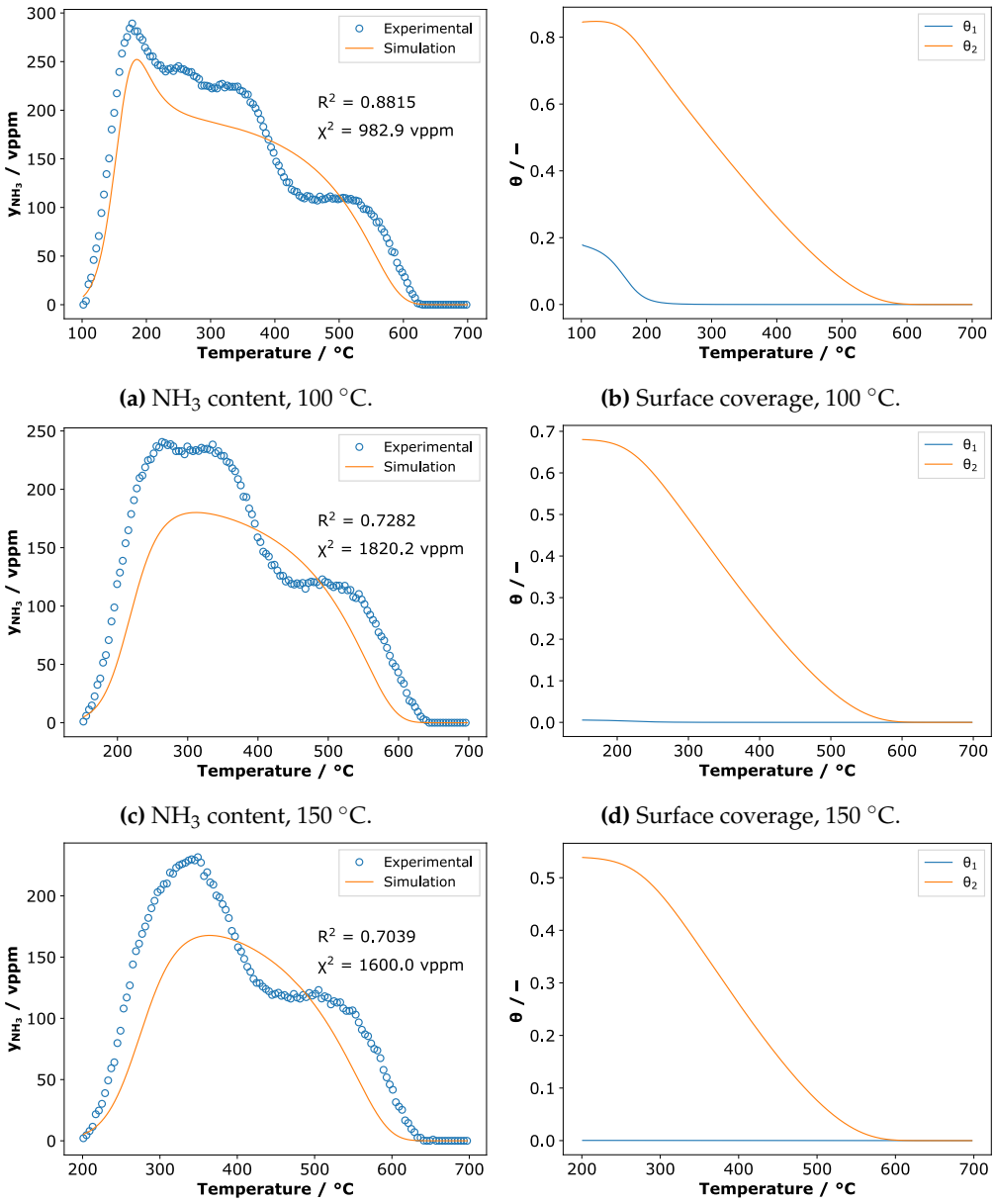

(a) NH_3 content, 100 °C.

(b) Surface coverage, 100 °C.

(c) NH_3 content, 150 °C.

(d) Surface coverage, 150 °C.

(e) NH_3 content, 200 °C.

(f) Surface coverage, 200 °C.

Figure B.14: Validation of the kinetic model for 1.2Cu-ZSM-5 at several temperatures of adsorption.

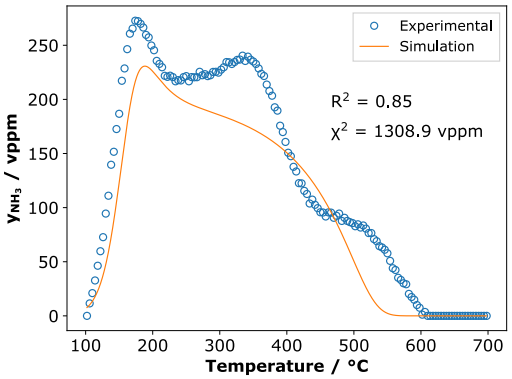

(a) NH_3 content, 100 °C.

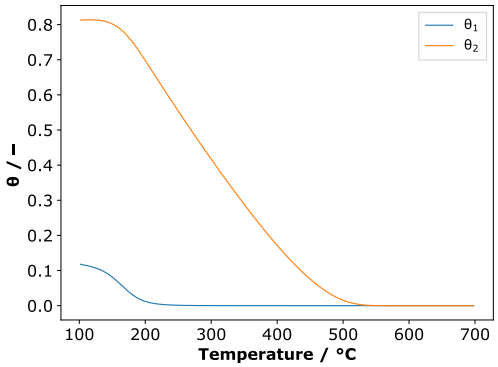

(b) Surface coverage, 100 °C.

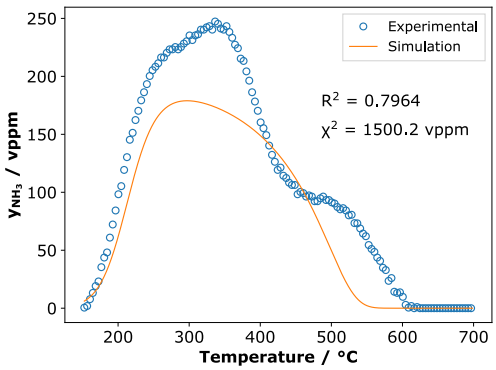

(c) NH_3 content, 150 °C.

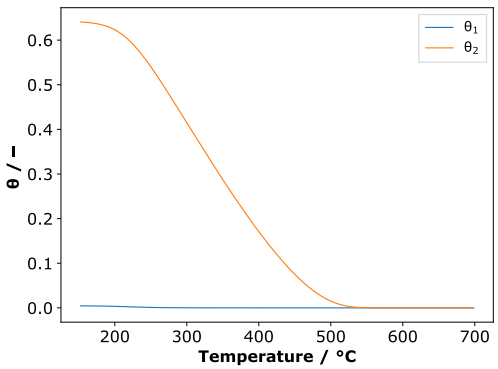

(d) Surface coverage, 150 °C.

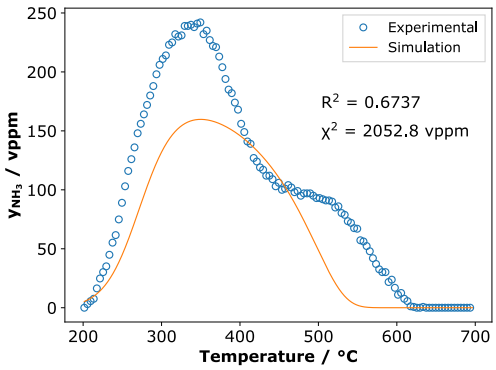

(e) NH_3 content, 200 °C.

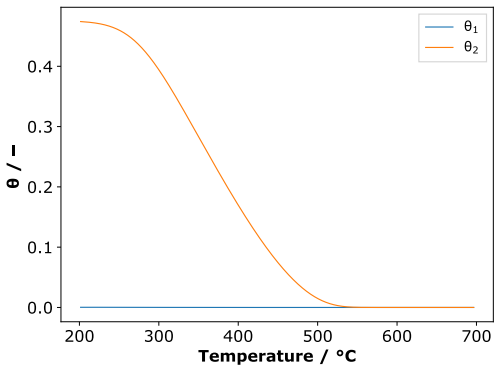

(f) Surface coverage, 200 °C.

Figure B.15: Validation of the kinetic model for 1.2Cu/ZSM-5 at several temperatures of adsorption.

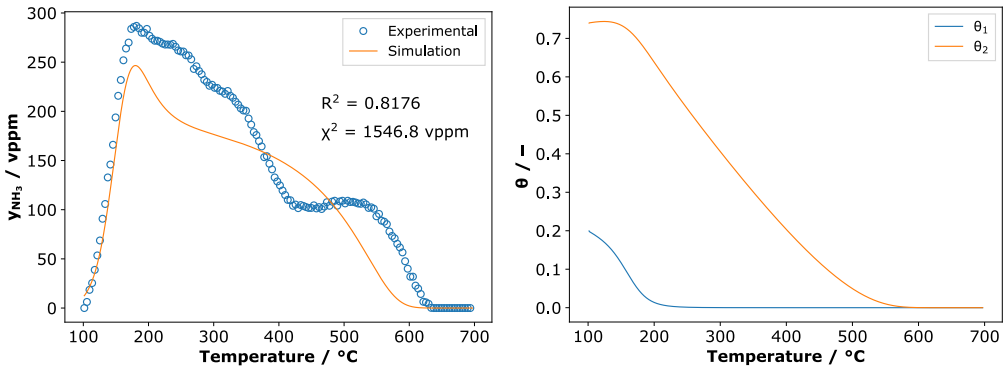

(a) NH_3 content, 100 °C.

(b) Surface coverage, 100 °C

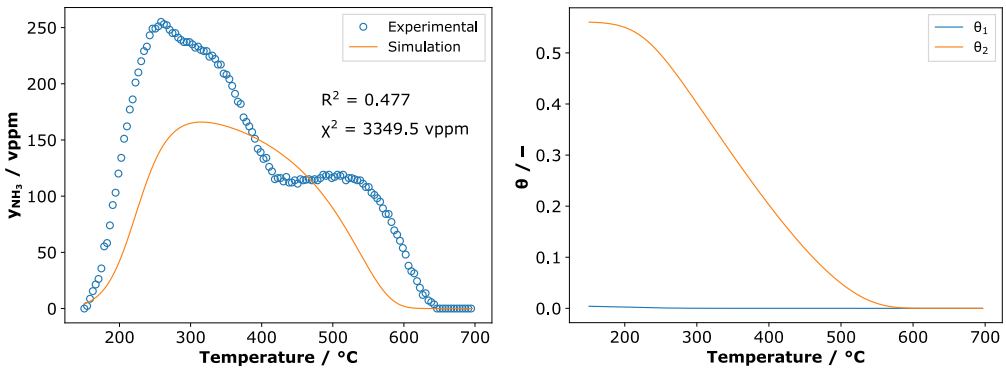

(c) NH_3 content, 150 °C.

(d) Surface coverage, 150 °C.

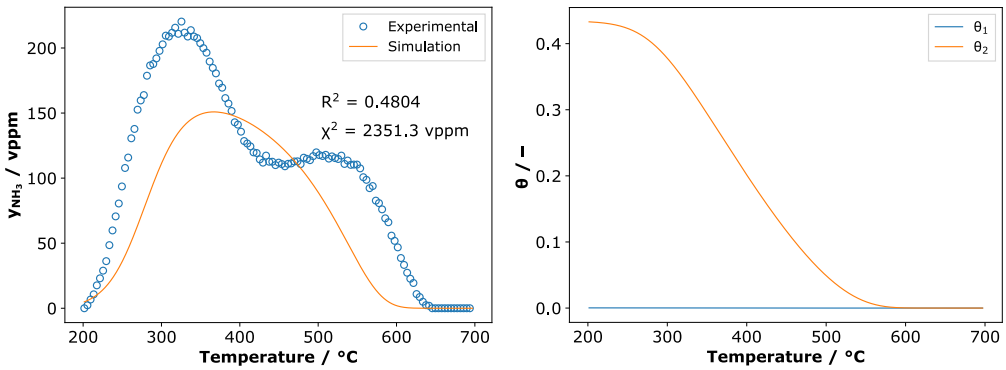

(e) NH_3 content, 200 °C.

(f) Surface coverage, 200 °C.

Figure B.16: Validation of the kinetic model for 2.0Cu/ZSM-5 at several temperatures of adsorption.

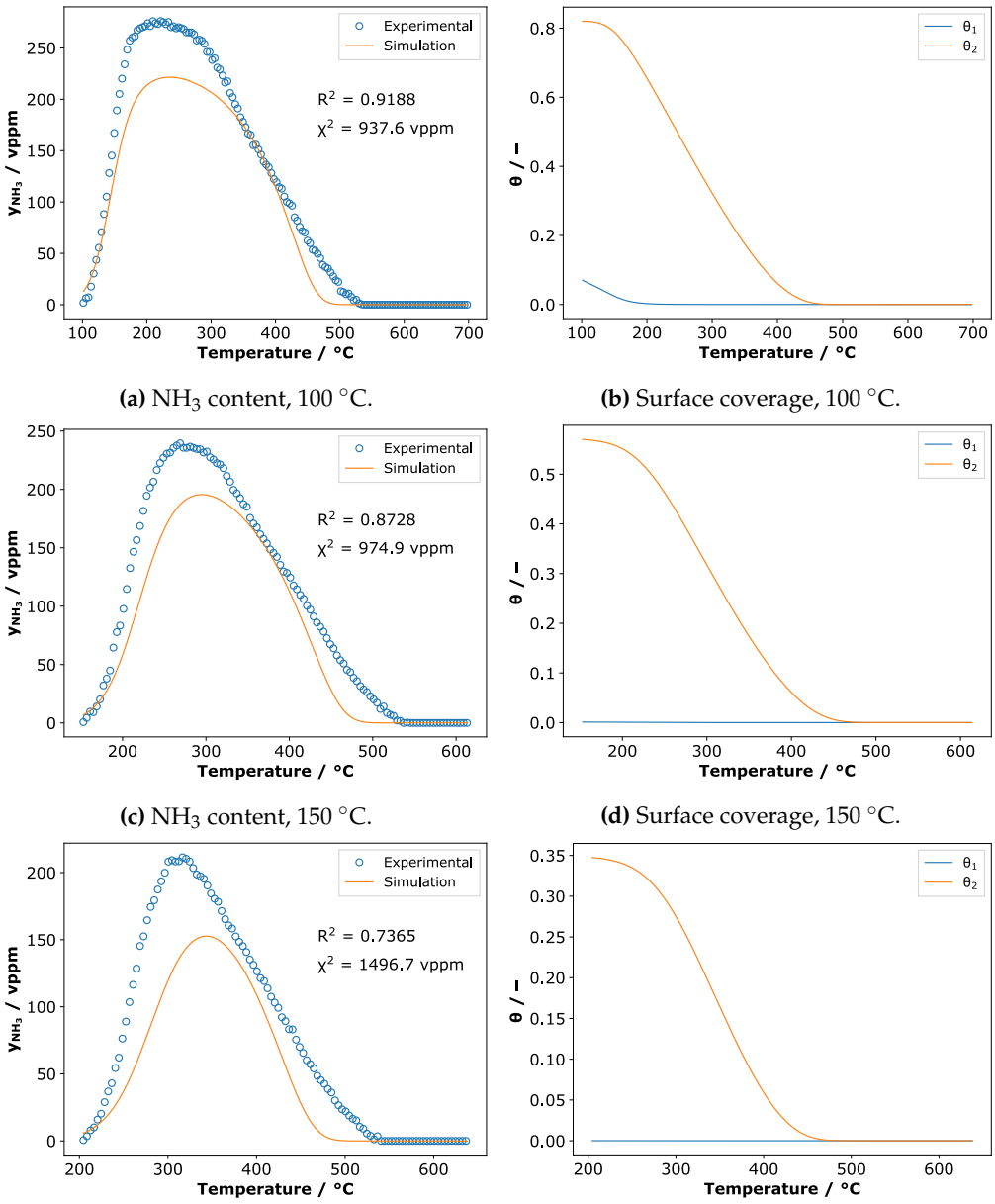

(a) NH_3 content, 100 °C.

(b) Surface coverage, 100 °C.

(c) NH_3 content, 150 °C.

(d) Surface coverage, 150 °C.

(e) NH_3 content, 200 °C.

(f) Surface coverage, 200 °C.

Figure B.17: Validation of the kinetic model for 2.6Cu-SAPO-34 at several temperatures of adsorption.

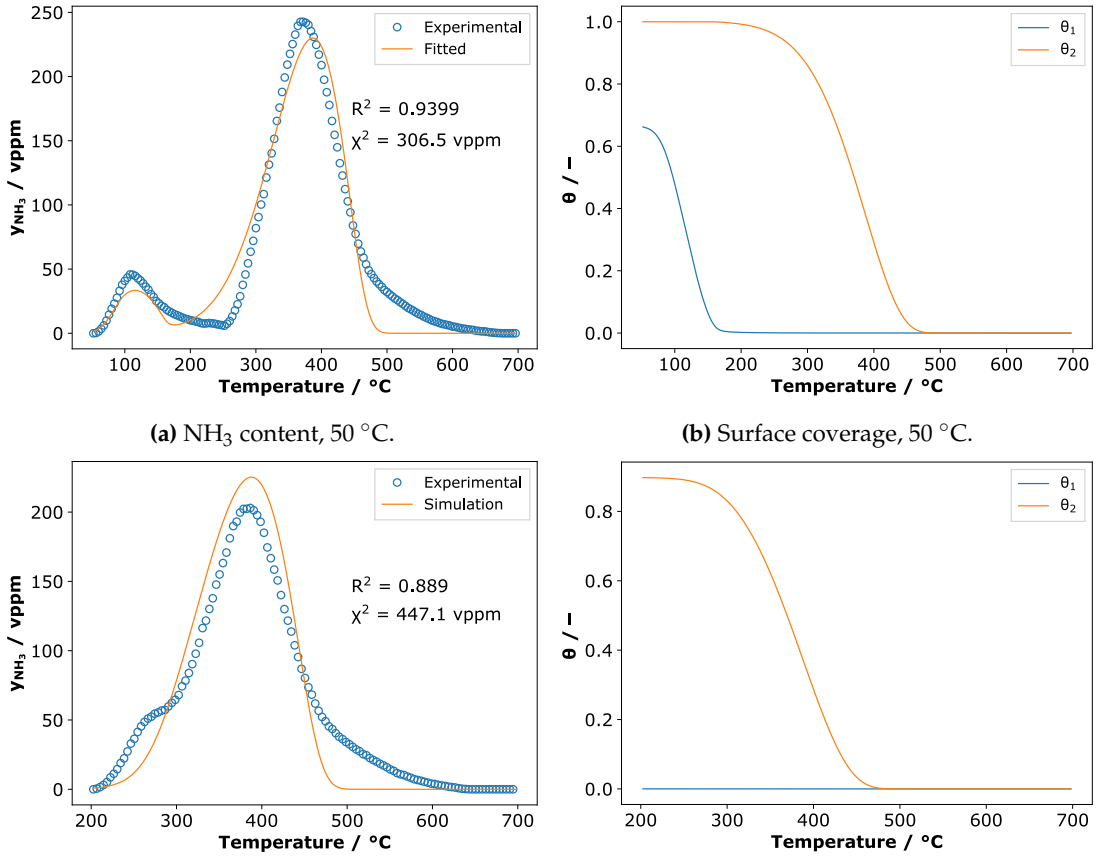

(a) NH_3 content, 50 °C.

(b) Surface coverage, 50 °C.

(c) NH_3 content, 200 °C.

(d) Surface coverage, 200 °C.

Figure B.18: Fitting of the NH_3-TPD profiles of HZSM-5 at adsorption temperatures of 50 °C and 200 °C.

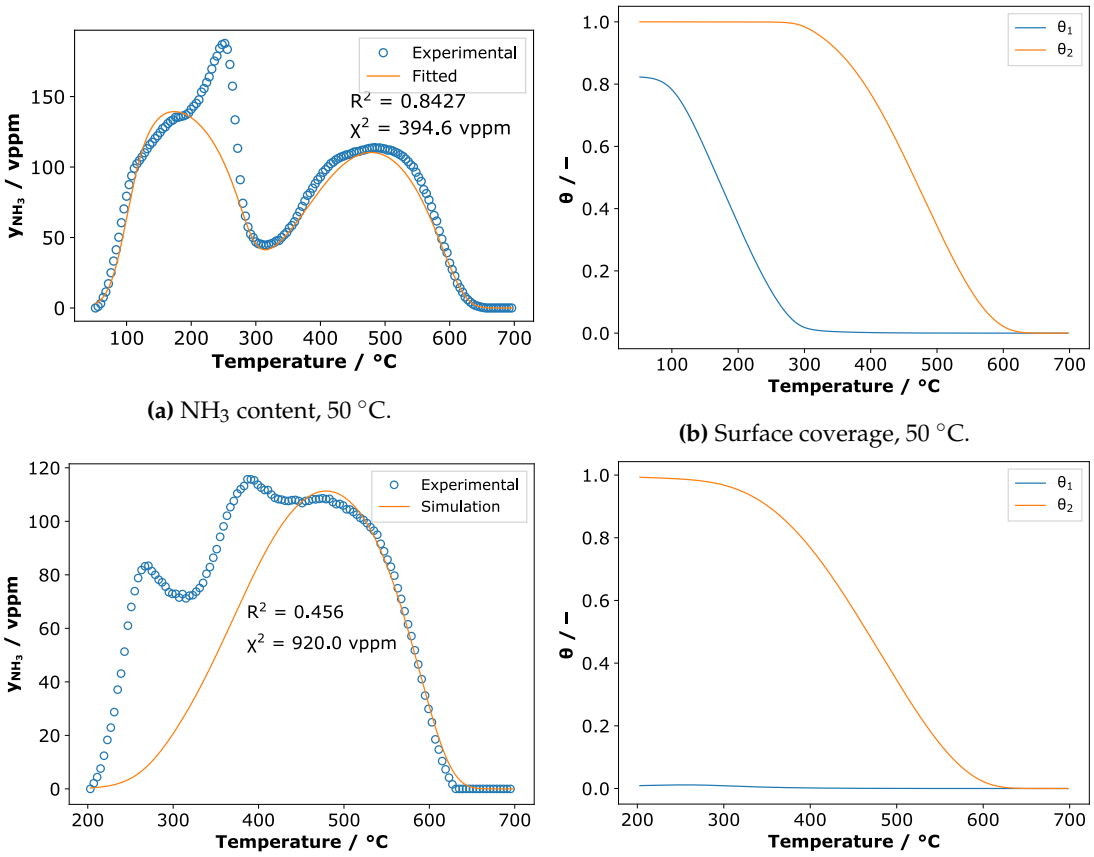

(a) NH_3 content, 50 °C.

(b) Surface coverage, 50 °C.

(c) NH_3 content, 200 °C.

(d) Surface coverage, 200 °C.

Figure B.19: Fitting of the NH_3-TPD profiles of 1.2Cu-ZSM-5 at adsorption temperatures of 50 °C and 200 °C.

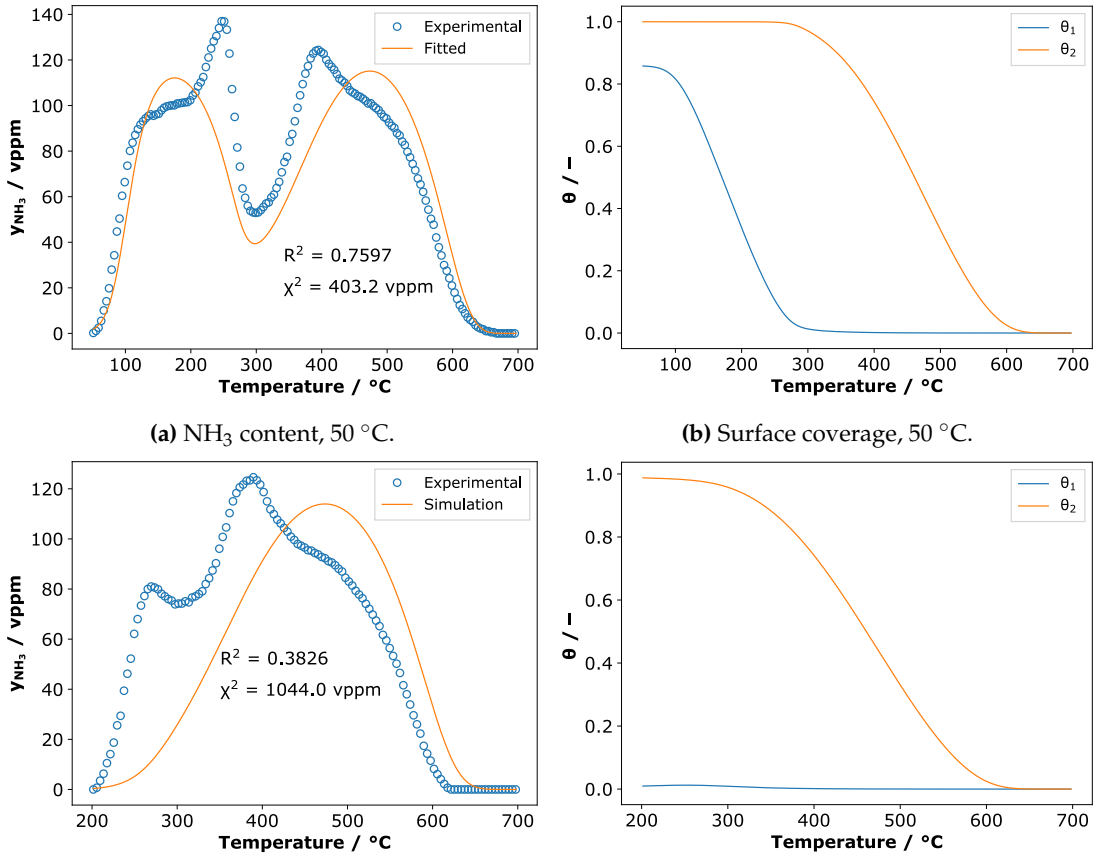

(a) NH_3 content, 50 °C.

(b) Surface coverage, 50 °C.

(c) NH_3 content, 200 °C.

(d) Surface coverage, 200 °C.

Figure B.20: Fitting of the NH_3-TPD profiles of 1.2Cu/ZSM-5 at adsorption temperatures of 50 °C and 200 °C.

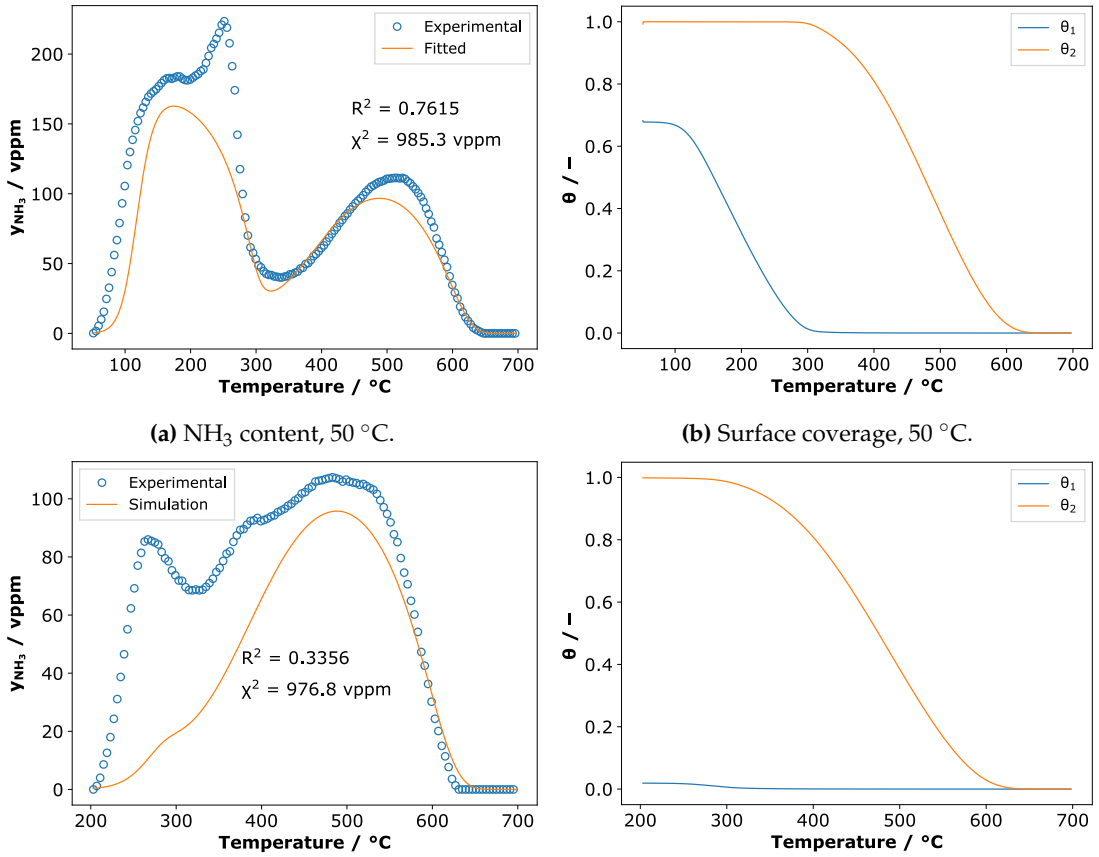

(a) NH_3 content, 50 °C.

(b) Surface coverage, 50 °C.

(c) NH_3 content, 200 °C.

(d) Surface coverage, 200 °C.

Figure B.21: Fitting of the NH_3-TPD profiles of 2.0Cu/ZSM-5 at adsorption temperatures of 50 °C and 200 °C.

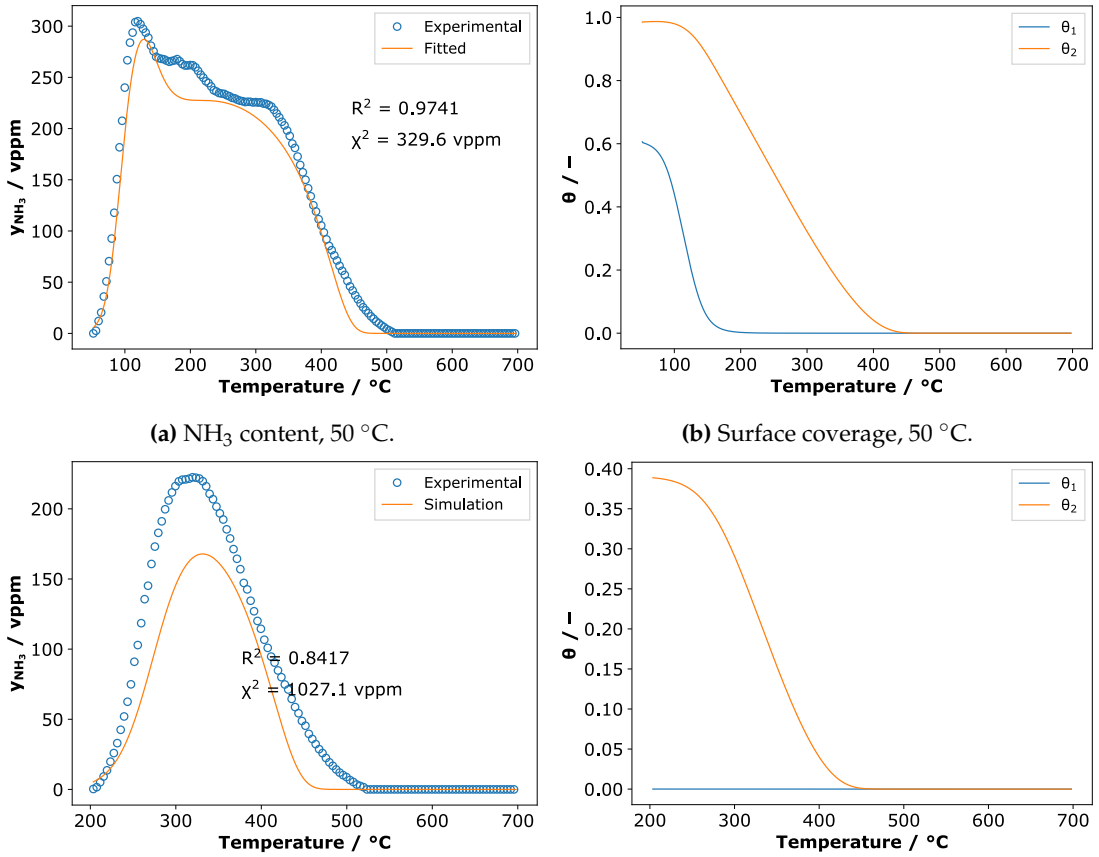

(a) NH_3 content, 50 °C.

(b) Surface coverage, 50 °C.

(c) NH_3 content, 200 °C.

(d) Surface coverage, 200 °C.

Figure B.22: Fitting of the NH_3-TPD profiles of 2.6Cu-SAPO-34 at adsorption temperatures of 50 °C and 200 °C.

Appendix C

Additional graphs for Chapter 3

C.1 NH_3-SCR of NO

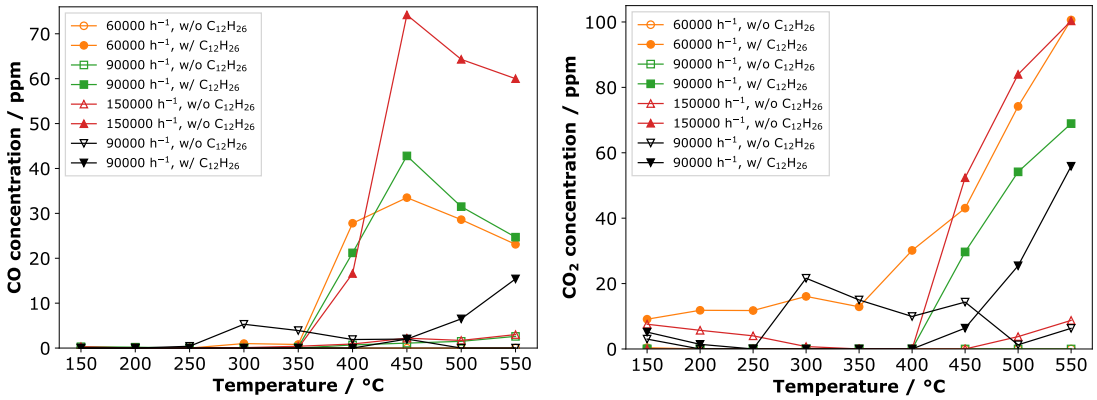

(a) CO concentration. **(b)** CO_2 concentration.

Figure C.1: Effect of GHSV on CO and CO_2 concentration in the NH_3-SCR of NO over Cu-SSZ-13. Reaction conditions: 400 ppm NH_3, 8% O_2, 5% H_2O, balance argon.

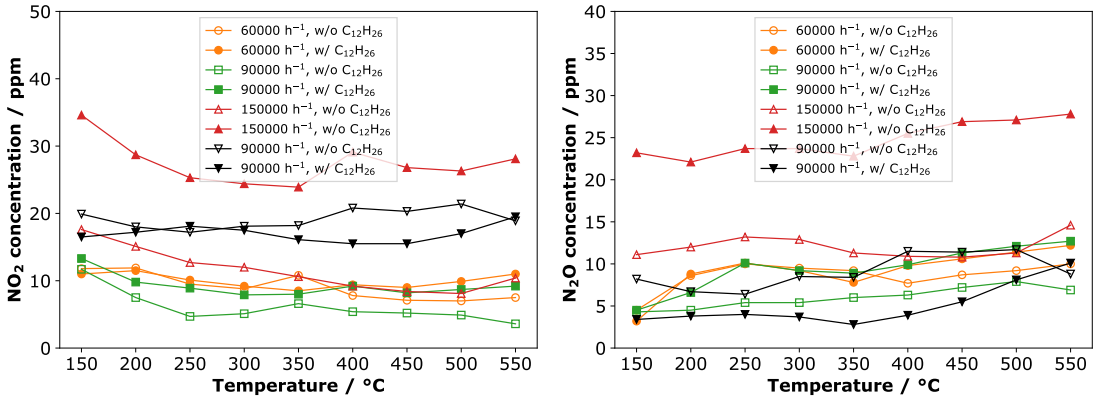

(a) NO_2 concentration. **(b)** N_2O concentration.

Figure C.2: Effect of GHSV on NO_2 and N_2O concentration in the NH_3-SCR of NO over Cu-SSZ-13. Reaction conditions: 400 ppm NH_3, 8% O_2, 5% H_2O, balance argon.

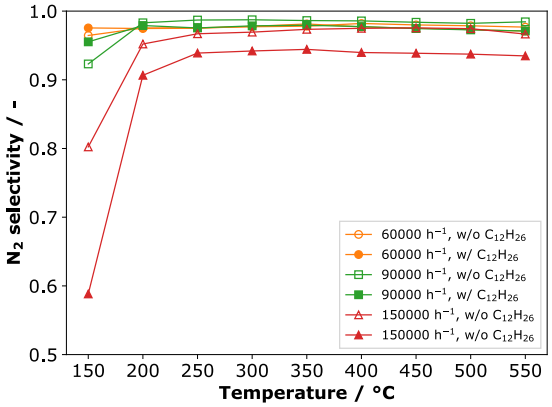

Figure C.3: Effect of GHSV on the N_2 selectivity in the NH_3-SCR of NO over Cu-SSZ-13. Reaction conditions: 400 ppm NO, 400 ppm NH_3, 8% O_2, 5% H_2O, 300 ppm $C_{12}H_{26}$ when used, balance argon.

C.2 NH_3 oxidation

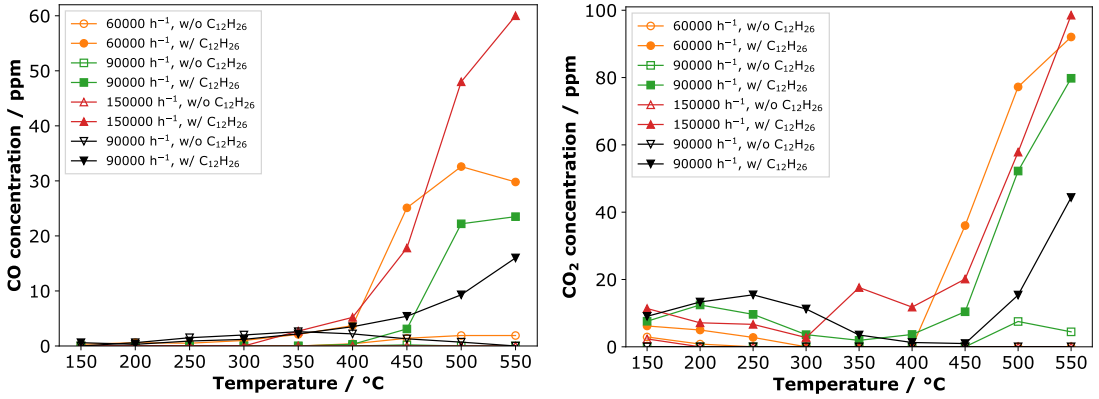

(a) CO concentration. **(b)** CO_2 concentration.

Figure C.4: Effect of GHSV on CO and CO_2 concentration in the NH_3 oxidation over Cu-SSZ-13. Reaction conditions: 400 ppm NH_3, 8% O_2, 5% H_2O, balance argon.

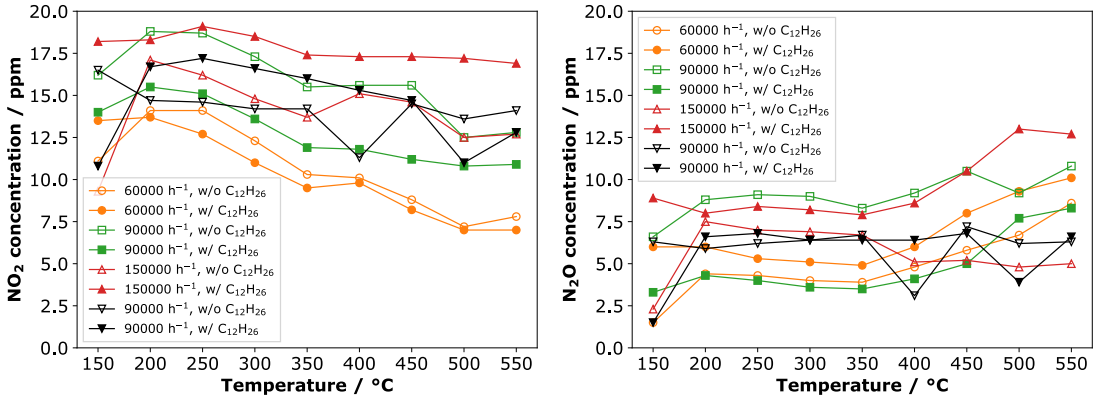

(a) CO concentration. **(b)** CO_2 concentration.

Figure C.5: Effect of GHSV on NO_2 and N_2O concentration in the NH_3 oxidation over Cu-SSZ-13. Reaction conditions: 400 ppm NH_3, 8% O_2, 5% H_2O, balance argon.

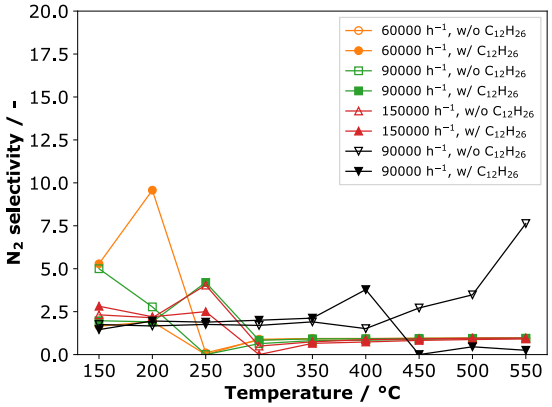

Figure C.6: Effect of GHSV on the N_2 selectivity in the NH_3 oxidation over Cu-SSZ-13. Reaction conditions: 400 ppm NO, 400 ppm NH_3, 8% O_2, 5% H_2O, 300 ppm $C_{12}H_{26}$ when used, balance argon.

C.3 NO oxidation

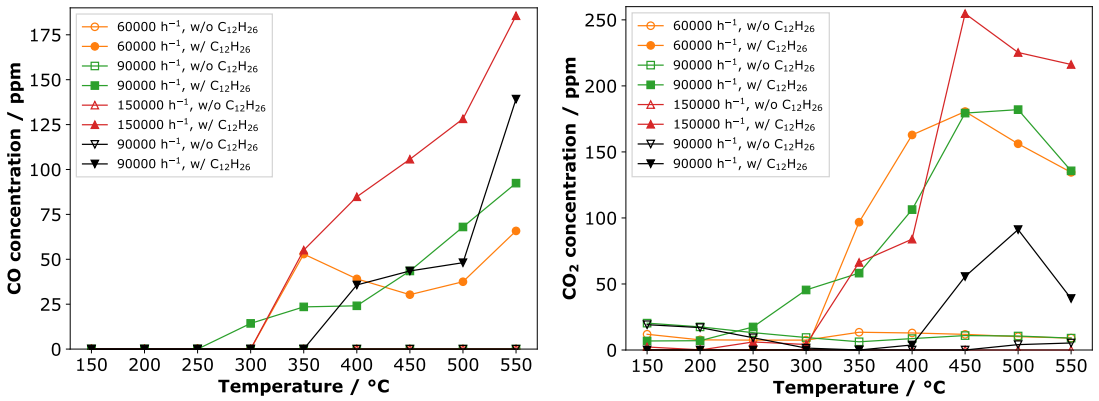

(a) CO concentration. **(b)** CO_2 concentration.

Figure C.7: Effect of GHSV on CO and CO_2 concentration in the NO oxidation over Cu-SSZ-13. Reaction conditions: 400 ppm NH_3, 8% O_2, 5% H_2O, balance argon.

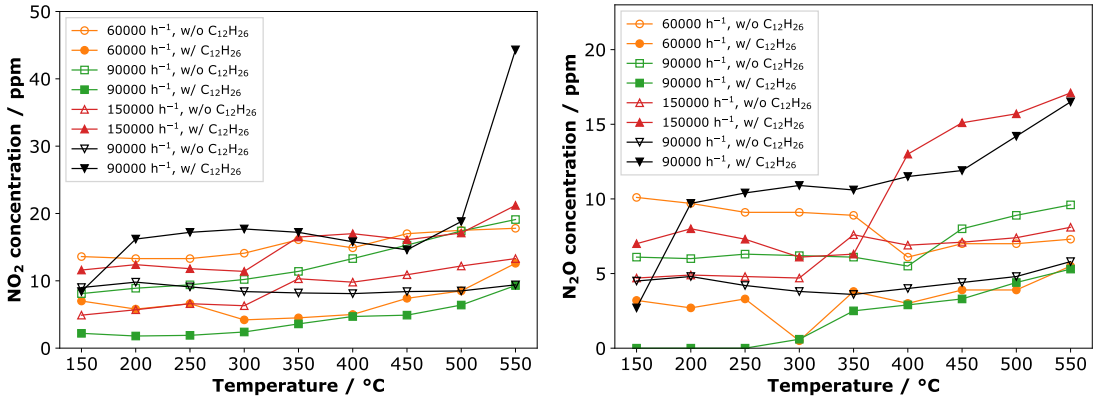

(a) CO concentration. **(b)** CO_2 concentration.

Figure C.8: Effect of GHSV on NO_2 and N_2O concentration in the NO oxidation over Cu-SSZ-13. Reaction conditions: 400 ppm NH_3, 8% O_2, 5% H_2O, balance argon.

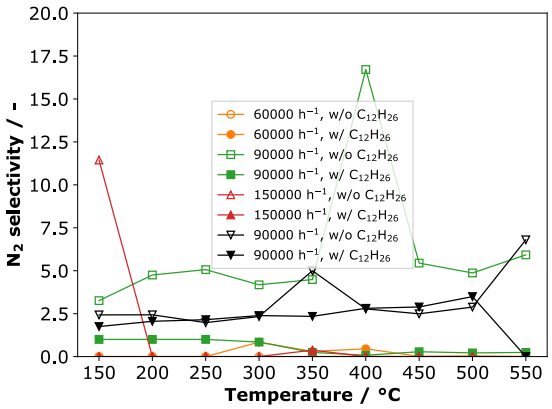

Figure C.9: Effect of GHSV on the N_2 selectivity in the NO oxidation over Cu-SSZ-13. Reaction conditions: 400 ppm NO, 400 ppm NH_3, 8% O_2, 5% H_2O, 300 ppm $C_{12}H_{26}$ when used, balance argon.

Appendix D

Weisz-Prater criterion

The Weisz-Prater criterion [139] estimates the influence of the interparticle and intracrystalline diffusions on a catalytic system. If the Weisz-Prater number (Equation D.1) $N_{w-p} \leq 0.3$ [140], the observed reaction rates should have negligible internal mass transfer limitations. Where r_{cal} is the calculated reaction rate in mole·kg_{cat}^{-1}·s^{-1}, R_p is the radius of the catalyst particle in m, ρ_c is the apparent density of the catalyst bed in kg·m^{-3}, D_{eff} is the effective diffusivity in m^2·s^{-1}, C_s is the gas concentration of NO at the external surface of the catalysts in mole·m^{-3}.

$$N_{w-p} = \frac{r_{cal}\rho_c R_p^2}{C_s D_{eff}} \tag{D.1}$$

The effective diffusivity can be calculated by Equation D.2, in which ν is the average velocity of the NO molecules in m·s^{-1}, which can be calculated with Equation D.3, where k_B is the Boltzmann constant, T is the temperature, m is the mass of a molecule; and d_p is the crystallite grain size of the catalyst, which can be calculated by the Scherrer equation (Equation D.4), where D_{hkl} is the crystallite size in the direction perpendicular to the lattice planes, hkl are the Miller indices of the planes being analyzed, K is a dimensionless crystallite-shape factor, λ is the X-ray wavenumber, B is the width (full width at half-maximum) of the X-ray diffraction peak in radians, and θ is the Bragg angle.

$$D_{eff} = \frac{\nu \cdot d_p}{3} \tag{D.2}$$

$$\nu = \sqrt{\frac{8 \cdot k_B T}{\pi m}} \tag{D.3}$$

$$D_{hkl} = \frac{K\lambda}{B\cos\theta} \tag{D.4}$$

Bibliography

[1] Konrad Reif. *Diesel Engine Management: Systems and Components*. Springer Fachmedien Wiesbaden, 2014. ISBN: 9783658039813. URL: https://books.google.com.co/books?id=OdklBAAAQBAJ.

[2] Paul Breeze. "Diesel Engines". In: *Piston Engine-Based Power Plants*. Elsevier, 2018, pp. 47–57. ISBN: 9780128129043. DOI: 10.1016/B978-0-12-812904-3.00005-7.

[3] United Nations Environmental Programme, International Labour Organisation, and World Health Organization. *Diesel fuel and exhaust emissions: Evironmental Health Criteria 171*. Geneva, 1996. URL: http://www.inchem.org/documents/ehc/ehc/ehc171.htm (visited on 07/17/2019).

[4] Gerhard Knothe. "Introduction". In: *The Biodiesel Handbook: Second Edition*. Elsevier Inc., 2010, pp. 1–3. ISBN: 9780983507260. DOI: 10.1016/B978-1-893997-62-2.50006-1.

[5] İbrahim Aslan Reşitoğlu, Kemal Altinişik, and Ali Keskin. "The pollutant emissions from diesel-engine vehicles and exhaust aftertreatment systems". In: *Clean Technologies and Environmental Policy* 17.1 (2015), pp. 15–27. ISSN: 1618-954X. DOI: 10.1007/s10098-014-0793-9.

[6] Fuyan Liang et al. "The organic composition of diesel particulate matter, diesel fuel and engine oil of a non-road diesel generator". In: *Journal of environmental monitoring : JEM* 7.10 (2005), pp. 983–988. ISSN: 1464-0325. DOI: 10.1039/b504728e.

[7] Jerald A. Caton and Zhiyong Xia. "The Selective Non-Catalytic Removal (SNCR) of Nitric Oxides From Engine Exhaust Streams: Comparison of Three Processes". In: *Journal of Engineering for Gas Turbines and Power* 126.2 (2004), p. 234. ISSN: 0028-0836. DOI: 10.1115/1.1688366.

[8] Craig T. Bowman. "Control of combustion-generated nitrogen oxide emissions: Technology driven by regulation". In: *Symposium (International) on Combustion* 24.1 (1992), pp. 859–878. ISSN: 00820784. DOI: 10.1016/S0082-0784(06)80104-9.

[9] Bolin Zhang et al. "High N_2 selectivity in selective catalytic reduction of NO with NH_3 over Mn/Ti-Zr catalysts". In: *Royal Society of Chemistry Advances* 8 (2018), pp. 12733–12741. DOI: 10.1039/c8ra00336j.

[10] WebStockReview. *Engine clipart diesel engine*. 2019. URL: https://webstockreview.net/explore/engine-clipart-diesel-engine/.

[11] Lina Gan et al. "High-Performance V_2O_5-WO_3/TiO_2 Catalyst for Diesel NO_X Reduction at Low Temperatures". In: *Energy Procedia* 61 (2014), pp. 1115–1118. ISSN: 18766102. DOI: 10.1016/j.egypro.2014.11.1035.

[12] Bin Guan et al. "Review of state of the art technologies of selective catalytic reduction of NO_X from diesel engine exhaust". In: *Applied Thermal Engineering* 66.1-2 (2014), pp. 395–414. ISSN: 13594311. DOI: 10.1016/j.applthermaleng.2014.02.021.

[13] Junhua Li et al. "Mechanism of propene poisoning on Fe-ZSM-5 for selective catalytic reduction of NO_X with ammonia". In: *Environmental science & technology* 44.5 (2010), pp. 1799–1805. DOI: 10.1021/es903576d.

[14] Isabella Nova and Enrico Tronconi, eds. *Urea-SCR technology for deNO_X after treatment of diesel exhausts*. Fundamental and applied catalysis. New York, Heidelberg, and Dordrecht: Springer, 2014. ISBN: 9781489980717. URL: https://www.loc.gov/catdir/enhancements/fy1613/2014934157-b.html.

[15] Zhiguo Xie et al. "One-pot hydrothermal synthesis of CuBi co-doped mesoporous zeolite Beta for the removal of NO_X by selective catalytic reduction with ammonia". In: *Scientific reports* 6 (2016), p. 30132. DOI: 10.1038/srep30132.

[16] Paweł Boroń, Lucjan Chmielarz, and Stanislaw Dzwigaj. "Influence of Cu on the catalytic activity of FeBEA zeolites in SCR of NO with NH_3". In: *Applied Catalysis B: Environmental* 168-169 (2015), pp. 377–384. ISSN: 09263373. DOI: 10.1016/j.apcatb.2014.12.052.

[17] Oana Mihai et al. "The effect of Cu-loading on different reactions involved in NH_3-SCR over Cu-BEA catalysts". In: *Journal of Catalysis* 311 (2014), pp. 170–181. ISSN: 00219517. DOI: 10.1016/j.jcat.2013.11.016.

[18] Choong-Kil Seo et al. "Effect of ZrO_2 addition on de-NO_X performance of Cu-ZSM-5 for SCR catalyst". In: *Chemical Engineering Journal* 191 (2012), pp. 331–340. ISSN: 13858947. DOI: 10.1016/j.cej.2012.03.027.

[19] Masakazu Iwamoto and Hideaki Hamada. "Removal of nitrogen monoxide from exhaust gases through novel catalytic processes". In: *Catalysis Today* 10.1 (1991), pp. 57–71. ISSN: 09205861. DOI: 10.1016/0920-5861(91)80074-J.

[20] Qing Ye, Lifeng Wang, and Ralph T. Yang. "Activity, propene poisoning resistance and hydrothermal stability of copper exchanged chabazite-like zeolite catalysts for SCR of NO with ammonia in comparison to Cu/ZSM-5". In: *Applied Catalysis A: General* 427-428 (2012), pp. 24–34. ISSN: 0926860X. DOI: 10.1016/j.apcata.2012.03.026.

[21] Feng Gao et al. "A comparative kinetics study between Cu/SSZ-13 and Fe/SSZ-13 SCR catalysts". In: *Catalysis Today* 258 (2015), pp. 347–358. ISSN: 09205861. DOI: 10.1016/j.cattod.2015.01.025.

[22] Ja Hun Kwak et al. "The Effect of Copper Loading on the Selective Catalytic Reduction of Nitric Oxide by Ammonia Over Cu-SSZ-13". In: *Catalysis Letters* 142.3 (2012), pp. 295–301. ISSN: 1011-372X. DOI: 10.1007/s10562-012-0771-y.

[23] Dustin W. Fickel et al. "The ammonia selective catalytic reduction activity of copper-exchanged small-pore zeolites". In: *Applied Catalysis B: Environmental* 102.3-4 (2011), pp. 441–448. ISSN: 09263373. DOI: 10.1016/j.apcatb.2010.12.022.

[24] Ja Hun Kwak et al. "Excellent activity and selectivity of Cu-SSZ-13 in the selective catalytic reduction of NO_X with NH_3". In: *Journal of Catalysis* 275.2 (2010), pp. 187–190. ISSN: 00219517. DOI: 10.1016/j.jcat.2010.07.031.

[25] Carmine Colella and William S. Wise. "The IZA Handbook of Natural Zeolites: A tool of knowledge on the most important family of porous minerals". In: *Microporous and Mesoporous Materials* 189 (2014), pp. 4–10. ISSN: 1387-1811. DOI: 10.1016/j.micromeso.2013.08.028. URL: https://www.sciencedirect.com/science/article/abs/pii/S1387181113004162.

[26] International Zeolite Association. *Welcome to the IZA Website*. 15/08/2017. URL: http://www.iza-online.org/default.htm.

[27] Herman van Bekkum et al. *Introduction to zeolite science and practice*. 2. completely rev. and expanded ed. Vol. 137. Studies in Surface Science and Catalysis. Amsterdam: Elsevier, 2001. ISBN: 0444824219. URL: http://site.ebrary.com/lib/alltitles/docDetail.action?docID=10190971.

[28] Christian Baerlocher, Lynne B. McCusker, and David H. Olson. *Atlas of Zeolite Framework Types*. Sixth Edition. Amsterdam et al.: Elsevier, 2007. ISBN: 978-0-444-53064-6.

[29] Philip L. Llewellyn and Guillaume Maurin. "Gas Adsorption in Zeolites and Related Materials". In: *Introduction to Zeolite Science and Practice*. Vol. 168. Studies in Surface Science and Catalysis. Elsevier, 2007, pp. 555–XVI. ISBN: 9780444530639. DOI: 10.1016/S0167-2991(07)80805-6.

[30] Zeolite Store. *Zeolites*. 2010. URL: https://www.zeolitestore.com/en/zeolites (visited on 07/24/2019).

[31] Luca Lietti et al. "Dynamics of the SCR-DeNO$_X$ reaction by the transient-response method". In: *AIChE Journal* 43.10 (1997), pp. 2559–2570. ISSN: 0001-1541. DOI: 10.1002/aic.690431017.

[32] Donald W. Breck. *Zeolite molecular sieves: structure, chemistry, and use*. Wiley-Interscience Publication. Wiley, 1973. ISBN: 9780471099857. URL: https://books.google.com.co/books?id=aY0vAQAAIAAJ.

[33] Hayim Abrevaya. *Unique Aspects of Mechanisms and Requirements for Zeolite Catalysis in Refining and Petrochemicals*. Wiley Online Books. 2010. ISBN: 9783527629565. DOI: 10.1002/9783527629565.ch13.

[34] Nasir M. Tukur and Sulaiman Al-Khattaf. "Catalytic cracking of n-dodecane and alkyl benzenes over FCC zeolite catalysts: Time on stream and reactant converted models". In: *Chemical Engineering and Processing: Process Intensification* 44.11 (2005), pp. 1257–1268. ISSN: 02552701. DOI: 10.1016/j.cep.2005.02.009.

[35] Hiroshi Oikawa et al. "Highly selective conversion of ethene to propene over SAPO-34 as a solid acid catalyst". In: *Applied Catalysis A: General* 312.1-2 (2006), pp. 181–185. ISSN: 0926860X. DOI: 10.1016/j.apcata.2006.06.045.

[36] Oliver Kröcher and Martin Elsener. "Combination of V_2O_5/WO_3-TiO_2, Fe-ZSM5, and Cu-ZSM5 Catalysts for the Selective Catalytic Reduction of Nitric Oxide with Ammonia". In: *Industrial & Engineering Chemistry Research* 47.22 (2008), pp. 8588–8593. DOI: 10.1021/ie800951a.

[37] Kirsten Leistner et al. "Comparison of Cu/BEA, Cu/SSZ-13 and Cu/SAPO-34 for ammonia-SCR reactions". In: *Catalysis Today* 258 (2015), pp. 49–55. ISSN: 09205861. DOI: 10.1016/j.cattod.2015.04.004.

[38] Beñat Pereda-Ayo et al. "Role of the different copper species on the activity of Cu/zeolite catalysts for SCR of NO$_X$ with NH_3". In: *Applied Catalysis B: Environmental* 147 (2014), pp. 420–428. ISSN: 09263373. DOI: 10.1016/j.apcatb.2013.09.010.

[39] "Low-temperature selective catalytic reduction of NOx with NH_3 over metal oxide and zeolite catalysts-A review". In: *Catalysis Today* 175.1 (2011), pp. 147–156. ISSN: 09205861. DOI: 10.1016/j.cattod.2011.03.034. URL: http://dx.doi.org/10.1016/j.cattod.2011.03.034.

[40] Li Zhang et al. "SO_2 poisoning impact on the NH_3-SCR reaction over a commercial Cu-SAPO-34 SCR catalyst". In: *Applied Catalysis B: Environmental* 156-157 (2014), pp. 371–377. ISSN: 09263373. DOI: 10.1016/j.apcatb.2014.03.030. URL: http://www.sciencedirect.com/science/article/pii/S0926337314001933.

[41] Kurnia Wijayanti et al. "Impact of sulfur oxide on NH_3-SCR over Cu-SAPO-34". In: *Applied Catalysis B: Environmental* 166-167 (2015), pp. 568–579. ISSN: 09263373. DOI: 10.1016/j.apcatb.2014.11.043. URL: http://www.sciencedirect.com/science/article/pii/S0926337314007516.

[42] Ashok Kumar et al. "Impact of different forms of feed sulfur on small-pore Cu-zeolite SCR catalyst". In: *Catalysis Today* 231 (2014), pp. 75–82. ISSN: 09205861. DOI: 10.1016/j.cattod.2013.12.038.

[43] Clifford Montreuil and Christine Lambert. "The Effect of Hydrocarbons on the Selective Catalyzed Reduction of NO_X over Low and High Temperature Catalyst Formulations". In: *SAE International Journal of Fuels and Lubricants* 1.1 (2008), pp. 495–504. DOI: 10.4271/2008-01-1030. URL: https://www.sae.org/gsdownload/?prodCd=2008-01-1030.

[44] Asima Sultana et al. "SCR of NO_X with NH_3 over Cu/NaZSM-5 and Cu/HZSM-5 in the presence of decane". In: *Catalysis Communications* 10.14 (2009), pp. 1859–1863. ISSN: 1566-7367. DOI: 10.1016/j.catcom.2009.06.015. URL: http://www.sciencedirect.com/science/article/pii/S1566736709002465.

[45] Chongheng He et al. "Activity, stability and hydrocarbon deactivation of Fe/Beta catalyst for SCR of NO with ammonia". In: *Applied Catalysis A: General* 368.1-2 (2009), pp. 121–126. ISSN: 0926860X. DOI: 10.1016/j.apcata.2009.08.020.

[46] Iljeong Heo et al. "Effect of hydrocarbon slip on NO removal activity of CuZSM5, FeZSM5 and V_2O_5/TiO_2 catalysts by NH_3". In: *Microporous and Mesoporous Materials* 141.1-3 (2011), pp. 8–15. ISSN: 13871811. DOI: 10.1016/j.micromeso.2010.02.005.

[47] Irene Malpartida et al. "An operando IR study of the unburnt HC effect on the activity of a commercial automotive catalyst for NH_3-SCR". In: *Applied Catalysis B: Environmental* 102.1-2 (2011), pp. 190–200. ISSN: 09263373. DOI: 10.1016/j.apcatb.2010.11.041.

[48] Jin-Yong Luo et al. "Hydrocarbon Poisoning of Cu-Zeolite SCR Catalysts". In: *SAE Technical Paper Series*. SAE Technical Paper Series. SAE International, 2012. DOI: 10.4271/2012-01-1096.

[49] Jin-Yong Luo et al. "Effect of C_3H_6 on selective catalytic reduction of NO_X by NH_3 over a Cu/zeolite catalyst: A mechanistic study". In: *Applied Catalysis B: Environmental* 123-124 (2012), pp. 296–305. ISSN: 09263373. DOI: 10.1016/j.apcatb.2012.04.038.

[50] Lei Ma et al. "Propene poisoning on three typical Fe-zeolites for SCR of NO_X with NH_3: from mechanism study to coating modified architecture". In: *Environmental science & technology* 46.3 (2012), pp. 1747–1754. DOI: 10.1021/es203070g.

[51] Ashok Kumar, Krishna Kamasamudram, and Aleksey Yezerets. "Hydrocarbon Storage on Small-Pore Cu-Zeolite SCR Catalyst". In: *SAE Int. J. Engines* 6 (2013), pp. 680–687. DOI: 10.4271/2013-01-0508. URL: https://doi.org/10.4271/2013-01-0508.

[52] Lei Ma et al. "Mechanism of propene poisoning on Cu-SSZ-13 catalysts for SCR of NO_X with NH_3". In: *Catalysis Today* 245 (2015), pp. 16–21. ISSN: 09205861. DOI: 10.1016/j.cattod.2014.05.027.

[53] Yang Zheng, Michael P. Harold, and Dan Luss. "Effects of CO, H_2 and C_3H_6 on Cu-SSZ-13 catalyzed NH_3-SCR". In: *Catalysis Today* 264 (2016), pp. 44–54. ISSN: 09205861. DOI: 10.1016/j.cattod.2015.06.028.

[54] T. Selleri et al. "Modelling Inhibition Effects of Short-Chain Hydrocarbons on a Small-Pore Cu-Zeolite NH_3-SCR Catalyst". In: *Topics in Catalysis* 60.3 (2017), pp. 214–219. ISSN: 1572-9028. DOI: 10.1007/s11244-016-0600-4. URL: https://doi.org/10.1007/s11244-016-0600-4.

[55] Tommaso Selleri et al. "The impact of light and heavy hydrocarbons on the NH_3-SCR activity of commercial Cu- and Fe-zeolite catalysts". In: *Catalysis Today* 320 (2019), pp. 100–111. ISSN: 09205861. DOI: 10.1016/j.cattod.2017.09.028.

[56] Di Wang et al. "A comparison of hydrothermal aging effects on NH_3 -SCR of NO_X over Cu-SSZ-13 and Cu-SAPO-34 catalysts". In: *Applied Catalysis B: Environmental* 165 (2015), pp. 438–445. ISSN: 09263373. DOI: 10.1016/j.apcatb.2014.10.020.

[57] Clean Air Technology Center. "Nitrogen Oxides (NOx), Why and How They Are Controlled". In: *Epa-456/F-99-006R* November (1999), p. 48. DOI: EPA456/F-99-006R. URL: http://www.epa.gov/ttncatc1/dir1/fnoxdoc.pdf.

[58] Alan C. Lloyd and Thomas A. Cackette. "Diesel engines: environmental impact and control." In: *Journal of the Air & Waste Management Association* 51.6 (2001), pp. 809–847. ISSN: 1096-2247 (Print). DOI: 10.1080/10473289.2001.10464315.

[59] J. L. Sullivan et al. "CO_2 Emission Benefit of Diesel (versus Gasoline) Powered Vehicles". In: *Environmental Science & Technology* 38.12 (2004), pp. 3217–3223. DOI: 10.1021/es034928d.

[60] Sounak Roy, M. S. Hegde, and Giridhar Madras. "Catalysis for NO_X abatement". In: *Applied Energy* 86.11 (2009), pp. 2283–2297. ISSN: 03062619. DOI: 10.1016/j.apenergy.2009.03.022.

[61] Antonio Grossale et al. "NH_3–NO/NO_2 SCR for Diesel Exhausts Aftertreatment: Reactivity, Mechanism and Kinetic Modelling of Commercial Fe- and Cu-Promoted Zeolite Catalysts". In: *Topics in Catalysis* 52.13-20 (2009), pp. 1837–1841. ISSN: 1022-5528. DOI: 10.1007/s11244-009-9354-6.

[62] Massimo Colombo, Isabella Nova, and Enrico Tronconi. "A comparative study of the NH_3-SCR reactions over a Cu-zeolite and a Fe-zeolite catalyst". In: *Catalysis Today* 151.3-4 (2010), pp. 223–230. ISSN: 09205861. DOI: 10.1016/j.cattod.2010.01.010.

[63] Maria Pia Ruggeri et al. "FTIR in situ mechanistic study of the NH_3NO/NO_2 "fast SCR" reaction over a commercial Fe-ZSM-5 catalyst". In: *Catalysis Today*. Vol. 184. 1. Elsevier, 2012, pp. 107–114. DOI: 10.1016/j.cattod.2011.10.036.

[64] Louise Olsson et al. "A multi-site kinetic model for NH_3-SCR over Cu/SSZ-13". In: *Applied Catalysis B: Environmental* 174-175 (2015), pp. 212–224. ISSN: 09263373. DOI: 10.1016/j.apcatb.2015.02.037. URL: http://www.sciencedirect.com/science/article/pii/S0926337315001095.

[65] Amir R. Fahami, Isabella Nova, and Enrico Tronconi. "A kinetic modeling study of NO oxidation over a commercial Cu-CHA SCR catalyst for diesel exhaust aftertreatment". In: *Catalysis Today* (2017). ISSN: 09205861. DOI: 10.1016/j.cattod.2017.05.098. URL: http://www.sciencedirect.com/science/article/pii/S0920586117304303.

[66] Kirsten Leistner et al. "Mechanistic study of hydrothermally aged Cu/SSZ-13 catalysts for ammonia-SCR". In: *Catalysis Today* 307 (2018), pp. 55–64. ISSN: 09205861. DOI: 10.1016/j.cattod.2017.04.015.

[67] Isabella Nova, Bill Epling, and Chuck Peden. "Novel Catalysis for Vehicle Emissions Control". In: *Catalysis Today* 320 (2019), p. 1. ISSN: 09205861. DOI: 10.1016/j.cattod.2018.10.044.

[68] Pranit S. Metkar, Michael P. Harold, and Vemuri Balakotaiah. "Selective catalytic reduction of NOx on combined Fe- and Cu-zeolite monolithic catalysts: Sequential and dual layer configurations". In: *Applied Catalysis B: Environmental* 111-112 (2012), pp. 67–80. ISSN: 09263373. DOI: 10.1016/j.apcatb.2011.09.019.

[69] Pranit S. Metkar, Michael P. Harold, and Vemuri Balakotaiah. "Experimental and kinetic modeling study of NH_3-SCR of NOx on Fe-ZSM-5, Cu-chabazite and combined Fe- and Cu-zeolite monolithic catalysts". In: *Chemical Engineering Science* 87 (2013), pp. 51–66. ISSN: 00092509. DOI: 10.1016/j.ces.2012.09.008.

[70] Dae Jung Kim, Jin Wang, and Mark Crocker. "Adsorption and desorption of propene on a commercial Cu-SSZ-13 SCR catalyst". In: *Catalysis Today* 231 (2014), pp. 83–89. ISSN: 09205861. DOI: 10.1016/j.cattod.2013.10.061.

[71] Hanna Sjövall, Richard J. Blint, and Louise Olsson. "Detailed Kinetic Modeling of NH_3 and H_2O Adsorption, and NH_3 Oxidation over Cu-ZSM-5". In: *The Journal of Physical Chemistry C* 113.4 (2009), pp. 1393–1405. ISSN: 1932-7447. DOI: 10.1021/jp802449s.

[72] Unai De La Torre, Beñat Pereda-Ayo, and Juan R. González-Velasco. "Cu-zeolite NH_3-SCR catalysts for NO_X removal in the combined NSR–SCR technology". In: *Chemical Engineering Journal* 207-208 (2012), pp. 10–17. ISSN: 13858947. DOI: 10.1016/j.cej.2012.06.092.

[73] Nasim Najafi, Sima Askari, and Rouein Halladj. "Hydrothermal synthesis of nanosized SAPO-34 molecular sieves by different combinations of multi templates". In: *Powder Technology* 254 (2014), pp. 324–330. ISSN: 00325910. DOI: 10.1016/j.powtec.2014.01.037.

[74] Kirsten Leistner et al. "Impact of Copper Loading on NH_3-Selective Catalytic Reduction, Oxidation Reactions and N_2O Formation over Cu/SAPO-34". In: *Energies* 10.4 (2017), p. 489. DOI: 10.3390/en10040489.

[75] Isak Rajjak Shaikh et al. "H-ZSM-5 Zeolite Synthesis by Sourcing Silica from the Wheat Husk Ash: Characterization and Application as a Versatile Heterogeneous Catalyst in Organic Transformations including Some Multicomponent Reactions". In: *Journal of Catalysts* 2015.4 (2015), pp. 1–14. ISSN: 2314-5102. DOI: 10.1155/2015/805714.

[76] Lei Wang et al. "Location and nature of Cu species in Cu/SAPO-34 for selective catalytic reduction of NO with NH_3". In: *Journal of Catalysis* 289 (2012), pp. 21–29. ISSN: 00219517. DOI: 10.1016/j.jcat.2012.01.012.

[77] Peter Balle et al. "Study of the selective catalytic reduction of NOx on an efficient Fe/HBEA zeolite catalyst for heavy duty diesel engines". In: *Applied Catalysis B: Environmental* 91.3-4 (2009), pp. 587–595. ISSN: 09263373. DOI: 10.1016/j.apcatb.2009.06.031. URL: http://www.sciencedirect.com/science/article/pii/S0926337309002677http://linkinghub.elsevier.com/retrieve/pii/S0926337309002677.

[78] Christoph Hahn et al. "Kinetic Modelling of the Adsorption and Desorption of NH_3 on Fe/BEA Zeolite". In: *Zeitschrift für Physikalische Chemie* 229.5 (2015). ISSN: 0942-9352. DOI: 10.1515/zpch-2014-0607.

[79] D. Klukowski et al. "On the mechanism of the SCR reaction on Fe/HBEA zeolite". In: *Applied Catalysis B: Environmental* 93.1-2 (2009), pp. 185–193. ISSN: 0926-3373. DOI: 10.1016/J.APCATB.2009.09.028. URL: http://www.sciencedirect.com/science/article/pii/S0926337309003828https://www.sciencedirect.com/science/article/pii/S0926337309003828.

[80] M. Weiss, G. Ertl, and F. Nitschké. "Adsorption and decomposition of ammonia on Fe(110)". In: *Applications of Surface Science* 2.4 (1979), pp. 614–635. ISSN: 03785963. DOI: 10.1016/0378-5963(79)90049-7.

[81] O. Hinrichsen, A. Hornung, and M. Muhler. "Modeling of Temperature-Programmed Surface Reactions". In: *Chemical Engineering & Technology* 22.12 (1999), pp. 1039–1042. ISSN: 1521-4125. DOI: 10.1002/(SICI)1521-4125(199912)22:12<1039::AID-CEAT1039>3.0.CO;2-5.

[82] T Finke et al. "Numerical modelling of the adsorption and thermal desorption of NH_3 on ZrO_2". In: *Thermochimica Acta* 473.1 (2008), pp. 32–39. ISSN: 0040-6031. DOI: https://doi.org/10.1016/j.tca.2008.04.006. URL: http://www.sciencedirect.com/science/article/pii/S0040603108001196.

[83] Daniel Chatterjee et al. "Numerical Simulation of Zeolite- and V-Based SCR Catalytic Converters". In: *SAE Paper No. 2007-01-1136* 2007.724 (2007). DOI: 10.4271/2007-01-1136.

[84] J. M. Kanervo et al. "Temperature-programmed desorption as a tool to extract quantitative kinetic or energetic information for porous catalysts". In: *Journal of Catalysis* 238.2 (2006), pp. 382–393. ISSN: 00219517. DOI: 10.1016/j.jcat.2005.12.026.

[85] Daniel Chatterjee et al. "Numerical Simulation of NO/NO2/NH3 Reactions on SCR-Catalytic Converters: Model Development and Applications". In: *SAE Technical Paper* (2006). DOI: 10.4271/2006-01-0468.

[86] Isabella Nova et al. "Dynamics of SCR reaction over a TiO_2-supported vanadia-tungsta commercial catalyst". In: *Catalysis Today* 60.1 (2000), pp. 73–82. ISSN: 09205861. DOI: 10.1016/S0920-5861(00)00319-9.

[87] J. A. Dumesic et al. "Kinetics of selective catalytic reduction of nitric oxide by ammonia over vanadia/titania". In: *Journal of Catalysis* 163.2 (1996), pp. 409–417. ISSN: 00219517. DOI: 10.1006/jcat.1996.0342.

[88] T. Z. Srnak et al. "Temperature-programmed desorption/reaction and in situ spectroscopic studies of vanadia/titania for catalytic reduction of nitric oxide". In: *Journal of Catalysis* 135.1 (1992), pp. 246–262. ISSN: 10902694. DOI: 10.1016/0021-9517(92)90283-N.

[89] The SciPy community. *scipy.interpolate.interp1d*. 2019. URL: https://docs.scipy.org/doc/scipy/reference/generated/scipy.interpolate.interp1d.html.

[90] Cheng Peng et al. "Design and Synthesis of Cu/ZSM-5 Catalyst via a Facile One-Pot Dual-Template Strategy with Controllable Cu Content for Removal of NO_X". In: *Industrial & Engineering Chemistry Research* 57.44 (2018), pp. 14967–14976. ISSN: 0888-5885. DOI: 10.1021/acs.iecr.8b03432.

[91] Tetsuya Nanba et al. "Active sites of Cu-ZSM-5 for the decomposition of acrylonitrile". In: *Applied Catalysis B: Environmental* 61 (2005), pp. 288–296. DOI: 10.1016/j.apcatb.2005.05.013.

[92] Parvaneh Nakhostin Panahi et al. "Effect of the preparation method on activity of Cu-ZSM-5 nanocatalyst for the selective reduction of NO by NH_3". In: *Environmental technology* 38.15 (2017), pp. 1852–1861. DOI: 10.1080/09593330.2016.1238964.

[93] Filippo Giordanino et al. "Characterization of Cu-exchanged SSZ-13: a comparative FTIR, UV-Vis, and EPR study with Cu-ZSM-5 and Cu-β with similar Si/Al and Cu/Al ratios". In: *Dalton transactions* 42.35 (2013), pp. 12741–12761. DOI: 10.1039/c3dt50732g.

[94] Tao Zhang et al. "Selective catalytic reduction of NO with NH_3 over HZSM-5-supported Fe–Cu nanocomposite catalysts: The Fe–Cu bimetallic effect". In: *Applied Catalysis B: Environmental* 148-149 (2014), pp. 520–531. ISSN: 09263373. DOI: 10.1016/j.apcatb.2013.11.006.

[95] Hui Hsin Tseng et al. "Synthesis, characterization, and promoter effect of Cu-Zn/γ-Al_2O_3 catalysts on NO reduction with CO". In: *Chemical Engineering Journal* 160.1 (2010), pp. 13–19. ISSN: 13858947. DOI: 10.1016/j.cej.2010.02.039.

[96] F. Benaliouche et al. "NH_3-TPD and FTIR spectroscopy of pyridine adsorption studies for characterization of Ag- and Cu-exchanged X zeolites". In: *Microporous and Mesoporous Materials* 111.1-3 (2008), pp. 80–88. ISSN: 13871811. DOI: 10.1016/j.micromeso.2007.07.006.

[97] Jungwon Woo et al. "Effect of various structure directing agents (SDAs) on low-temperature deactivation of Cu/SAPO-34 during NH_3-SCR reaction". In: *Catal. Sci. Technol.* 8 (12 2018), pp. 3090–3106. DOI: 10.1039/C8CY00147B. URL: http://dx.doi.org/10.1039/C8CY00147B.

[98] Feng Gao et al. "Synthesis and Evaluation of Cu-SAPO-34 Catalysts for Ammonia Selective Catalytic Reduction. 1. Aqueous Solution Ion Exchange". In: *ACS Catalysis* 3.9 (2013), pp. 2083–2093. ISSN: 2155-5435. DOI: 10.1021/cs4004672.

[99] A. Frache et al. "CuAPSO-34 catalysts for N_2O decomposition in the presence of H_2O. A study of zeolitic structure stability in comparison to Cu-SAPO-34 and Cu-ZSM-5". In: *Topics in Catalysis* 22.1/2 (2003), pp. 53–57. ISSN: 10225528. DOI: 10.1023/A:1021411628121.

[100] Dong Zhang and Ralph T. Yang. "NH_3-SCR of NO over one-pot Cu-SAPO-34 catalyst: Performance enhancement by doping Fe and MnCe and insight into N_2O formation". In: *Applied Catalysis A: General* 543 (2017), pp. 247–256. ISSN: 0926860X. DOI: 10.1016/j.apcata.2017.06.021.

[101] E. A. Urquieta-González et al. "Identification of Extra-Framework Species on Fe/ZSM-5 and Cu/ZSM-5 Catalysts Typical Microporous Molecular Sieves with Zeolitic Structure". In: *Journal of Catalysis* 5.3 (2002), pp. 321–327. ISSN: 00219517. DOI: 10.1590/S1516-14392002000300017.

[102] Huawang Zhao et al. "The promotion effect of Fe to Cu-SAPO-34 for selective catalytic reduction of NO_X with NH_3". In: *Catalysis Today* 297 (2017), pp. 84–91. ISSN: 09205861. DOI: 10.1016/j.cattod.2017.05.060.

[103] Paul E. Fanning and M.Albert Vannice. "A DRIFTS Study of Cu–ZSM-5 Prior to and during Its Use for N_2O Decomposition". In: *Journal of Catalysis* 207.2 (2002), pp. 166–182. ISSN: 00219517. DOI: 10.1006/jcat.2002.3518.

[104] A.V Ivanov, G.W Graham, and M. Shelef. "Adsorption of hydrocarbons by ZSM-5 zeolites with different SiO_2/Al_2O_3 ratios: a combined FTIR and gravimetric study". In: *Applied Catalysis B: Environmental* 21.4 (1999), pp. 243–258. ISSN: 09263373. DOI: 10.1016/S0926-3373(99)00021-1.

[105] Miki Niwa and Naonobu Katada. "Measurements of acidic property of zeolites by temperature programmed desorption of ammonia". In: *Catalysis Surveys from Asia* 1.2 (1997), pp. 215–226. ISSN: 1574-9266. DOI: 10.1023/A:1019033115091.

[106] Peirong Chen et al. "Local dynamics of copper active sites in zeolite catalysts for selective catalytic reduction of NO_X with NH_3". In: *Applied Catalysis B: Environmental* 237 (2018), pp. 263–272. ISSN: 09263373. DOI: 10.1016/j.apcatb.2018.05.091.

[107] I. Lezcano-Gonzalez et al. "Chemical deactivation of Cu-SSZ-13 ammonia selective catalytic reduction (NH_3-SCR) systems". In: *Applied Catalysis B: Environmental* 154-155.x (2014), pp. 339–349. ISSN: 09263373. DOI: 10.1016/j.apcatb.2014.02.037. URL: http://dx.doi.org/10.1016/j.apcatb.2014.02.037.

[108] G. V.A. Martins et al. "Quantification of Brønsted acid sites in microporous catalysts by a combined FTIR and NH_3-TPD study". In: *Journal of Physical Chemistry C* 112.18 (2008), pp. 7193–7200. ISSN: 19327447. DOI: 10.1021/jp710613q.

[109] Luz Rodríguez-González et al. "The acid properties of H-ZSM-5 as studied by NH_3-TPD and 27Al-MAS-NMR spectroscopy". In: *Applied Catalysis A: General* 328.2 (2007), pp. 174–182. ISSN: 0926860X. DOI: 10.1016/j.apcata.2007.06.003.

[110] Hao Wang et al. "Zeolite structure effects on Cu active center, SCR performance and stability of Cu-zeolite catalysts". In: *Catalysis Today* 327 (2019), pp. 295–307. ISSN: 09205861. DOI: 10.1016/j.cattod.2018.04.035.

[111] Jun Wang et al. "The influence of silicon on the catalytic properties of Cu/SAPO-34 for NO_X reduction by ammonia-SCR". In: *Applied Catalysis B: Environmental* 127 (2012), pp. 137–147. ISSN: 09263373. DOI: 10.1016/j.apcatb.2012.08.016.

[112] Di Wang et al. "In Situ-DRIFTS Study of Selective Catalytic Reduction of NO_X by NH_3 over Cu-Exchanged SAPO-34". In: *ACS Catalysis* 3.5 (2013), pp. 871–881. ISSN: 2155-5435. DOI: 10.1021/cs300843k.

[113] Tao Zhang et al. "Enhanced hydrothermal stability of Cu-ZSM-5 catalyst via surface modification in the selective catalytic reduction of NO with NH_3". In: *Applied Surface Science* 375 (2016), pp. 186–195. ISSN: 01694332. DOI: 10.1016/j.apsusc.2016.03.049.

[114] Hanna Sjövall et al. "Identification of adsorbed species on Cu-ZSM-5 under NH_3 SCR conditions". In: *Topics in Catalysis* 42-43.1-4 (2007), pp. 113–117. ISSN: 1022-5528. DOI: 10.1007/s11244-007-0162-6.

[115] T. E. Hoost, K. A. Laframboise, and K. Otto. "Co-adsorption of propene and nitrogen oxides on Cu-ZSM-5: An FTIR study". In: *Applied Catalysis B: Environmental* 7.1-2 (1995), pp. 79–93. ISSN: 09263373. DOI: 10.1016/0926-3373(95)00181-6.

[116] Kamasamudram Krishna and Michiel Makkee. "Coke formation over zeolites and CeO_2-zeolites and its influence on selective catalytic reduction of NO_X". In: *Applied Catalysis B: Environmental* 59.1 (2005), pp. 35–44. ISSN: 0926-3373. DOI: https://doi.org/10.1016/j.apcatb.2005.01.003. URL: http://www.sciencedirect.com/science/article/pii/S0926337305000287.

[117] Sandro Brandenberger et al. "The role of Brønsted acidity in the selective catalytic reduction of NO with ammonia over Fe-ZSM-5". In: *Journal of Catalysis* 268.2 (2009), pp. 297–306. ISSN: 00219517. DOI: 10.1016/j.jcat.2009.09.028. URL: http://www.sciencedirect.com/science/article/pii/S0021951709003327.

[118] Michael Schwidder et al. "The role of Brønsted acidity in the SCR of NO over Fe-MFI catalysts". In: *Microporous and Mesoporous Materials* 111.1-3 (2008), pp. 124–133. ISSN: 13871811. DOI: 10.1016/j.micromeso.2007.07.019. URL: http://linkinghub.elsevier.com/retrieve/pii/S1387181107004258.

[119] Moses O. Adebajo, Mervyn A. Long, and Ray L. Frost. "Spectroscopic and XRD characterisation of zeolite catalysts active for the oxidative methylation of benzene with methane". In: *Spectrochimica Acta - Part A: Molecular and Biomolecular Spectroscopy* 60.4 (2004), pp. 791–799. ISSN: 13861425. DOI: 10.1016/S1386-1425(03)00302-0.

[120] Asima Sultana et al. "Influence of co-cations on the formation of Cu^+ species in Cu/ZSM-5 and its effect on selective catalytic reduction of NO_X with NH_3". In: *Applied Catalysis B: Environmental* 101.1-2 (2010), pp. 61–67. ISSN: 09263373. DOI: 10.1016/j.apcatb.2010.09.007.

[121] John B. Heywood. *Internal Combustion Engine Fundamentals, Second Edition*. 2nd edition. New York: McGraw-Hill Education: New York, Chicago, San Francisco, Athens, London, Madrid, Mexico City, Milan, New Delhi, Singapore, Sydney, Toronto, 2018. ISBN: 9781260116106. URL: https://www.accessengineeringlibrary.com/content/book/9781260116106.

[122] Asima Sultana et al. "Selective catalytic reduction of NO_X with NH_3 over different copper exchanged zeolites in the presence of decane". In: *Catalysis Today* 164.1 (2011), pp. 495–499. ISSN: 09205861. DOI: 10.1016/j.cattod.2010.11.036.

[123] Sachi Shrestha et al. "Selective oxidation of ammonia to nitrogen on bi-functional Cu-SSZ-13 and Pt/Al2O3 monolith catalyst". In: *Catalysis Today* 267 (2016), pp. 130–144. ISSN: 0920-5861. DOI: https://doi.org/10.1016/j.cattod.2015.11.035. URL: http://www.sciencedirect.com/science/article/pii/S0920586115007762.

[124] Ante Kozina, Gojmir Radica, and Sandro Nižetić. "Analysis of methods towards reduction of harmful pollutants from diesel engines". In: *Journal of Cleaner Production* 262 (2020), p. 121105. ISSN: 09596526. DOI: 10.1016/j.jclepro.2020.121105.

[125] T. Komatsu et al. "Kinetic Studies of Reduction of Nitric Oxide with Ammonia on Cu^{2+}-Exchanged Zeolites". In: *Journal of Catalysis* 148.2 (1994), pp. 427–437. ISSN: 0021-9517. DOI: 10.1006/jcat.1994.1229.

[126] Sandro Brandenberger et al. "The determination of the activities of different iron species in Fe-ZSM-5 for SCR of NO by NH_3". In: *Applied Catalysis B: Environmental* 95.3-4 (2010), pp. 348–357. ISSN: 09263373. DOI: 10.1016/j.apcatb.2010.01.013.

[127] Shane A. Bates et al. "Identification of the active Cu site in standard selective catalytic reduction with ammonia on Cu-SSZ-13". In: *Journal of Catalysis* 312 (2014), pp. 87–97. ISSN: 00219517. DOI: 10.1016/j.jcat.2014.01.004. URL: http://www.sciencedirect.com/science/article/pii/S0021951714000141http://dx.doi.org/10.1016/j.jcat.2014.01.004https://linkinghub.elsevier.com/retrieve/pii/S0021951714000141.

[128] Saurabh Y. Joshi et al. "New insights into the mechanism of NH_3-SCR over Cu- and Fe-zeolite catalyst: Apparent negative activation energy at high temperature and catalyst unit design consequences". In: *Applied Catalysis B: Environmental* 226 (2018), pp. 565–574. ISSN: 09263373. DOI: 10.1016/j.apcatb.2017.12.076.

[129] Scott A. Stevenson, James C. Vartuli, and Carlton F. Brooks. "Kinetics of the Selective Catalytic Reduction of NO over HZSM-5". In: *Journal of Catalysis* 190.2

(2000), pp. 228–239. ISSN: 00219517. DOI: 10.1006/jcat.1999.2747. URL: http://linkinghub.elsevier.com/retrieve/pii/S0021951799927471.

[130] Daniel Chatterjee et al. "Numerical simulation of ammonia SCR-catalytic converters: Model development and application". In: *SAE Technical Papers*. SAE International, 2005. DOI: 10.4271/2005-01-0965. URL: https://www.sae.org/publications/technical-papers/content/2005-01-0965/.

[131] Unai De-La-Torre et al. "Steady-state NH_3-SCR global model and kinetic parameter estimation for NOx removal in diesel engine exhaust aftertreatment with Cu/chabazite". In: *Catalysis Today* 296 (2017), pp. 95–104. ISSN: 09205861. DOI: 10.1016/j.cattod.2017.04.011.

[132] Wataru Eijima et al. "Kinetic modeling of steady-state NH_3-SCR over a monolithic Cu-CHA catalyst". In: *Catalysis Today* 352 (2020), pp. 237–242. ISSN: 09205861. DOI: 10.1016/j.cattod.2019.09.005.

[133] Gérard Delahay et al. "Kinetics of the selective catalytic reduction of NO by NH_3 on a Cu-faujasite catalyst". In: *Applied Catalysis B: Environmental* 52.4 (2004), pp. 251–257. ISSN: 0926-3373. DOI: 10.1016/j.apcatb.2004.04.008.

[134] Enrico Tronconi et al. "Modelling of an SCR catalytic converter for diesel exhaust after treatment: Dynamic effects at low temperature". In: *Catalysis Today* 105.3-4 (2005), pp. 529–536. ISSN: 09205861. DOI: 10.1016/j.cattod.2005.06.043.

[135] Michel Boudart. "Turnover Rates in Heterogeneous Catalysis". In: *Chemical Reviews* 95.3 (1995), pp. 661–666. ISSN: 0009-2665. DOI: 10.1021/cr00035a009.

[136] Feng Gao et al. "Structure–activity relationships in NH_3-SCR over Cu-SSZ-13 as probed by reaction kinetics and EPR studies". In: *Journal of Catalysis* 300 (2013), pp. 20–29. ISSN: 0021-9517. DOI: 10.1016/j.jcat.2012.12.020.

[137] M. P. Ruggeri et al. "Structure–Activity Relationship of Different Cu–Zeolite Catalysts for NH_3-SCR". In: *Topics in Catalysis* 59.10 (2016), pp. 875–881. ISSN: 1022-5528. DOI: 10.1007/s11244-016-0562-6. URL: https://doi.org/10.1007/s11244-016-0562-6.

[138] Junjie Xue et al. "Characterization of copper species over Cu/SAPO-34 in selective catalytic reduction of NOx with ammonia: Relationships between active Cu sites and de-NOx performance at low temperature". In: *Journal of Catalysis* 297.Supplement C (2013), pp. 56–64. ISSN: 0021-9517. DOI: https://doi.org/10.1016/j.jcat.2012.09.020. URL: http://www.sciencedirect.com/science/article/pii/S0021951712002990.

[139] P. B. Weisz and C. D. Prater. "Interpretation of Measurements in Experimental Catalysis". In: *Advances in Catalysis*. Ed. by W.G Frankenburg, V.I Komarewsky, and E.K Rideal. Vol. 6. Academic Press, 1954, pp. 143–196. ISBN: 0360-0564. DOI: 10.1016/S0360-0564(08)60390-9. URL: http://www.sciencedirect.com/science/article/pii/S0360056408603909.

[140] M. Albert Vannice. *Kinetics of catalytic reactions*. New York and London: Springer, 2005. ISBN: 0387259724.